SEDIMENT DYNAMICS AND ASSOCIATED HEAVY METALS IN A SMALL RIVER- AND WAVE-DOMINATED INNER SHELF (BARCELONA CITY, NW MEDITERRANEAN)

PROGRAMA DE DOCTORAT EN CIÈNCIES DEL MAR, UPC/UB/CSIC

Memòria presentada per

LAURA LÓPEZ FERNÁNDEZ

per optar al grau de Doctora per la Universitat Politècnica de Catalunya

Dirigida per

Dr. JORGE GUILLÉN

i

Dr. ALBERT PALANQUES

CONTENTS

Acknowledgements i

Summary i

Resumen iv

List of Figures i

List of Tables vi

1 Introduction 1

1.1 Effects of floods and storms on the continental shelf 1
1.2 The role of across-shelf gradients in sediment dynamics 5
1.3 Heavy metals in the littoral system 7
1.4 Study area 9
1.5 Main objectives 14

2 Methods 15

2.1 Field work and instrumentation 15
2.1.1 Benthic tripods 16
2.1.2 Hydrographical and meteorological data 21
2.1.3 Bottom sediment sampling 22
2.2 Laboratory Works 26
2.2.1 Preparation and treatment of sediment traps samples 26
2.2.2 Treatment of sediment cores and grabs 27
2.2.3 Grain size analysis 27
2.2.4 Major elements and heavy metal analysis 28
2.2.5 Enrichment factor of main heavy metals in sediments 30
2.3 Data calculations 30
2.3.1 Near-bottom wave orbital velocity 30
2.3.2 Calibration of Seapoint turbidimeters 31
2.3.3 Calibration of Aanderaa turbidimeters 32
2.3.4 Along- and across-shelf currents and advective fluxes 32
2.3.5 Downward total mass fluxes 33
2.3.6 Altimeter calibration and Seabed erosion/deposition 33
2.3.7 One-dimensional (vertical) sediment transport model 34
2.3.8 Definition of sediment flux events 35

3 Forcing conditions 36

3.1 Wind and waves 36
3.2 Hydrography and water river discharge 41
3.3 Near-bottom currents 44
3.4 Processes affecting currents during the study period 51

4 Sediment characteristics 53

4.1 Bottom sediment variability..... 53
4.2 Particulate matter downward fluxes..... 60
4.3 Near-bottom suspended sediment concentration and shear stress..... 61
4.4 Factors controlling SSC..... 64

5 Patterns of sediment transport 67

5.1 Near-bottom sediment fluxes..... 67
5.2 Evaluation of a 1D Sediment transport model 70
5.3 Sediment dynamics across the shelf 77

6 Heavy metal pollution in sediments 82

6.1 Distribution and pollution levels of heavy metals 82
6.2 Temporal variability of heavy metals concentrations 85
6.3 Implications for the fate of heavy metals in the inner shelf off Barcelona 89

7 Conclusions and further research..... 92

8 References 95

Acknowledgements

La presente tesis ha sido llevada a cabo gracias al proyecto SEDMET (CMTM2006-06919) financiado por el Ministerio de Economía y Competitividad. Y no hubiera sido posible sin la supervisión y el conocimiento de mis directores de tesis, Albert Palanques y Jorge Guillén. Gracias a los dos por confiar en mi y darme la oportunidad de participar en casi todos los pasos de un proyecto de investigación. Ha sido una gran experiencia.

Brevemente me gustaría agradecer a todas las personas que me han ayudado directa o indirectamente al desarrollo de la tesis:

A los compañeros de despacho y de tertulias en los primeros años en el ICM: Elena Ojeda, Ruth Duran, Marta Nuez, Marga García, y en los últimos Amanda Sancho, Marta Ribó, Jaume Llopart y Laia Beni.

A todo el personal del ICM y la UTM. En especial a Silvia de Diago, Neus Maestro y Mª Angeles Millán por su gran ayuda y excelente compañía en las largas tandas de laboratorio. A Maribel Lloret, Oriol Mulet, Jordi el patrón y demás compañeros de PUDEM por esas campañas fantásticas de verano y el calor durante las de invierno. A Pere Puig, Gonzalo Simarro, Sara Soto, Oscar Chic y Toni Bermúdez por su disponibilidad a compartir sus conocimientos y experiencia.

A toda la tripulación del B/O García del Cid y Sarmiento de Gamboa. Por sus buenas maniobras y su excelente compañía.

Als professors i companys de la UB i de la UPC. En especial, a Jordi Serra per conduir-me cap a l'ICM a fer el treball de fi de carrera, i per extensió, al Professor Dan Bowman i l'Enzo Pellegrino per la bona feina durant aquest.

Thanks to Mike Collins, Erwan Garel and all the staff of the NOC (Southampton, UK) and Chris Sherwood and colleagues from the USGS and the Woods Hole Oceanographic Institution (USA). Your openness and advices have been crucial to get here. And, of course, to all the friends I made during my stay there, specially to Cass, Rich, Matt and Alma Road's people.

I per últim però primers al meu cor. A la meva petita família, Màrius, Oriol i Llorenç. Als meus nebots Pau i Maria. A mis padres, mi hermana Sandra y al Manel, a los mejores suegros Maica y Rufino y a Jordi. A mi prima Eva y la extensa familia que me han hecho parte de lo que soy. I per descomptat, als meus amics que m'han acompanyat i m'han carregat les piles en els moments de desconnexió.

Summary

Wave storms and river inputs have been found to be the dominant forcing mechanism of sediment transport in continental shelves dominated by medium to large rivers around the world (e.g. Drake and Cacchione, 1985; Sherwood et al., 1994; Ogston and Stemberg, 1999; Traykovski et al., 2000; Wadman and McNinch, 2008) and in the northwestern Mediterranean Sea (Jiménez et al., 1999; Puig et al., 2001; Guillén et al., 2002, 2006; Palanques et al., 2002, 2011; Ferré et al., 2005; Roussiez et al., 2005; Ulses et al., 2008). However, the contribution of "small" Mediterranean river systems in fine-grained sediment dynamics is not well known. Flood and storm events redistribute not only sediment but also all the associated matter as well, such a heavy metals, which are indicators of the impact of industrial and urban activities. For these reasons, the present thesis project involves studying the dynamics of sediments and associated heavy metals across the inner continental shelf off the Besòs River (Barcelona), and in particular determining the effect of floods and storms in a littoral system affected by industrial and urban activities. To this end, several oceanographic surveys were carried out between 20 and 40 m water depths in the Barcelona continental shelf to obtain a variety of data: to register vertical hydrographical profiles (temperature, salinity and turbidity); to record time series of physical parameters (currents, salinity, temperature, turbidity and seabed variation) by deploying oceanographic equipment; and to take sediment samples (short cores and Van Veen grabs) and suspended and downward particulate matter from water samples and sediment traps for further sedimentological and geochemical analysis.

The time period of the present study comprised three seasons, from autumn 2007 to spring 2008, which showed distinct features between them. The purpose of section 3 was to describe the main hydrographic and hydrodynamic conditions during the study period to support the interpretation of sediment transport processes. Three different periods in terms of storm and river activity matched the natural seasons of the year: The period comprised between end of September 2007 and December 2007 (autumn) was characterized by an intense frequency of northeastern-eastern storms mostly coupled with high but short river discharges and a convergence of the across-shelf current between 20 m and 30 m water depths; between January and early March 2008 (winter), the wave and river activity and frequency were reduced significantly with offshore currents dominating the across component; and finally, from March to mid June 2008 (spring), specially between May and June 2008, river discharges lasted

more than one month and occurred under low wave energy conditions or in conjunction with S-SE and SW wave storms.

The sediment response to the forcing conditions observed during the study period was analyzed in section 4. The grain size and porosity measurements taken in all the sediment samples collected during the experiment (sediment cores, sediment grabs and sediment traps) showed a high spatial and temporal variability of the bottom sediment properties, downward sediment fluxes and near-bottom sediment concentrations across the inner-shelf. Those changes were associated to periods of high wave shear stress, river and current energy and therefore, were more intense in autumn 2007 and spring 2008. However, an across shelf spatial variability was observed during this period which was associated to the sediment availability (i.e. critical shear stress gradients). As a result, the same storm produced larger near-bottom sediment concentration in deeper waters due to the limitation on the availability of resuspendable sediment in the near-shore.

The resultant sediment dynamics across the inner shelf and results in sediment transport modeling during a resuspension event were then addressed in section 5. In the inner shelf off Barcelona, the general circulation of sediment transport was mainly directed towards the southwest (along-shelf) during the study period, however, the seaward component was considerably relevant and favored the segregation of coarse and fine sediment from the nearshore towards deeper areas. Nonetheless, noticeable differences in sediment transport patterns were observed across the inner shelf. Near-bottom sediment transport at 20 m water depth was mainly offshore, while in deeper parts of the inner shelf the along-shelf component dominated the sediment transport. The resulting sediment transport and its variability across the shelf, deposited riverine and storm-derived fine sediment in an along-shelf path towards the southwest between 20 m and 30 m water depth and only under the strong storms were transferred seaward toward the 40 m water depth site and to deeper areas. These differences had in turn a strong seasonal component related to the availability of fine sediments from river inputs and the energy of waves and currents. In this sense, autumn and spring registered events affected mostly at 20 m water depth and autumn and early winter months were more energetic at deeper waters reversing the sing of sediment transport gradients across the shelf. During this event, the sediment transport model captured adequately the transport rates across the inner shelf and allowed the estimation of the integrated vertical sediment flux in 10 meters of the water column above the seabed. Consequently with the observed and modelled pattern of sediment transport, the

seabed variation was higher at 30 m than at 20 m water depth, with a total seabed erosion of about 10 cm and 4 cm, respectively.

The implications of the sediment dynamics during the study period in the transference of heavy metals from the Besòs River across the shelf was analyzed in section 6. The Besòs River introduced heavy metal pollutants into the nearshore continuously associated with the regular regime and sporadically during increments in river discharge. Only during high wave and current energy the anthropogenic contamination, previously deposited in the shallow inner-shelf, reached deeper areas. As a result, the most contaminated sediment accumulated southwestward from the river and sewer mouths along the inner shelf decreasing offshore. The most affected area associated to the Besòs river influence was located around the tripod sites, especially between 20 m and 30 m water depths decreasing offshore.

Finally, the main conclusions and proposals for future research of this thesis are discussed in section 7. In it, the importance of "small" Mediterranean river systems in the transfer of sediment across the continental shelf is highlighted from the sediment transport events observed during the study period.

Resumen

El oleaje durante temporales y los aportes fluviales han sido considerados como los mecanismos de forzamiento dominantes del transporte de sedimento en las plataformas continentales afectadas por ríos medianos y grandes en todo el mundo (por ejemplo, Drake y Cacchione, 1985; Sherwood et al., 1994; Ogston y Stemberg, 1999; Traykovski et al., 2000; Wadman y McNinch, 2008) y en el Mediterráneo noroccidental (Jiménez et al., 1999; Puig et al., 2001; Guillén et al., 2002, 2006; Palanques et al., 2002, 2011; Ferré et al., 2005; Roussiez et al., 2005; Ulses et al., 2008). Sin embargo, la contribución de "pequeños" sistemas fluviales mediterráneos en la dinámica de sedimento está poco estudiada. El oleaje y las tormentas no solo redistribuyen sedimentos si no también toda la materia asociada, así como, metales pesados, que son indicadores del impacto de las actividades industriales y urbanas. Por estas razones, el presente proyecto de tesis implica el estudio de la dinámica de sedimento y metales pesados asociados a través de la plataforma continental del río Besòs (Barcelona), y en particular, determinar el efecto de los temporales y tormentas en un sistema litoral afectado por actividades industriales y urbanas. Para este fin, varias campañas oceanográficas se llevaron a cabo entre 20 y 40 m de profundidad en la plataforma continental de Barcelona donde se tomaron gran variedad de datos y muestras: perfiles verticales hidrográficos (temperatura, salinidad y turbidez); series temporales de parámetros físicos (corrientes, salinidad, temperatura, turbidez y la variación del fondo) mediante el anclaje de equipos oceanográficos, y muestras de sedimento (testigos cortos de sedimento y dragas Van Veen) y de partículas en suspensión (a partir de muestras de agua y trampas de sedimentos) para análisis sedimentológicos y geoquímicos.

El período de estudio comprendió tres estaciones, desde otoño de 2007 a primavera de 2008, que mostraron características distintas entre ellas. En la sección 3 se describen las principales condiciones hidrográficas y la hidrodinámica durante el período de estudio para apoyar la interpretación de los procesos de transporte sedimentario. Se identificaron tres periodos diferentes en función de la actividad fluvial y la del oleaje que coincidieron con las estaciones naturales del año: El período comprendido entre finales de septiembre de 2007 y diciembre de 2007 (otoño) se caracterizó por una intensa frecuencia de temporales del noreste-este junto con incrementos en la descarga del río y una convergencia de la componente *across-shelf* de la corriente entre 20 m y 30 m de profundidad; entre enero y principios de marzo de 2008 (invierno), la actividad y la frecuencia del oleaje y del río se redujeron

significativamente con predominio de la componente *offshore* de la corriente; y, por último, de marzo a mediados de junio de 2008 (primavera), especialmente entre mayo y junio de 2008, las descargas fluviales se intensificaron durante más de un mes produciéndose en condiciones de baja energía del oleaje o en combinación con temporales del S-SE o SW.

La respuesta del sedimento del fondo a las condiciones de forzamiento observadas durante el período de estudio se analizó en la sección 4. El tamaño medio de grano y la porosidad de todas las muestras de sedimento recogidas durante el experimento (testigos, dragas y trampas) mostraron una alta variabilidad espacial y temporal. Los flujos verticales de sedimento y la concentración de sedimento en suspensión cerca del fondo también variaron a través de la plataforma interna durante el periodo de estudio. Estos cambios se asociaron a eventos de fuerte oleaje y corrientes y a descargas del río y, por tanto, fueron más intensas en otoño de 2007 y primavera de 2008. Sin embargo, se observó una variabilidad espacial a través de la plataforma interna durante estos eventos que se asoció a la disponibilidad de sedimento (es decir, a gradientes de “critical shear stress”). Como resultado, una misma tormenta produjo una concentración de sedimento cerca del fondo mayor en aguas más profundas debido a que la disponibilidad de sedimento fino era limitada en aguas someras.

En la sección 5, se analiza la dinámica de sedimento resultante a través de la plataforma interna y los resultados obtenidos en el modelado del transporte de sedimento durante un evento de resuspensión. En la plataforma interna de Barcelona, la circulación general del transporte sedimentario se dirigió principalmente hacia el suroeste (*along-shelf*) durante el período de estudio, sin embargo, la componente *onshore* fue bastante relevante y favoreció la segregación de sedimento grueso y fino desde la costa hacia zonas más profundas. Sin embargo, se observaron diferencias notables en el transporte de sedimento a través de la plataforma interna. A 20 m de profundidad, el transporte de sedimento fue principalmente *onshore*, mientras que zonas más profundas de la plataforma interna la componente *along-shelf* dominó el transporte. Este patrón de transporte, depositó sedimentos del río y depositados previamente en una trayectoria *along-shelf* hacia el suroeste entre 20 m y 30 m de profundidad y sólo durante los temporales más fuertes fueron transportados hacia 40 m de profundidad y probablemente a zonas más profundas de la plataforma continental. Estas diferencias tuvieron a su vez una fuerte componente estacional relacionada con la disponibilidad de sedimentos fluviales finos y la energía del oleaje y las corrientes. En este sentido, en otoño y primavera los eventos registrados afectaron

mayormente a 20 m de profundidad y a finales de otoño y comienzos del invierno fueron más activos en aguas profundas, cambiando el gradiente del transporte sedimentario a través de la plataforma. Durante este evento, el modelo de transporte sedimentario capturó adecuadamente las tasas de transporte a través de la plataforma y permitió estimar el flujo vertical integrado de sedimento en 10 metros de columna de agua sobre el fondo marino. En consecuencia con el patrón de transporte de sedimento observado y modelado, la variación del fondo marino fue superior a 30 m que a 20 m de profundidad, con una erosión de alrededor de 10 cm y 4 cm, respectivamente.

Las implicaciones de la dinámica sedimentaria durante el período de estudio en la transferencia de metales pesados des del río Besòs a través de la plataforma se analizó en la sección 6. El río Besòs introdujo metales pesados cerca de la costa continuamente durante el régimen de descarga regular y esporádicamente en incrementos de caudal del río. Sólo durante las condiciones más altas de oleaje y corrientes la contaminación antropogénica, previamente depositada en la parte somera de la plataforma, alcanzó zonas más profundas. Como resultado, el sedimento más contaminado se acumuló hacia el suroeste del río y de las desembocaduras de los pluviales. La zona más afectada asociada a la influencia del río Besòs se localizó especialmente entre 20 m y 30 m de profundidad disminuyendo en profundidad.

Por último, las principales conclusiones y propuestas de futura investigación de la presente tesis se abordan en la sección 7. En ella, se destaca la importancia de "pequeños" sistemas fluviales mediterráneos en la transferencia de sedimento a través de la plataforma continental que se manifiesta a partir de la secuencia de eventos de transporte sedimentario observada durante el periodo de estudio.

List of Figures

Figure 1.1. Map of the Barcelona continental shelf showing the study area and the wave data points used in this project. The map projection is UTM zone 31N datum ED50. 9

Figure 1.2. Sketch showing the general zonation of the Barcelona shelf. Map projection is UTM 31N WGS84. From Liquete et al. (2007). 12

Figure 1.3. Distribution of surface contaminated sediments by heavy metals on the continental shelf of Barcelona. * Pipeline Mouth of the treatment plant. From Palanques et al. (1998). 13

Figure 2.1. Position of the benthic tripods deployed: Be09 at 20 m water depth, Be08 at 30 m depth and Be07 at 40 m depth. The map projection is UTM zone 31N datum ED50. 17

Figure 2.2. Picture of the benthic tripod used in this project. 18

Figure 2.3. Schematic drawing of the sediment trap used in this study. 19

Figure 2.4. Location of hydrographic stations during SEDMET surveys. WANA 2066051 is the model point of oceanographic data and the text annotation BESÒS RIVER marks the mouth of the river. The thick black line is the old pipeline from the water waste plant located near the river mouth. The map projection is UTM zone 31N datum ED50. 21

Figure 2.5. Location of sediment cores sampling stations during SEDMET surveys. WANA 2066051 is the model point of oceanographic data and the text annotation BESÒS RIVER marks the mouth of the river. The rectangle is the old pipeline from the water waste plant located near the river mouth. The map projection is UTM zone 31N datum ED50. 23

Figure 2.6. Picture of the box corer used in this project (model Haps corer by KC-Denmark). 24

Figure 2.7. Sediment grabs sampling locations in the study area during two monthly monitoring surveys. WANA 2066051 is the model point of oceanographic data and the text annotation BESÒS RIVER marks the mouth of the river. The thick black line is the

old pipeline from the water waste plant located near the river mouth. The map projection is UTM zone 31N datum ED50. 25

Figure 3.1 Wave, wind and river discharge conditions during the experiment, collected nearby the study area. (A) Wind speed at WANA model point 2066051; (B) and (C) wave data at WANA model point 2066051 calibrated with Llobregat buoy data; (D) water discharge at the Besòs River gateway. 37

Figure 3.2. Time-series of significant wave orbital velocity at location (A) Be09-20m, (B) Be08-30m and (C) Be07-40m. 38

Figure 3.3. Time series of wave (A1) and wind (B1) directions at WANA model point 2066051 during the study period. (A2) and (B2) rose diagram of the relative frequency of the record of wave and wind direction, respectively. 38

Figure 3.4. Spectral analysis of forcing agents time series. (A) Significant near-bottom wave orbital velocity, (B1) Across-shelf winds and (B2) Along-shelf winds. 40

Figure 3.5. Across-shelf sections of temperature, salinity, SSC and density over the study area during (A) the SEDMET-I (September 2007) and (B) SEDMET-II (November 2007) cruises. The location of the stations is shown in the left map of each box. 42

Figure 3.6. Across-shelf (lower box) sections of temperature, salinity, SSC and density over the study area during (A) the SEDMET-III (February 2008) and (B) the SEDMET-IV (June 2008) cruises. The location of the stations is shown in the left map of each box. 43

Figure 3.7. Time series of current speed during the study period (left boxes) and current components fields (right boxes) measured at 0.58 mab at the study sites (A1) and (A2) Be09-20m, (B1) and (B2) Be08-30m and (C1) and (C2) Be07-40m. 46

Figure 3.8. Times series of transformed across-shelf and along-shelf current components and the progressive vectors in those directions at (A1) and (A2) Be09-20m, (B1) and (B2) Be08-30m and (C1) and (C2) Be07-40m, respectively. Positive values are towards the NE in the along-shelf direction and offshore across the shelf. 49

Figure 3.9. Spectral analysis of across-shelf (left boxes) and along-shelf (right boxes) current components. (A1) and (A2) Be09-20m location, (B1) and (B2) Be08-30m location and (C1) and (C2) Be07-40m location. Note different scales for the Y axis. 50

Figure 4.1. (A) and (B) Mud content (%) and (C) and (D) median grain size of the superficial bottom sediment from Barcelona continental shelf. Red diamonds correspond to the surface sediment samples (grabs) taken in October 2007 monitoring survey (A and C) and April 2008 monitoring survey (B and D). The black lines correspond to the bathymetry of the study area. The maps projection is UTM zone 31N datum ED50. 56

Figure 4.2. Down-core logs of grain size, porosity and organic and inorganic carbon content of the studied sediment cores taken in the tripods transect in September 2007. See location at Figure 2.5. 57

Figure 4.3. Down-core logs of grain size, porosity and organic and inorganic carbon content of the studied sediment cores taken at 30 m and 40 m depth in September, 2007. From north to south. See location at Figure 2.5. 58

Figure 4.4. Temporal variability of (A) median grain size (d50 in mm) and (B) porosity between 0 and 10 cm depth of the cores sampled at 20, 30 and 40m water depth (Be09-20m, Be08-30m and Be07-40m sites) from figure top to bottom. 59

Figure 4.5. Bar graphs illustrate the time series of total mass fluxes of particulate matter for each sediment trap during the study period: (A) Be09-20m trap at 20 m water depth, (B) Be08-30m trap at 30 m depth and (C) Be07-40m trap at 40 m water depth. 60

Figure 4.6. Temporal variability of the median grain size (d50 in μm) of the trap samples collected at the tripod sites (Be09-20m, Be08-30m and Be07-40m) during the experiment. 61

Figure 4.7. Time series of (A) current shear velocity, (B) wave shear velocity, and (C) SSC at 20 m depth (Be09-20m site). 62

Figure 4.8. Time series of (A) current shear velocity, (B) wave shear velocity, and (C) SSC at 30 m depth (Be08-30m site). 63

Figure 4.9. Time series of (A) current shear velocity, (B) wave shear velocity, and (C) SSC at 40 m depth (Be07-40m site). 63

Figure 4.10. Temporal variability of the across-shelf critical shear stress estimated for median grain size of sediment samples from the inner-shelf off Barcelona. 66

Figure 5.1. Time series of the magnitude of sediment flux near the bottom at the three tripod locations. (A) Be09-20m at 20 m depth, (B) Be08-30m at 30 m depth and (C) Be07-40m at 40 m depth. Letters indicated the selected sediment fluxes events defined at site Be09-20m..... 69

Figure 5.2. Model evaluation of observed (blue) and calculated (red) SSC at 0.53 mab at sites (A) Be09-20m and (B) Be08-30m..... 71

Figure 5.3. Correlation forced to zero between observed data (after removing background levels) and model results: (A) and (B) along the study period and between December 2007 and February 2008 at Be09-20m and Be08-30m, respectively; and (C) and (D) for the December 2007 storm and at the peak of the event at Be09-20m site and Be08-30m site, respectively..... 73

Figure 5.4. Model profiles of SSC, current speed and components at Event H1 peak (A1 and A2) and along-shelf (B1 and B2) and across-shelf (C1 and C2) sediment fluxes during Event H1 at 20 m and 30 m water depth, respectively. * Reference level during the peak of Event H1. 76

Figure 5.5. Along-shelf and across-shelf cumulative sediment transport near the bottom for the recording period at (A) Be09-20m site, (B) Be08-30m site and (C) Be07-40m site. Positive values are towards the NE in the along-shelf direction and offshore, across the shelf. Letters inside the plots represent the selected events. 78

Figure 5.6. Seabed evolution at (A) Be09-20m and (B) Be08-30m sites. Letters inside the plots represent the selected events. 78

Figure 5.7. CTD profile of temperature and turbidity in June 2008 waters at the Be08-30m site. 81

Figure 6.1. Maps showing the surface distribution of the most important heavy metal contaminants in the fine fraction of the bottom sediment sampled in October 2007. Metal concentrations are expressed in ppm. 84

Figure 6.2. Temporal variability of heavy metals concentration in the Besòs River suspended sediment during the study period. 85

Figure 6.3.Temporal variability of heavy metals concentration in the settling particulate matter during the study period at A) Be09-20m site, B) Be08-30m site and C) Be07-40m site. 87

Figure 6.4.Temporal variability of heavy metals concentration in the bottom sediment during the study period at A) Be09-20m site, B) Be08-30m and C) Be07-40m. 88

List of Tables

Table 2.1. Available field data along the SEDMET project. * The last sample container did not closed and the sample period changed to 27 days. 20

Table 2.2. Timing and depths of sediment cores extractions. 24

Table 5.1. Near-bottom sediment fluxes in mg/m^{2}s at the tripod locations during the three surveys. 69

Table 5.2. Characteristics of sediment flux events at 20 m water depth from September 2007 to June 2008. Italic and bold numbers correspond to mean and maximum values, respectively. 70

Table 6.1. Mean concentration of heavy metals in the Besòs River suspended sediment and settling particulate matter and bottom sediment of the three tripod locations in September 2007. 85

Table 6.2. Enrichment Factor of the mean concentration of heavy metals in the Besòs River suspended sediment and settling particulate matter and bottom sediment of the three tripod locations in September 2007. 85

1 Introduction

1.1 Effects of floods and storms on the continental shelf

The importance of events like floods and storms on sediment delivery and reworking on river-dominated continental shelves has been recognized in many studies during the last few decades. Wave storms and river inputs have been found to be the dominant forcing mechanism of sediment flux in continental shelves (e.g. Drake and Cacchione, 1985; Sherwood et al., 1994; Ogston and Stemberg, 1999).

The delivery of sediment from rivers to inner shelves occurs as hypopycnal and hyperpycnal plumes, whose trajectories, the timing of the high discharge conditions and their relationship with physical oceanographic processes in the receiving basin can impact the fate of fluvial sediment in the marine environment. In large river systems as the Mississippi or the Amazon (Wright and Coleman, 1974; Nittrouer and DeMaster, 1987; Cacchione et al., 1995), the annual sediment load is delivered continuously to the shelf mainly as hypopycnal plumes. Periods of elevated water discharge last over 3-4 months and are associated with seasonal flooding. Due to the size of the drainage basin and the duration of the elevated discharge, there is little direct coupling between season floods and conditions in the coastal ocean. A fraction of the fine-grained sediments deposited over these months are transported to the distal portions of the dispersal system during the remainder of the year (Palinkas et al., 2005). Instead, in small rivers systems (drainage basins < 10^4 km^2), where most of the annual sediment load is discharged during episodic events, the short duration of floods may lead to a more important role of synoptic scale (days to weeks) meteorological forcing on the fate of the sediment discharged onto the continental shelf (Geyer et al., 2000).

In continental shelves controlled by tides and swells, the interactions of small rivers sediment supply and physical oceanographic energy have been defined as “oceanic storm” (Wheatcroft and Borgeld, 2000), “wet/dry storms” (Ogston et al., 2000) and “high/low concentration regimes” (Fan et al., 2004). The terms oceanic storm, wet storm and high concentration regime have been used to describe events of small mountainous river systems where flooding and sediment delivery often coincide with energetic oceanic conditions such as large waves and fast currents. The magnitude and distribution of sediment-suspension and transport events are controlled primarily by storms and episodic floods, the concurrence of which provides conditions for strong

across-shelf transport. Under these conditions, deposition in shallow water is limited and sediment can be widely dispersed, resulting in a seabed deposit that is located offshore and downstream of the river mouth (e.g. the Eel River - California, USA: Geyer et al., 2000). In this context, Geyer et al. (2000), Ogston et al. (2000) and Traykovski et al. (2000) showed that the river plumes formed by the Eel River did not provide the offshore transport of sediment required to reach the mid-shelf. Rather, the river deliver the sediment to the bottom boundary layer on the inner shelf, possibly leading to the formation of an ephemeral mud deposit, and then the transport of sediment into the mid-shelf and off-shelf must occur due to processes within the bottom boundary layer, including wave induced resuspension and the gravity-driven transport of dense suspensions.

However, recent studies presented a challenge to the preceding ideas suggesting that other factors are important in the fate of sediment in the shelf, particularly differences in shelf gradients and timing of floods and storms. In this context, although, gravity-driven flows have been reported off other small high-load river systems discharging into energetic shelves, such as the Fly River in Papua New Guinea or the Waiapu and Waipaoa rivers in New Zealand (Wright and Friedrichs, 2006), the pattern of flood and sedimentation seemed to vary for each system. Wadman and McNinch (2008) and Bever et al. (2011) showed that the Waipaoa River dispersal system differed from a paradigm developed for those small rivers because significant sediment deposition occurred in the nearshore during oceanic storms.

Conversely, small river floods that occur during the onset of relatively quiet physical conditions, when limited tidal currents and generally small significant wave heights result in limited bed shear stress for reworking and advection offshore, the discharged sediment can remain in shallow water close to the river mouth. Sediments that are deposited nearshore can be subsequently resuspended and transported to distal portions of the dispersal system when shear stresses become sufficiently high. The suspended load is then the main sediment transport mechanism resulting in sediment winnowing and erosion across the shelf and bypassing of a portion of the sediment over the shelf edge. Allison et al. (2000) inventoried the formation of a 1-3 cm thick annual flood deposit on the Atchafalaya (Louisiana – USA) inner shelf during the high river discharge period (March-April) that persisted for several months as a function of the relatively low energy of this margin. The subsequent winter resuspension events redistributed the sediment from shallower to deeper parts of the shelf.

In this context, the NW Mediterranean Sea is a micro-tidal, low-energy system. However, most of the fluvial systems that discharge into the NW Mediterranean Sea are smaller and have lower sediment and water supplies than “small” rivers around the world. In fact, “small” rivers around the world, such as the Eel River or the Atchafalaya River, have similar dimensions (water and sediment supplies) to “medium” rivers in the Mediterranean Sea. Therefore, the dominant of hydrodynamic forcing are likely to be different from that shelves that receive higher water and sediment discharges from rivers.

Floods and storm-generated wave effect on coastal sediment resuspension and transport in the shelf has been emphasized by several studies in “medium” to “large” Mediterranean Rivers systems on the Ebro margin (Jiménez et al., 1999; Puig et al., 2001; Guillén et al., 2002; Palanques et al., 2002) and on other margin of the north-western Mediterranean such as the Gulf of Lions (Ferré et al., 2005; Roussiez et al., 2005; Guillén et al., 2006; Ulses et al., 2008; Palanques et al., 2011). These studies revealed that the wave-induced bottom shear stress is generally the main stirring factor for sediment resuspension which is counteracted by the immersed density of the particles. The near-bottom suspended sediment concentration and wave-orbital velocity are generally correlated during storms that occur without relevant continental runoff. When wave-storm and floods occur simultaneously, the effect is combined and the results in terms of sediment dynamics are diverse depending on the intensity, duration and the sequence of events. Although along-shelf sediment fluxes are dominant during most of the time in NW Mediterranean continental shelves, such as the Ebro (Palanques et al., 2002), in the Gulf of Lions, extreme floods and storms can lead to an across- and along-shelf sediment transport about the same order of magnitude (Bourrin et al., 2008; Ulses et al., 2008; Palanques et al., 2011). However, the Gulf of Lions is probably a privileged area in the Mediterranean Sea for across-shelf export due to be more often affected by relatively stronger storms, dense shelf water cascading and the wind-induced cyclonic circulation (Durrieu de Madron et al., 2005; Palanques et al, 2006; Canals et al., 2006; Ogston et al., 2008).

Nonetheless, few studies have addressed sediment dynamics in continental shelves off a typical “small” Mediterranean river system (e.g. Têt River in the Gulf of Lions: Guillén et al., 2006; Bourrin et al., 2008). In these regard, Guillén at al. (2006) differentiated episodes of sediment dispersal in the inner shelf of the Têt River (Gulf of Lions) during “wet storms” when storm conditions coincided with local precipitation and elevated river discharge and “dry storms” when wave storms occur in the absence of significant river

discharge. The main differences between the wet and dry storms arose after the storm. This “small” Mediterranean river system allows the deposition of fine-grained particulate material near the river mouth during flood events as ephemeral layers. Their location above the storm wave base make them subjected to regular resuspension events that transport these fine materials further offshore.

Available 1D theoretical models can be useful for the study of the interactions between bottom sediments and combined wave and current flows in continental shelves (Wiberg et al., 1994; Harris and Wiberg, 1997; Wiberg et al., 2002; Traykovski et al., 2007; Ferré et al., 2010; Bever et al., 2011). These models use as input observational waves, currents and sediment characteristics to calculate suspended sediment profiles, velocity profiles and sediment transport (e.g. Wiberg and Smith, 1983; Wiberg et al., 1994; Harris and Wiberg, 2001). Most models of continental shelf transport have been applied over times for which detailed flow and sediment data are available, with implementations ranging from a single transport event to a number of months, and are fitted to measurements of flow velocity and water turbidity at different points above the bottom. Although, a reference concentration or flux boundary condition at the bottom is required to establish the concentration of sediment at each water level, Wiberg et al. (1994) argued that adding a limit on the depth in the bed from which sediment available for resuspension imposes a maximum suspended volume for each fraction. This surface sediment bottom layer within which bed sediment is “well mixed”, and can therefore reach the surface and be suspended, is referred as the “active layer depth”, and in the Wiberg et al. (1994) one-dimensional sediment transport model is used for a dynamic representation of the bed armoring.

In this context, the grain size of the available sediment is one of the crucial parameters for the application of models because it determines the bottom roughness, the critical conditions for resuspension and the presence of armoring. However, the inputs and changes of bottom sediment characteristics due to the presence of sediment sources are not taken into account in these models. A detailed bottom and suspended grain size characterization is required of any site, specially those close to a sediment source if an accurate estimation of the sediment fluxes is to be achieved, and therefore, an evaluation of the model performance in the study site.

In any case, the majority of open-coast studies directed towards understanding sediment dynamics have focused on the mid to outer parts of energetic shelves or in the inner shelves of medium-sized Mediterranean river systems. However, the

contribution of “small” Mediterranean river systems in fine-grained sediment dynamics is not well known. In this context, the amount of sediment captured in these regions, the time-scales of deposition-erosion and the patterns of sediment transport across the shelf in these typical Mediterranean systems are poorly understood.

1.2 The role of across-shelf gradients in sediment dynamics

On many shelves, including those off Barcelona and the Mediterranean coast, along-shelf transport often dominates sediment flux (Palanques et al., 2002). However, the largest gradients in sediment flux are across the shelf (Harris and Wiberg, 2002). These flux gradients may arise from spatial gradients in wave energy, current velocity, sediment properties and/or the proximity to sediment sources. The net deposition or erosion of sediments in the continental shelf is leaded for those cross-shelf divergences and convergences in sediment flux (Harris and Wiberg, 2002). Therefore, to adequately analyze sediment dynamics on the shelf, it is important to resolve the across shelf variation of sediment resuspension and dispersion processes (Wright et al., 1999) and the factors that may enhance or prevent these processes such as seabed sediment properties (e.g. Drake and Cacchione, 1989; Wiberg et al., 1994) or biological control (e.g. Wright et al., 1997).

For given surface wave conditions, the magnitude of the wave-generated bed shear stress decreases with increasing water depth. These shear stress gradients are present on any wave-dominated shelf, and they may produce gradients in suspended sediment flux that contribute to erosion and deposition across the shelf (Harris and Wiberg, 2002).

Further, Wright et al. (2002) concluded that pulsational gravity-induced transport of sediment suspended by waves is likely to be an important mode of across-shelf transport on the inner shelf of energetic sandy environments and the mid-shelf of energetic muddy environments.

The continental shelf may be also affected by intense currents near the bottom which can be able to transport particles resuspended by waves. The influence of local wind in shelf motions and sediment dynamics has been widely reported (e.g. Lentz et al., 1999; Geyer et al., 2000; Hendrickson and MacMahan, 2009). While in the mid-shelf the wind stress together with the Coriolis Force is the dominant across-shelf transport mechanism (Ekman transport – Lentz et al., 1999), on the inner shelf, as the water

depth decreases, the along-shelf surface stress becomes increasingly balanced by the bottom stress instead of the Coriolis force reducing Ekman surface boundary layer (Dever et al., 2006). Observations in some inner shelf regions along the US coast (Lentz et al., 1999; Fewings et al., 2008; Kirincich et al., 2009) found that alongshore winds are not sufficient mechanism in driving across-shelf exchange on the inner shelf. Hendrickson and MacMahan (2009) observed that when onshore winds (Sea breeze) occur the cross-shelf exchange of material is onshore near the surface and offshore near the sea bed but during the relaxation period (land breeze), the surface stress is not large enough and material is not transported cross-shore.

The importance of physical sediment properties such as particle size and water content on seabed erosion has long been recognized (e.g. Einsele et al., 1974; Amos et al., 1997, 2004; Stevens et al., 2007; Law et al., 2008) and how they can limit or enhance transport rates across the shelf (Wiberg et al., 1994; Amos et al., 1997; Harris and Wiberg, 2002; Roussiez et al., 2005; Guillén et al., 2006). In a heterogeneous bed, the wave and current shear stresses preferentially resuspend fine sediment leaving a coarser layer of sediment at the bed surface that prevents the flow from suspending underlying fine sediment. This process is referred to as “bed armoring” (Wiberg et al., 1994). In a consolidated muddy bed, cohesive strengths reduce erodibility (Amos et al., 1997, 2004). Bed texture on many shelves grades from coarser sediments on the inner shelf to fine-grained sediments over the middle and outer shelf. Seabed off of some rivers, including those of the NW Mediterranean Sea, exhibits a distinct mud deposit that can be traced to fluvial sources (Palanques and Diaz, 1994). Therefore, bed texture varies across the shelf and thereby their potential erodibility under storm conditions as well. However, previous observations documented the episodic nature of flood sediment deposition and the modification of seabed texture (grain size, sorting, grading) and therefore, the rates of suspended sediment flux on the continental shelf (e.g., Sommerfield and Nittrouer, 1999; Wheatcroft and Borgeld, 2000; Harris and Wiberg, 2002; Roussiez et al., 2005; Guillén et al., 2006; Bever et al., 2011). Those flood or storm event muddy beds with high water content are more easily resuspended and, having a lower settling velocity, are more likely to remain in suspension once mobilized.

Guillén et al. (2005) observed that sedimentation and erosion events produced changes in the grain size of the surface bottom sediment as well as along a 20-cm thick layer on the Ebro inner shelf. The main processes responsible for sediment changes were associated to sedimentation events caused by river floods or wave

storms, and selective winnowing of the sediment during low-energy conditions and probably by bioturbation of the bottom sediment. Roussiez et al. (2005) showed that in the Gulf of Lions (NW Mediterranean), fine-grained deposits from the rivers prodeltaic structures that according to their mean grain size mainly stand below the storm wave base, also exist above the storm wave limits due to an intense mud accumulation creating cohesive strengths that limit significantly post-deposit erosion. Further, Stevens et al. (2007) observed, along the 20 m isobath of the western Adriatic Sea, that during wintertime muddy sediment with lower porosity were more easily eroded due to the presence of sand-sized particles than those without it suggesting that the presence of sand-sized particles enhances erodibility.

One-dimensional models cannot capture spatial gradients in wave energy, current velocity or sediment properties and although the temporal and spatial (in the vertical) variability of the sediment grain size can be a major source of error in models like that which consider a moving active layer in a homogeneous sediment (Guillén et al., 2005), those models are useful to examine sediment resuspension in response to oceanographic forcing and to easily realize a sensitivity test of locals factors before applying more complex sediment transport models.

Therefore, the sediment physical properties (grain size and porosity), the mutual interaction between cohesive and non-cohesive sediment, the bioturbation of the bottom sediment as well as their variability in time and space, determined by the sediment dispersion system and sequence of flood and storm events, influence the amount of near-bottom suspended sediment concentration and therefore, the seabed sediment erosion, transport and deposition across the inner shelf.

1.3 Heavy metals in the littoral system

Flood and storm events redistribute not only sediment but also all the associated matter as well, such an organic matter and pollutants. A frequent group of contaminants in sediment of Mediterranean coastal systems and continental shelves are heavy metals, which are indicators of the impact of industrial and urban activities. In areas heavily affected by these activities, the irregular regime of rivers, storm sewers and outfalls along with the episodic character of many of the discharges made through them makes the contaminants to reach the sea in sporadic pulses that are difficult to predict and quantify.

Heavy metals have a high affinity with fine sediment particles (silt and clay) (Gibbs, 1973; Eisma, 1981, 1993) and therefore, the transport and fate of these contaminants are also associated with the transport and deposition of suspended particulate matter (SPM) discharged into the sea. The SPM and its associated contaminants are dispersed by mixing and advective processes. The ultimate sink is influenced by the prevailing short-term currents (Csandady, 1981). After sedimentation, contaminants can be resuspended either by bioturbation or by physical erosion. However, due to processes of particle aggregation, to the micro-tidal regime and the moderate wave energy of the Mediterranean Sea, an important part of sludge contaminated with heavy metals and waste is deposited near the coast, before being sufficiently diluted, generating anomalous contents on the seabed. Thus, the distribution of the heavy metals anomalies found in the sediments of some Mediterranean continental shelves show a maximum pattern located nearby contaminant discharge points, such as rivers and collectors, with a preferred distribution along the internal shelf near the shore (Frignani et al., 1978; Added et al., 1980; Modamio, 1986b; Alonso et al., 1986; Palanques and Diaz, 1994; Puig et al., 1999).

The dynamic of the contaminated sediment deposits is more complex nearby urban and industrial areas with a heavy anthropogenic pressure because the marine environment not only receives inputs from natural sources (rivers, wind) but also by artificial regulations systems (storm sewers and outfalls) some of them located offshore (sewage pipelines, or dump sites).

Nowadays, developed countries control the levels and address the problem of heavy metals pollution in the marine environment to estimate the economic and social impact of the different sources of contamination and to undertake preventive and corrective actions.

Numerous studies have demonstrated that the near-shore sediments from coastal areas near large industrial and urban areas are highly contaminated with heavy metals (Duedall et al. 1983; Krom et al. 1983) and some of this studies have detected heavy metals anthropogenic impact on the suspended particulate matter (SPM) and sediments discharged by the Besòs River (Cros and García-Rey, 1980; Modamio, 1986a; Palanques and Díaz, 1994; Palanques, 1994) and the Llobregat River (Modamio, 1986b; Puig et al., 1999; Palanques et al., 2008). Those authors showed that the inner part of the Barcelona continental shelf, in front of Barcelona, was one of the most polluted areas in the Mediterranean. This littoral system was affected by a

complex situation with a variety of pollution sources (rivers, sewage collectors, sewers, etc.) and a historic contamination dating from the early 20Th century at the Besòs prodeltaic deposit was reported (Palanques et al., 1998).

However, all these studies reported historical contamination or where carried out previously to the generalization of the implementation of corrective actions in industries and urban areas. A detailed spatial and temporal resolution study of heavy metals downward fluxes and bottom sediment pollution levels in the inner continental shelf of Barcelona have been carried out to understand the present day transfer and deposition of suspended particulate matter and associated heavy metal pollution across this contaminated area.

1.4 Study area

Barcelona is located in the NE coast of Spain in the NW Mediterranean Sea (Figure 1.1). The Barcelona continental shelf extents from the Foix Canyon (southern limit) to the Blanes Canyon (northern limit). It is a narrow shelf (6 – 20 km) consisting on an inner, middle and outer regions separated by the 30 – 40 and the 80 m isobaths, respectively, with the shelf break at 110 – 120 m depth (ITGE, 1989).

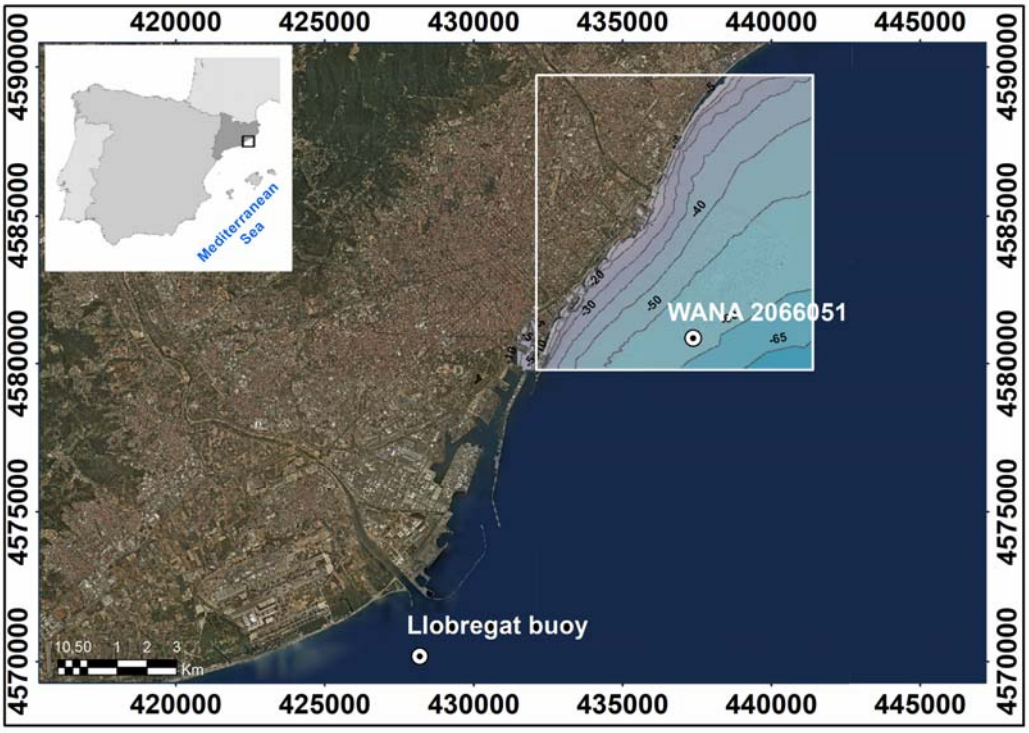

Figure 1.1. Map of the Barcelona continental shelf showing the study area and the wave data points used in this project. The map projection is UTM zone 31N datum ED50.

Our study focused on the Besòs River and the adjacent part of the Barcelona inner continental shelf (NW Mediterranean Sea) (Figure 1.1). The Llobregat and Besòs rivers discharges represent the main sediment supply to this region of the Barcelona continental shelf. The suspended load in the lower part of the Besòs river is variable and relatively high (Palanques, 1994). These values are usual for a short river with mountainous basin affected seasonally by heavy rains. The Besòs river basin has an area of 1029 km^2 and its main course flows north-south along 52 km from the Catalan Coastal Ranges to the Mediterranean Sea. The Besòs River annual sediment discharge has been averaged in 15000 T/year which forms a delta of 8.3 km^2 with a coastal development of 7.6 km shifted south-westwards from the river mouth as a result of the dominant littoral circulation (Liquete et al., 2007). Mean water discharge between 1968 and 2008 was 6.8 m^3/s at Santa Coloma de Gramenet gauging station, 2.8 km far from the water mouth (433347.3; 4589242.6; UTM zone 31N; datum ED50), where the maximum water discharge of 270 m^3/s was measured in May 9th 1991 (Liquete et al., 2009).

In this region the tidal range is lower than 0.2 m, and the waves are the main hydrodynamic forcing acting on the continental shelf. Statistical analysis of wave conditions in the region from 1984 to 2004 shows mean significant wave height values (Hs) of 0.70 m, with Hs maxima of 4.61, maximum wave heights of 7.80 m and averaged mean period of 4.29 s (Gómez et al., 2005). Storms occur mainly from October to April and the most important ones are those coming from the East, due to the combination of the coast orientation and the Mediterranean climate. The wind regime is characterized by small inter-annual variability (Font, 1990). The predominant winds come from the north and northwest, primarily during autumn and winter, where its energy concentrated in low frequencies associated with synoptic passage of low-pressure systems, which in the Catalan Sea corresponds to 3-12 days. In summer and spring, the dominant winds are southwesterly, with the dominant frequencies being the synoptic and diurnal (sea breeze) bands (Font, 1990). Grifoll et al. (2012) identified that, in the Catalan Sea, the variability of the along-shelf current flow is influenced basically by local wind-forcing and sea level gradients, and also by water column stratification and the influence of rapid pulses of river discharge.

Sediment resuspension in the Western Mediterranean Sea is caused primarily by the wave-storm activity when wave heights and periods increase significantly (Jiménez et al., 1999; Puig et al., 2001; Guillén et al., 2002; Palanques et al. 2002; Ferré et al., 2005). Guillén et al. (2002) showed that sediment resuspension, in response to storm

waves on the Ebro area is mainly effective on the inner-shelf region. In addition, Puig et al. (2001) reported that strong north-eastern wave-storm (Hs>4.5 m and Ts>11 s) could also resuspend fine-grained sediments from the mid-shelf mud-belt, at 60 m depth, and transported off-shelf through the bottom nepheloid layer. The surface sediment distribution and the location of the prodeltaic mud deposits were observed to be coherent with the hydrodynamic processes and induced near-bottom sediment fluxes. Palanques et al. (2002) reported that on the Ebro shelf, fine sediment accumulated mainly on the mid-shelf, where the lowest mean combined wave-current shear stresses occurred, whereas on the inner shelf some mud accumulated, but was frequently resuspended due to the high combined wave-current shear stresses occurring on that region. On the Barcelona continental shelf, sediment tends to be transported south-westward due to the action of the dominant littoral drift and the Northern Current, a geostrophic current that flows over the continental slope and shows episodic incursions on the continental shelf and some permanent mesoscale features (Font el al., 1995; Flexas et al., 2002; Rubio et al., 2005). Fine-grained suspended sediment derived from rivers plumes or storms resuspension can be transferred to the slope and beyond through permanent nepheloid layers (Puig and Palanques, 1998; Palanques et al., 2008).

Liquete et al. (2007) recognized two main morphosedimentary domains (Figure 1.2): a modern, river-influenced area, and a relict sediment depleted area. The modern, river-influenced shelf includes the Llobregat and Besòs adjacent prodeltas, which represents the main Holocene depocenter in the area. The finest fluvial material is preferentially accumulated along-shelf, south-westwards, from both river mouths as a result of the dominant littoral circulation.

The sediment distribution has the same characteristics of other Mediterranean shelves that receive significant discharges by rivers (Palanques et al 1990; Diaz et al., 1994; Palanques and Diaz, 1994; Puig et al., 1999; Liquete et al., 2010): (1) medium well sorted sand (2 phi) in less than 15 to 20 m water depth; (2) mostly silt and clay (7 - 8 phi) distributed to the south from the mouth of the Besòs River between isobaths of 20 and 60 m; and (3) biogenic relict silty sand (3 to 4 phi), which covers the shelf between 60 m depth until the continental slope.

Barcelona city has approximately 13 km of coastline containing the city harbor, in the southernmost part of the city, three marinas, some storm sewers and more than three kilometers of beaches. The northern area of the beaches had almost disappeared by

the 1980s due to the invasion of urban and industrial areas to the harbor and marinas proliferation and to the decrease in the input of sediments to the coastal zone. The current beaches were created as part of the renewal plan that took place for the 1992 Olympic Games, when the old industrial infrastructures were demolished to create the Olympic Village (now transformed into a residential district) and new beaches were built north and south of the Olympic Marina.

In 1979, the Barcelona-Besòs water treatment plant was built near the Besòs River mouth, which discharged sludge waste through a 4-km-long pipeline at 56 m depth until the 1990s. Nearshore the pipe was placed within up to 2 m deep narrow trench, while seaward the tube emerged progressively till lying on the sea floor. Leakages from the Besòs pipeline resulted in several mound-shaped features along its path (Liquete et al., 2007). This pipeline was taken away and a new one was built. The new one, following the environmental regulations, only discharge water treated from the Barcelona-Besòs water treatment plant.

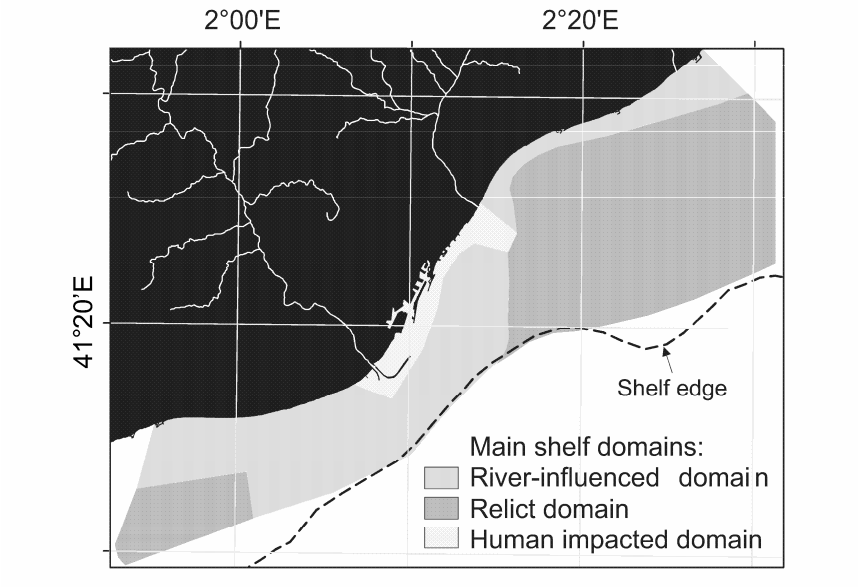

Figure 1.2. Sketch showing the general zonation of the Barcelona shelf. Map projection is UTM 31N WGS84. From Liquete et al. (2007).

The continental shelf in front of the city of Barcelona is an example of a coastal environment heavily affected by human action. This shelf receives the impact of heavy metals contamination discharged from the Besòs River, the water treatment plant and the old sewers of the city. In addition, present day storm sewers and many human infrastructures and activities have major impacts on sediment dispersal patterns that

are reflected on the seafloor cover, which is largely reworked by dredging, anchoring, and trawling activities (Liquete et al. 2007, 2010; Palanques et al., 2009).

The distribution of heavy metal pollution associated with suspended particulate matter on the Barcelona continental shelf was addressed by Palanques (1994) and Palanques et al. (1998) that reported high levels of Pb, Cr, Cu, Cd and Ni in the suspended particulate matter (SPM) and the surface sediments on the inner shelf of this Mediterranean area. The Besòs River, the Bogatell sewer and the sewage sludge produced in the Barcelona-Besòs wastewater treatment plant were identified as the main sources of heavy metal pollution in the continental shelf of Barcelona. Palanques and Díaz (1994) also reported anthropogenic heavy metal pollution associated to the sediment fine fraction (clay and silt) of the Besòs prodelta shallower than 50 m, between the river mouth and about 10 km southward. These authors showed that, in this continental shelf, the highest values of heavy metals were located around the Besòs river and the Bogatell sewer mouths and in the mound-shaped features along the sewage pipeline path (Figure 1.3) where the silt + clay content was higher than 90 %. Heavy metals pollution decreased from that point southward. In the outer shelf, contamination by heavy metals was relatively low, except at the mouth of the old pipeline of the water treatment plant (56 m depth) in the transitional zone between the prodeltaic sediments and the relict sand of the outer shelf (Palanques and Diaz, 1994).

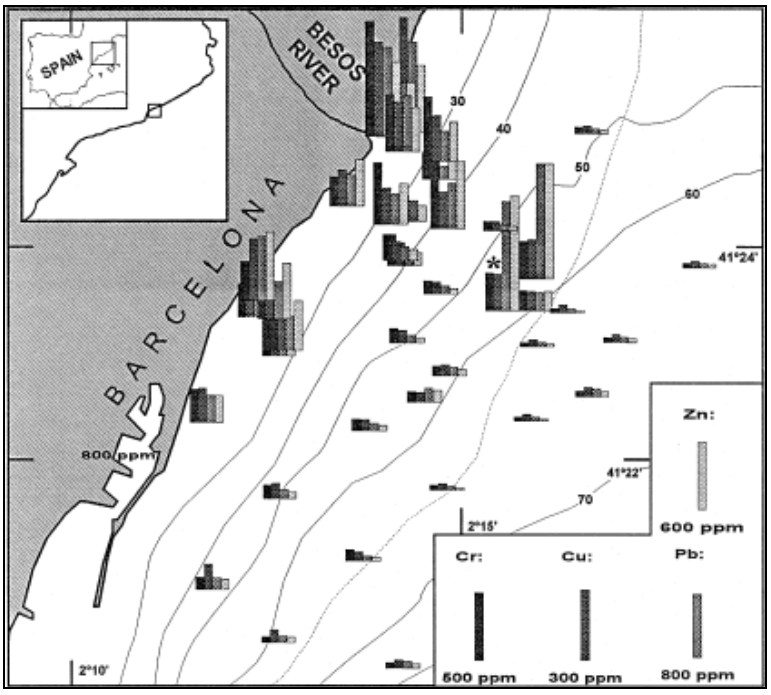

Figure 1.3. Distribution of surface contaminated sediments by heavy metals on the continental shelf of Barcelona. * Pipeline Mouth of the treatment plant. From Palanques et al. (1998).

Nowadays, the corrective actions that have been implemented in industries and urban areas in the Besòs basin should have been produce a decrease in the heavy metals contamination levels discharged by the Besòs River and the waste treatment plant pipeline, which is only discharging water waste.

1.5 Main objectives

The present thesis project involves studying the dynamics of sediments and associated heavy metals across the inner continental shelf off the Besòs River (Barcelona), and in particular determining the effect of floods and storms in a littoral system affected by industrial and urban activities.

The continental shelf off Barcelona has been previously studied in terms of dispersion processes (Font, 1990; Grifoll et al., 2012), modern and relict sedimentary features (Liquete et al., 2007, 2010), sediment accumulation rates (Sanchez-Cabeza et al., 1999) and heavy metal contamination (e.g. Palanques and Diaz, 1993; Palanques, 1994; Palanques et al., 1998, 2002). These studies provided a first interpretation of the inner-shelf motions and sediment properties that can support studies of sediment transport dynamics and associated contaminants in this area. However, these authors also reported the need of investigation in terms of across-shelf dynamics of sediments and associated heavy metal contamination.

In addition, the study of sediment dynamics across the shelf and the quantification of sediment transport in a micro-tidal inner shelf, influenced by a “small” Mediterranean river and moderate wave energy is necessary to complete the knowledge of the fate of sediment from rivers into oceans and how the particles are dispersed and accumulated across different sedimentary environments of the continental margins.

Particularly, the aims of the study are: 1) to characterize the discharges of sediment and associated heavy metals from the Besòs River and to determine the conditions in which they occur; 2) To quantify the sediment fluxes and associated heavy metals; 3) To study the transport and resuspension processes in the Besòs system sedimentary deposit addressing the factors controlling sediments dynamics across the inner shelf and; 4) To obtain valuable data for applying numerical models of sediment dynamics in the study area. In all these aims, special emphasis is placed on storm events, heavy rainfalls and fast currents.

2 Methods

2.1 Field work and instrumentation

During the SEDMET Project, several oceanographic surveys were carried out to obtain a variety of data: to register vertical hydrographical profiles (temperature, salinity and turbidity); to record time series of physical parameters (currents, salinity, temperature, turbidity and seabed variation) by deploying oceanographic equipment; and to take sediment samples (short cores and Van Veen grabs) and suspended and downward particulate matter from water samples and sediment traps for further sedimentological and geochemical analysis.

Four SEDMET cruises were carried out between September 2007 and June 2008 in the inner continental shelf off Barcelona (Figure 1.1) aboard of the R/V *García del Cid* of the *Consejo Superior de Investigaciones Científicas* and the *R/V Sarmiento de Gamboa* of the *Ministerio de Ciencia y Tecnologia*:

The SEDMET-I cruise was carried out between the 27th and 29th of September of 2007, at the beginning of the autumn season which is the most energetic season of the year in this Mediterranean region. The objective of this cruise was to perform the hydrographic profiles to characterize the water column at this time of the year which corresponded to beginning of the study period, to deploy the equipment and to take representative samples of the bottom sediment.

The SEDMET-II cruise (28^{th} – 30^{th} of November 2007) was scheduled for the end of the energetic season in order to recover the data from the equipment and take some representative samples of the bottom sediment and the hydrographic conditions at end of autumn and beginning of winter.

During the SEDMET-III (28^{th} and 29^{th} of February of 2008), the maintenance tasks of the deployed equipment was performed, the bottom sediment was sampled and the hydrographic structure was recorded.

Finally, during SEDMET-IV (19^{th} of June 2008) the equipment was recovered and the bottom sediment sampling and the hydrographic profiles were performed to characterize the area at the end of the spring season which corresponded to the end of the study period.

In addition, monitoring monthly oceanographic surveys were carried out along the study period. The objective of these surveys was to register vertical hydrographical profiles (temperature, salinity and turbidity); to collect suspended particulate matter samples (SPM) from water samples; and to take sediment samples (Van Veen grabs) in order to track the study area and to calibrate some equipment during the deployments period.

Suspended sediment matter samples were also collected from the Besòs River close to the water discharge gauging located nearby the river mouth. The river sampling period was scheduled to one month interval, approximately.

The locations of the recording and sampling sites are shown in the following sections.

2.1.1 Benthic tripods

The use of benthic tripods coupled with numerous sensors for the study of the hydrodynamic and sedimentary processes in coastal seas has been widely applied. Investigations from benthic tripods over the past fifty years have had a major impact on scientific knowledge: 1) validation and application of boundary-layer and sediment transport theory in the sea; 2) documentation and identification of the range of physical processes and associated sediment transport on continental shelves; and 3) data input for development and evaluation of numerical models of shelf circulation and sedimentology (Sternberg, 2005).

In addition, the use of these instrumented tripod coupled with an altimeter to observe event-scale sedimentary dynamics was applied as a new approach to quantify changes in seabed level (erosion or accumulation) that occur during discrete resuspension or deposition events in muddy inner-shelf shelves (Guillén et al., 2006; Palinkas et al., 2010). These studies showed that the altimeter can be used to directly observe changes in sea bed on a muddy inner shelf and allowed quantification of the net seabed change during short-lived resuspension events that are difficult to observe with other methods.

Three benthic tripods were deployed in the Barcelona continental shelf at 20, 30 and 40 m water depth (Be09, Be08 and Be07, respectively, Figure 2.1) during the field cruises SEDMET to evaluate vertical and horizontal sedimentary fluxes and their driving forcing conditions in the inner northern Barcelona continental shelf.

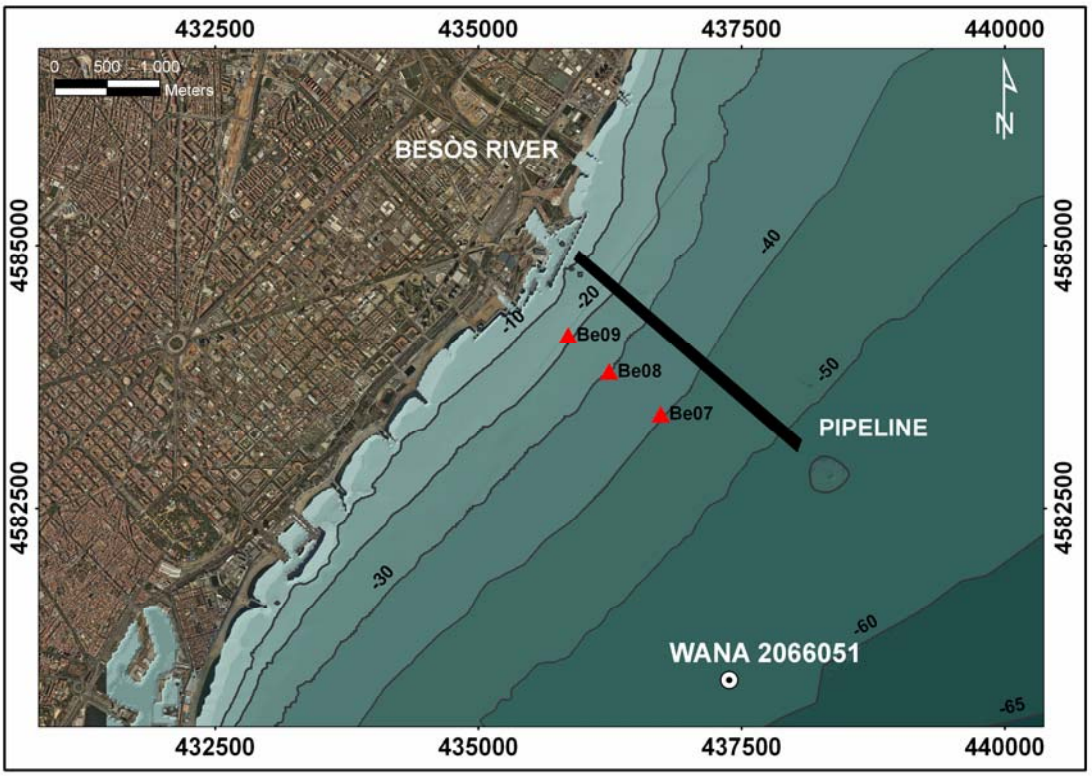

Figure 2.1. Position of the benthic tripods deployed: Be09 at 20 m water depth, Be08 at 30 m depth and Be07 at 40 m depth. The map projection is UTM zone 31N datum ED50.

Each tripod was equipped with several sensors and instruments (Figure 2.2):

- An Aanderaa Doppler current meter (RCM-9) that measured current speed and direction every 20 minutes. The RCM-9 uses the Doppler Shift principle as the basis for its measurements. The sensor transmits acoustic pulses of 2 MHz into the water in sequence. As the sound propagates, small particles or air bubbles in the water reflect a portion of the energy. The black-scattered energy is picked up by the transducers and analyzed. A microprocessor computes vector averages current speed and direction over the last sampling interval in an area of 0.5 – 2 m from the instrument. The sensor was placed at 0.58 meters above bottom (mab).

- Together with the current speed and direction, RCM units are coupled with a pressure sensor set at a range of 0-20 MPa for the two shallower tripods (20 and 30 m water depth) and the deepest one (40 m water depth) set at a 0-700 KPa range, a temperature sensor (Low range: 9.3 – 33.4 C) and an inductive cell conductivity sensor (0 – 74 mS). In addition, RCM-9 models were also equipped with two Aanderaa optical back-scatter turbidimeters calibrated with Formazin into two different sensitivity range 0 – 20 NTU (Nephelometric

Turbidity Unit) for normal hydrodynamic conditions, and 0 – 500 NTU for storm conditions. These sensors were at 0.53 meters above bottom (mab).

Figure 2.2. Picture of the benthic tripod used in this project.

- An NKE ALTUS 2 Hz altimeter that measured the seabed position and water depth every 15 minutes. Altus is a high frequency acoustic submersible recording altimeter. It is based on a 2 MHz echo sounder which transducer was located on a light frame at 0.22 cm from the bed. This frame avoids any sediment scouring in the measurement area. A separate container includes altimeter electronics, data logger, pressure sensor and energy.

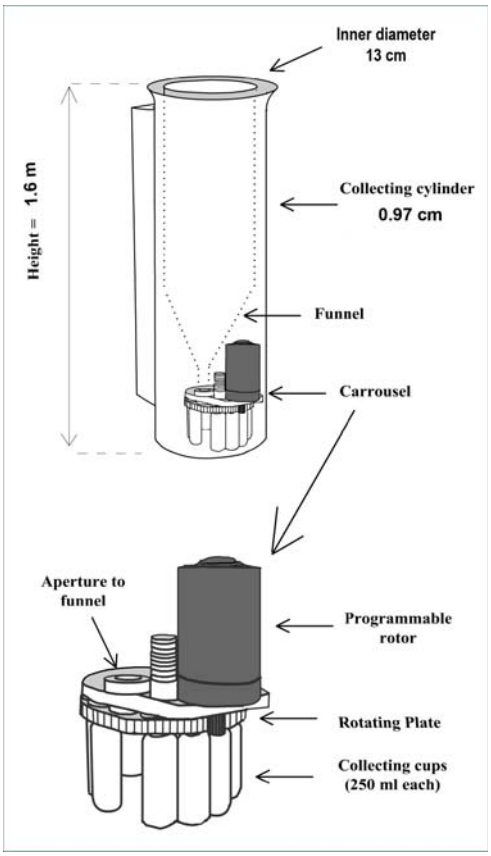

Figure 2.3. Schematic drawing of the sediment trap used in this study.

- A sediment trap which incorporates a carousel with 12 rotary collectors for sampling settling particulate matter (Figure 2.3). Sediment traps are tools for studying downward particle composition and fluxes to the seafloor over periods of weeks to years. The trap collecting hull is mainly cylindrical with a height of 97 cm and an inner diameter of 13 cm with an aspect ratio (height/diameter) of 7.5. Many trap-users (see Reynolds et al., 1980) have chosen an aspect ratio of either 3.0 or 5.0 as the minimum value to prevent particle resuspension in traps. In fact, the minimum trap aspect ratio to prevent particle resuspension can be even lower and depends on the bottom shear stress inside the trap (and thus, on R) and on the particles collected (Butman et al. 1986). The lower part is conical and ends in a connecting cylinder. The carousel (Technicap model PPS3) is controlled by a programmable motor that allow the presetting of variable sampling intervals for each of the 12 sample tubes (Heussner et al., 1990). During the experiment, the sampling interval was set at 5 days for the first deployment (SEDMET-I) and 7.5 days for the second and the third deployment (SEDMET-II and SEDMET-III), depending on the recording period (2 and 3 months, respectively), and the total sampling period was from October 2007 until June 2008. The top of the trap remained at 1.51 mab.

During the tripods recording period, there were some problems in the functioning and the localization of the instruments and some of the data and samples were not recovered. Table 2.1 shows a recompilation of all the data available along the study period. During SEDMET-I and SEDMET-II the three tripods were deployed and all the sensors recorded data for the entire deployment period, except for the altimeter sensors. However, at SEDMET-III cruise only the tripods located at Be09 and Be08 (20 and 30 m isobaths) were recovered, so for the SEDMET-III and SEDMET-IV only data from those locations was recorded. In addition, the current meter installed at 30 m water depth broke down during the SEDMET-III recording period (at the end of March 2008), no data was recovered from this time to the end of the study period.

		SEDMET-I (27/09/07)	SEDMET-II (28/11/07)	SEDMET-III (28/02/08)	SEDMET-IV (19/06/08)
Be09 (20 m)	CURRENT METERS	DEPLOYMENT	Ok	Ok	Ok
	PRESSURE		Ok	Ok	Ok
	TEMPERATURE		Ok	Ok	Ok
	TURBIDITY (0-20 NTU range)		Ok	Ok	Ok
	TURBIDITY (0-500 NTU range)		Ok	Ok	Ok
	SALINITY		Ok	Ok	Ok
	ALTIMETER (Seabed Variation)		Failed	Ok	Ok
	SEDIMENT TRAP SAMPLES		12	12	12*
Be08 (30 m)	CURRENT METERS		Ok	Ok	Ok
	PRESSURE		Ok	Ok	Ok
	TEMPERATURE		Ok	Ok	Ok
	TURBIDITY (0-20 NTU range)		Ok	Ok	Ok
	TURBIDITY (0-500 NTU range)		Ok	Ok	Ok
	CONDUCTIVITY		Ok	Ok	Ok
	ALTIMETER (Seabed Variation)		Ok	Ok	Ok
	SEDIMENT TRAP SAMPLES		12	12	Failed
Be07 (40 m)	CURRENT METERS		Ok	TRIPOD NOT FOUND	NONE
	PRESSURE		Ok		
	TEMPERATURE		Ok		
	TURBIDITY (0-20 NTU range)		Ok		
	TURBIDITY (0-500 NTU range)		Ok		
	CONDUCTIVITY		Ok		
	ALTIMETER (Seabed Variation)		Ok		
	SEDIMENT TRAP SAMPLES		12		

Table 2.1. Available field data along the SEDMET project. * The last sample container did not closed and the sample period changed to 27 days.

2.1.2 Hydrographical and meteorological data

In order to characterize the hydrographic and nepheloid structure in the study area, 17 vertical profiles distributed in four hydrographic transects were made during the SEDMET oceanographic surveys. The hydrographic profiles along the tripods transect (Be10, Be09, Be08, Be07 and Be06, Figure 2.4) were made using a Sea-Bird SBE 9 CTD. Selected hydrographic sections along and across the inner Barcelona continental shelf were represented, using the "Ocean Data View" software (Schlitzer, 2003). Along this transect, water samples were collected during each cast near the bottom and at the surface by means of twelve-liter Niskin bottles mounted on a General Oceanics CTD rosette sampler. The remaining hydrographic stations (see Figure 2.4 for location) were made using a Sea-Bird SBE 25 CTD. Both CTD were coupled with a Seapoint turbidimeter. Data collection was carried out in one day in order to obtain a quasi-synoptic picture of the hydrographic and nepheloid structures.

In addition, during the monthly monitoring surveys, hydrographic profiles were performed at the tripod sites using the Sea-Bird SBE 25 CTD coupled with a Seapoint turbidimeter. Water samples were collected from the deepest tripod site (Be07 site, Figure 2.4) with a Niskin bottle mounted on the winch used with the CTD.

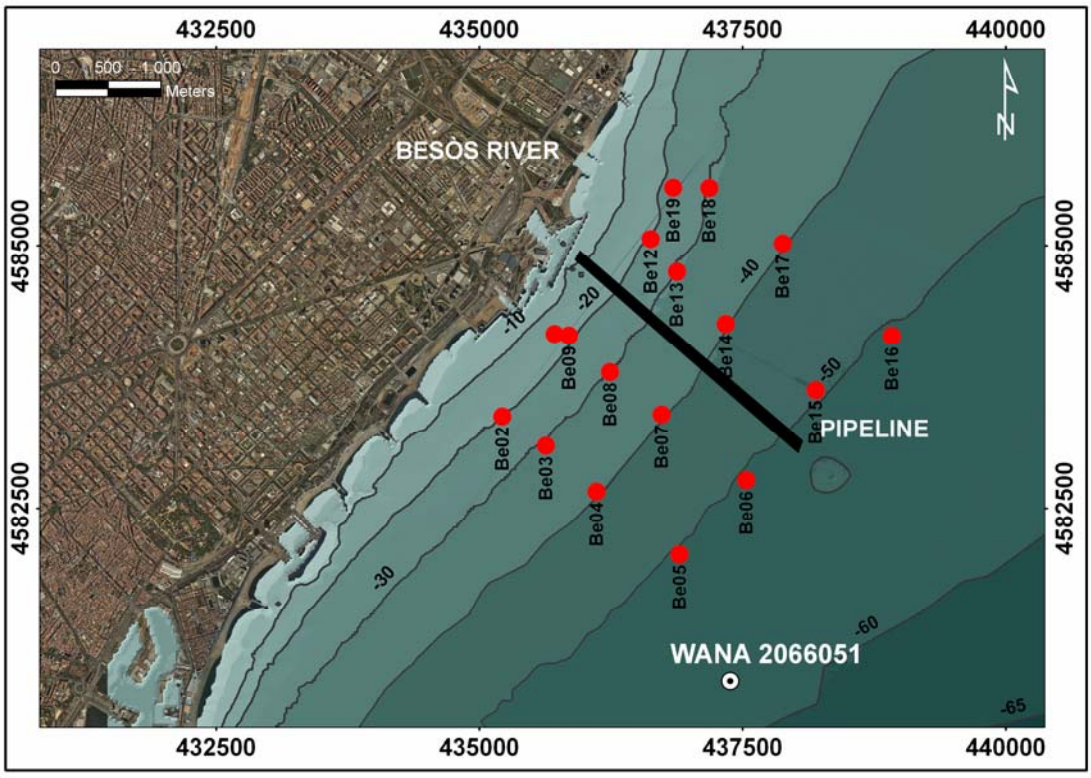

Figure 2.4. Location of hydrographic stations during SEDMET surveys. WANA 2066051 is the model point of oceanographic data and the text annotation BESÒS RIVER marks the mouth of

the river. The thick black line is the old pipeline from the water waste plant located near the river mouth. The map projection is UTM zone 31N datum ED50.

During the surveys, water samples were filtered through three different types of filters to determine suspended particulate matter concentration and heavy metals concentration (see section 2.2).

Wave measurement from the Llobregat buoy (*XIOM, www.xiom.cat*) were used as wave conditions during the study period. This buoy is located at a depth of 45 m (417205.22; 4542537.95; UTM zone 31N; datum ED50, Figure 1.1) and has been directional since 2004, recording data every hour. Interruptions in the buoy time series were filled in with data from the WANA model (node 2066051: 437376.97; 4580862.89; UTM zone 31N; datum ED50; 50m water depth, Figure 1.1), which provides directional wave information every three hours. The WANA data has been computed by the Spanish National Institute of Meteorology using the HIRLAM and WAM numerical model since 1991 (*Spanish Port Authority, www.puertos.es*). Wave height and period data from the WANA model were calibrated through linear regression using the buoy observations from October 2001 to December 2008 (Sancho-García et al., 2012).

The Besòs river daily discharge was obtained from the *Agència Catalana de l'Aigua* (*Generalitat de Catalunya*) water discharge gauging located at Santa Coloma de Gramenet gauging station, 2.8 km from the Besòs river mouth (433347.3; 4589242.6; UTM zone 31N; datum ED50).

2.1.3 Bottom sediment sampling

During the four SEDMET cruises, 20 sediments short cores were collected from the northern Barcelona continental shelf (see Figure 2.5 for location): 8 during SEDMET-I, 3 during SEDMET-II and SEDMET-III (Be07, Be08 and Be09) and 6 during SEDMET-IV (Be07, Be08, Be09, Be21, Be03 and Be22). The timing and depths of core extractions are shown in Table 2.2.

In addition, 19 sediment grabs were taken in the monthly monitoring survey carried out from approximately the beginning of the study period in October 2007 and in April 2008 (Figure 2.7). The samples were stored at 4 degrees Celsius for further laboratory analysis (see section 2.2).

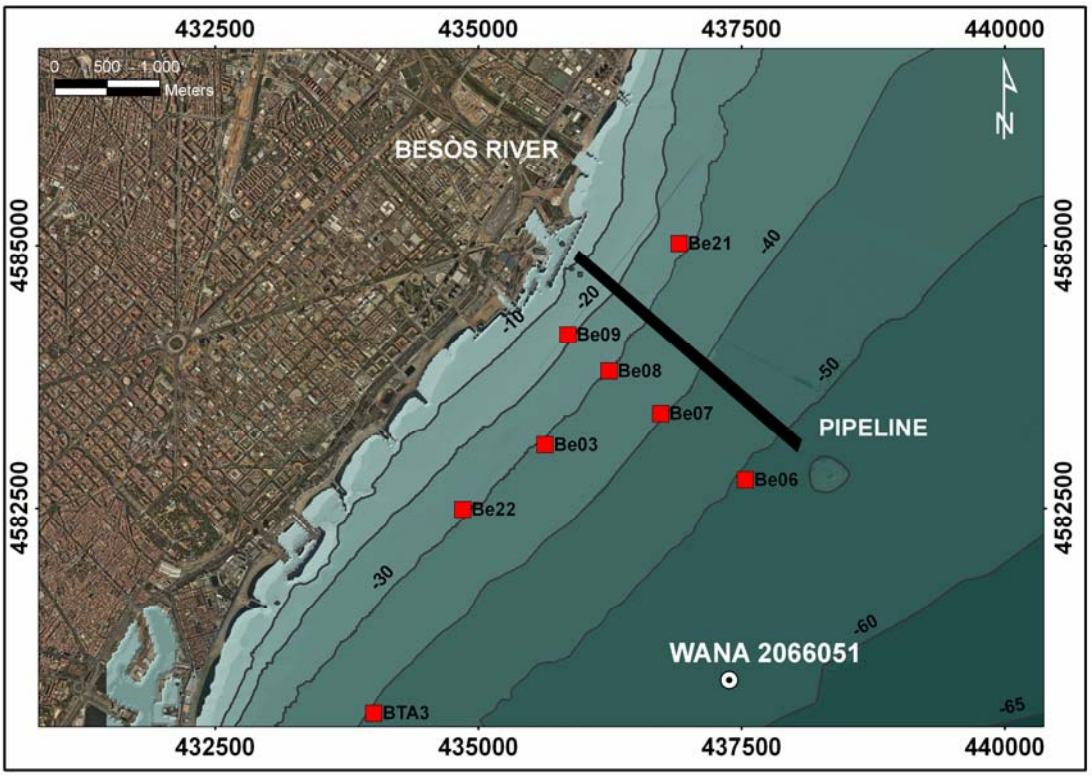

Figure 2.5. Location of sediment cores sampling stations during SEDMET surveys. WANA 2066051 is the model point of oceanographic data and the text annotation BESÒS RIVER marks the mouth of the river. The rectangle is the old pipeline from the water waste plant located near the river mouth. The map projection is UTM zone 31N datum ED50.

A small box corer with one acrylic cylindrical core tube (inner diameter = 135 mm) was used (Figure 2.6). This corer is designed to obtain an undisturbed sediment core with a maximum length of 30 cm by plunging through the water column and penetrate by striking the bottom with velocity. The corer is lowered vertically until it impacts with the seabed. While pulling the corer out of the sediment a spade swings underneath the sample to prevent loss. When hauled back onboard, the spade is under the box.

The cores were sliced in 1 cm thick intervals aboard the vessel and stored at 4 degrees Celsius for further laboratory analysis (see section 2.2).

Cruise	Core identifier	Depth (m)	Core length (cm)
SEDMET-I (09/28/07)	BTA3	43.0	30.0
	Be03	35.1	28.0
	Be06	53.0	29.0
	Be07	42.4	30.0
	Be08	33.6	30.0
	Be09	23.4	21.0
	Be21	28.0	26.0
	Be22	31.1	26.0
SEDMET-II (11/29/07)	Be07	41.2	13.0
	Be08	30.0	19.0
	Be09	23.3	8.0
SEDMET-III (02/28/08)	Be07	42.6	27.0
	Be08	31.6	10.0
	Be09	26.1	23.0
SEDMET-IV (06/19/08)	Be03	35.1	10.0
	Be07	43.0	10.0
	Be08	34.4	10.0
	Be09	20.4	10.0
	Be21	28.0	10.0
	Be22	31.1	10.0

Table 2.2. Timing and depths of sediment cores extractions.

Figure 2.6. Picture of the box corer used in this project (model Haps corer by KC-Denmark).

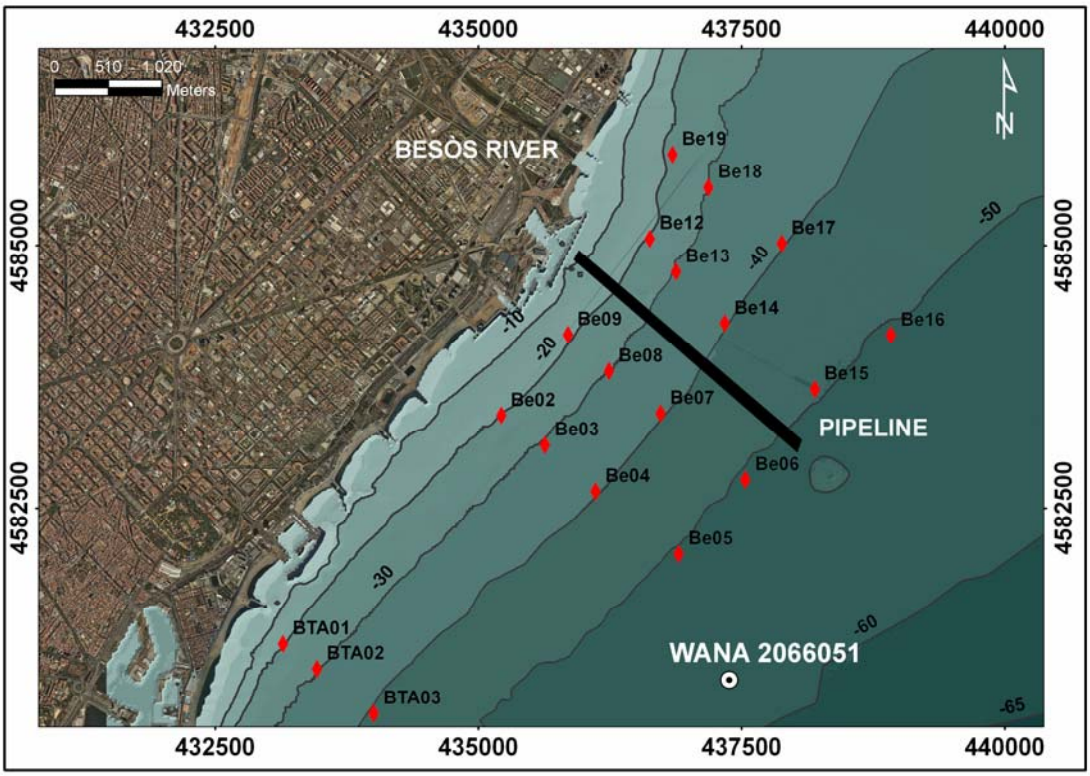

Figure 2.7. Sediment grabs sampling locations in the study area during two monthly monitoring surveys. WANA 2066051 is the model point of oceanographic data and the text annotation BESÒS RIVER marks the mouth of the river. The thick black line is the old pipeline from the water waste plant located near the river mouth. The map projection is UTM zone 31N datum ED50.

The Van Veen grab, used in this project, is a lightweight sampler designed to take large samples in soft bottoms. The weighted jaws, chain suspension, and doors and screens allow flow-through during lowering to the bottom and assure vertical descent where strong underwater currents exist. The relatively large surface area and the strong closing mechanism allow the jaws to excavate relatively undisturbed sediments.

2.2 Laboratory Works

2.2.1 Preparation and treatment of sediment traps samples

Before trap deployments, the sample tubes were rinsed and filled with a 5% formalin solution prepared from formaldehyde 40% mixed with 0.45 µm filtered seawater to avoid the degradation of organic matter in the trapped sediment. The solution was buffered (pH = 7.5 – 8) with sodium borate. After recovery of the sediment traps, pH was checked and the tubes were kept at 4º Celsius in the dark, until they were processed in the laboratory.

Before the sample treatment, two kinds of filters were prepared: 47 mm diameter glass microfibre Whatmann GF/F filter of approximately 0.45 µm mesh (GFF) and 47 mm, 0.45 µm mesh nitro-cellulose white HAWP Millipore filter (NF). Before its use, the GFF were rinsed with distilled water and then placed for 24 hours in an oven at 550º Celsius allowing those to cool for another 24 h. The NF filters were rinsed with distilled water and dried at 40º Celsius for 24 h in a desiccation bowl.

The samples were treated following the procedures described by Heussner et al. (1990). Once all particles were completely settled after a period of repose and the solution above the material was crystal clear, the supernatant was gently pumped, its pH checked, and stored at 4º Celsius. Swimmers (those organism deemed to have actively entered the trap) were removed from the samples to avoid errors in the measured fluxes. They were separated by wet-sieving through a 1 mm nylon mesh with filtered sea water, and stored in 5% formalin solution for further analysis. Large aggregates were supposed to be part of the passive flux and hence returned to the samples.

The sieved material was poured in a 2000 ml flask and filled with 0.45 µm filtered seawater. The flask was placed in a shaking table in order to keep the material suspended and homogenized to guarantee equality between aliquots. The whole sample was equally fractioned and distributed with a peristaltic pump (Jencons Ltd) and a robot “xy” arm into several flasks.

Through successive partitions, the original sample was divided in order to obtain fractions of about 50 mg (dry weight) for geochemical analysis. Other fractions were also obtained and stored at 4º Celsius in formalin solution for further grain size

analysis. Subsamples for total and organic carbon and also Mercury concentrations were filtered onto GFF filters, while those for major and trace heavy metals analysis were filtered onto NF filters. The filters with the sample were dried to constant weight at 40º Celsius and then placed for 24 h in a desiccation bowl.

2.2.2 Treatment of sediment cores and grabs

The acrylic tubes containing the sediment cores were placed in an extruding device that works as a piston pushing the sediment upward, allowing subsampling the cores at desired intervals. They were split into 1 cm-slices, and each slice sealed in a plastic bag and frozen at -14º Celsius before treatment.

Sediment grabs also were sealed in a plastic bag and frozen at -14º Celsius just after their collection and before treatment.

Core samples and grabs were dried on a stove at 40º Celsius until constant weight was attained.

Water contents (% of total weight) and moisture (% of dry weight) were calculated from non-homogenized samples that were weighed before and after drying.

2.2.3 Grain size analysis

The grain size distribution from the cores and drags sediment samples were determined by a settling tube for the >50-µm fraction and by a Sedigraph 5100D (Micrometrics) for the <50-µm fraction following the method described by Giró and Maldonado (1985).

Best particle size distribution results are obtained from sediment samples free of organic matter, thus representing clay-silt and fine sand sized minerogenic material. Organic matter content causes unreliable and non reproducible results using Sedigraph. For that reason, the dry sample is treated with 20% H_2O_2 for a week, in order to eliminate organic matter. Ensuing, pyrophosphate is added (24-48 h) to avoid particle flocculation.

Coarse and fine fractions of the treated sample are separated with a 50-µm sieve. The <50-µm fraction is analyzed with a Sedigraph 5100 particle size analyzer.

The Sedigraph 5100 system uses both particle falling rates and the amount of X-ray absorption for particle size analysis. Particle falling rates (according to Stoke's Law) are used to determine the points in the cell beyond which certain particles have fallen. X-ray absorption is used to determine the percentage of total particle mass at different points in the cell. The resulting particle size distribution data are processed by the system computer. Since different particles usually have different shapes, the standard measure used to report particle size is the "equivalent spherical diameter". This is the diameter of a sphere of quartz with the same settling rate.

The >50-μm fraction is dried at 60º Celsius for 24-48 h and sorted with sieves of 50, 2000, 4000 and 6000 μm. The 50-2000 μm fraction is analyzed in the sedimentation tube.

The sedimentation tube is based on Stoke's Law (free falling of particles within a fluid) and measures the pressure difference between two water columns connected by a metallic membrane. This pressure difference is produced by the particles passing near the traducer and is proportional to the quantity of particles. These measurements are integrated through time to represent the distribution of grain size frequencies, given that grains fall more rapidly with increasing size.

Finally, data from the sedimentation tube, the Sedigraph and the >2000-μm fractions, are integrated by the program INTEGRA'03 to produce the full grain-size distribution. The software outputs the percentages of gravel, sand, silt and clay, and also provides the mean, mode, standard deviation and other statistics from the curve of granulometric distribution, in metric units (mm) and phi (Φ) units.

Traps sediment grain size was determined by a laser granulometer Horiba LA950 V2 in the *Laboratori de Sedimentologia* of the *Institut de Ciències del Mar* (ICM-CSIC).

2.2.4 Major elements and heavy metal analysis

Selected major elements and heavy metals were determined in all sediment samples taken during the study period: bottom sediment samples (cores and grabs) taken from the northern Barcelona continental shelf, settling particulate matter collected by the three sediment traps moored and suspended particulate matter (SPM) from the Besòs River water.

Core subsamples and drag samples, previously dried (see section 2.2.2), were homogenized in an agate mortar for the analysis of major elements and heavy metals.

Sediment samples (cores and drags) and settling particulate samples in the NF filters were totally digested using the acid digestion protocol. All samples are introduced into a Teflon container. 2.5 ml of pure nitric acid is added and the container is immediately closed to avoid gas leakage. Teflon containers are introduced into a stove at 90º Celsius during 4 h minimum. Samples are poured into a test tube using milliQ water. The tubes are centrifuged for 20 minutes at 2500 rpm and the supernatant is removed using a pipette from the tubes and are placed in a 100 ml flask. This process is repeated three times as to obtain a solid part in the tubes and another liquid part in the flasks.

The solid fraction remaining in the tubes is collected by 2.5 ml of nitric acid and 7.5 ml of pure hydrofluoric acid (HF) and placed again in Teflon containers. The containers are placed into the stove for at least 4 hours at a temperature of 90º Celsius. After that time are placed on a hot plate at 245º Celsius, adding 2.5 ml of perchloric acid after a while. Once the acid evaporates, a solid residue remains in the container that represents the non-volatile metal part of the sample attacked. This residue is removed by 2.5 ml of pure nitric acid and stored in the flask containing the supernatant of the sample. The Teflon containers are cleaned with milliQ water and made to volume end of the flasks of 100 ml with milliQ water. The samples are placed in special plastic containers and stored at 4º Celsius until further analysis.

Concentrations of selected major elements and heavy metals in the samples dissolved in the resultant HNO_3 solution were analyzed by atomic emission spectrometry using the induced coupled plasma spectrometers from the *Universitat de Barcelona* (*Serveis Científico Tècnics* UB). In each round of digestion, a duplicate, a blank and a certified reference material (CRM) PACS-2 coastal marine sediment are also analyzed following the same procedure explained above.

Mercury was determined directly from samples and fiberglass filters using a LECO Mercury Analyzer.

2.2.5 Enrichment factor of main heavy metals in sediments

It is widely known that the clay-silt fraction is the principal carrier of metal contamination. Thus, it is necessary to correct the sand fraction for each sample to obtain a good index of the extent of this contamination. This index was provided by dividing the metal concentration of each sample by the fraction of silt-clay (Krom et al., 1983). This procedure assumes that all of the acid-leachable metals are in the fine fraction of sediment.

The excess of heavy metals in the analyzed sediments was quantified using the concept of relative enrichment factor (REF). Heavy metal concentrations obtained in the previous analysis were compared to their natural levels extracted from uncontaminated samples collected along the Catalan coast (reference samples). The heavy metals concentrations from both, the reference samples and the study area samples, were normalized against the aluminium, obtaining the ratio of each heavy metal concentration according to the aluminium concentration. The levels of heavy metals contamination in the sediments analyzed from the study area are indicated for the enrichment factor equation (Baut-Ménard, 1979).

$$\mathbf{REF} = \frac{\mathbf{[M]\ sample}}{\mathbf{[Al]\ sample}} : \frac{\mathbf{[M]\ reference\ sample}}{\mathbf{[Al]\ reference\ sample}}$$

From all heavy metals analyzed, only those with enrichment factors above 2.5 (i.e. concentrations above 2.5 times more than their natural levels) were selected to evaluate the degree of contamination of the study area. Thus, the heavy metals selected for discussion were Cr, Pb, Cd, Cu, Zn and Hg.

2.3 Data calculations

2.3.1 Near-bottom wave orbital velocity

Interactions between surface waves and the seabed are most conveniently expressed in terms of the wave-induced orbital fluid motion close to the bed. Significant wave height (H_s), peak period (T_p) and the angular wave frequency (w) obtained from the Llobregat buoy and the WANA calibrated dataset were used to calculate the near-bed orbital velocity (U_b) for linear wave theory:

$$u_b = \frac{H\pi}{T\ \sinh(kh)} = \frac{\omega a}{\sinh(kh)}$$

Where H is the significant wave height (Hs), T the wave period, k the wavenumber, a the amplitude and ω the orbital velocity. The kh (wavenumber*depth), required for orbital-velocity calculations using linear theory, is calculated using a MATLAB function of the Soulsby (2006) Newton-Raphson interactive method implemented by Wiberg and Sherwood (2008).

2.3.2 Calibration of Seapoint turbidimeters

The Seapoint Turbidity Meter measures turbidity by detecting scattered light from suspended particles in the water using dual 880 nm light sources and dual silicon photodiode detectors with visible light blocking filters. The intensity of light scattering is calibrated to Formazin Turbidity Units (FTU) by the manufactured (Seapoint).

Along with the Seapoint turbidity sensor coupled to the Sea-Bird SBE 9 CTD, water samples were collected during the cruises near the bottom and at the surface by means of twelve-liter Niskin bottles mounted on a General Oceanics CTD rosette sampler along the tripod transect (Be10, Be09, Be08, Be07 and Be06 stations in Figure 2.4). For the turbidimeter attached to the Sea-Bird SBE 25 CTD, the water samples used for the calibration of the sensor were obtained during monthly surveys carried out during the SEDMET project.

The water samples were vacuum-filtered up to filter saturation into a pre-weighed Nuclepore polycarbonate filters (0.4 μm pore size). The weight of the dry residue, divided by the volume of water filtered, rendered suspended sediment concentration (SSC) in units of mg l^{-1}.

Therefore, two linear regressions were used to calibrate the optical sensors:

- For the Seapoint turbidimeter coupled to the Sea-Bird SBE 9 CTD used in the tripods hydrographic transect, Be10, Be09, Be08, Be07 and Be06 stations in Figure 2.4, the following equation was obtained:

$$\mathbf{SSC\ (mg\ l^{-1}) = 0.62\ x\ FTU + 0.11\ \ (n = 24;\ r^2 = 0.74)}$$

- For the Seapoint turbidimeter coupled to the Sea-Bird SBE 25 CTD used in the remaining hydrographic stations, Be02, Be03, Be04, Be05, Be12, Be13, Be14, Be15, Be16, Be17, Be18 and Be19 (Figure 2.4), the calibration equation obtained was:

$$\mathbf{SSC\ (mg\ l^{-1}) = 0.76\ x\ FTU + 0.07\ \ (n = 24;\ r^2 = 0.79)}$$

2.3.3 Calibration of Aanderaa turbidimeters

Aanderaa turbidimeters express the light scattering intensity as equivalent of Nephelometric or Formazin turbidity Units (NTU or FTU). This calibration was conducted by the manufacturer (Aanderaa) using Formazin (turbidity calibration standards).

No water samples were collected during the deployment periods at those locations. Therefore, in order to convert NTU units into concentration units (mg l^{-1}), turbidity sensors were transformed using the measurements carried out by Guillén et al. (2000) obtained from 25 northwestern Mediterranean samples, taken in a nearby area. The intensity of the light backscattered by particles was calibrated with a nephelometric solution to calculate the suspended sediment concentration (SSC) with the equation:

$$\mathbf{SSC\ (mg\ l^{-1}) = 1.21\ x\ NTU + 0.43 \qquad (r^2 = 0.46)}$$

Because the 0-20 NTU calibrated sensors were out of range in times of relatively elevated SSC, probably underestimating maximum values, data from the 0-500 NTU sensor was used in times when SSC was above of approximately 25 mg l^{-1}.

2.3.4 Along- and across-shelf currents and advective fluxes

Aanderaa current meters output the module of the current speed and the current direction measured from the North. These were previously decomposed to u and v components with positive values towards N and E, respectively. The along- and across-shelf components were then defined following the orientation of the isobaths at each site, with positive values towards the NE and offshore, respectively.

Assuming that the output of the back scatter sensors was largely attributable to suspended particles and that particles move with the velocity of the water within which

they are suspended (Wright, 1995), the instantaneous sediment flux of particles in g/m^2s is obtained as the product of the velocity module and the SSC (suspended sediment concentration, in mg/l), with the same direction as the flow:

$q(t) = c(t)*SSC(t)$,

Averaging the instantaneous sediment flux over time produces the estimated magnitude of the horizontal flux and its direction from each sampling site during the experiment.

The along-shelf and across-shelf instantaneous sediment flux components where obtained in the same manner, as the product of the SSC and the along and across components of the velocity fields. Integrating sediment flux values over time results in the amount of sediment transported and the direction of the transport at each site.

2.3.5 Downward total mass fluxes

Total dry mass of sediment trap samples was determined gravimetrically. Several replicates were filtered into preweighed Millipore cellulose acetate membrane filters, rinsed with distilled water (to remove sea salt) and dry to constant weight at 40 degrees Celsius.

Total max flux (TMF) expressed in mg m^{-2} d^{-1}, was calculated with the formula:

TMF = Sample dry weight (mg) / (collecting area (m^2) · sampling interval (days)).

2.3.6 Altimeter calibration and Seabed erosion/deposition

The ALTUS altimeter is an autonomous 2 MHz acoustic transducer coupled with a pressure sensor. This device allows long term monitoring (Deloffre et al., 2006), but is also suitable for high-frequency surveys (sampling frequency up to 1 Hz) with a data storage capacity of several weeks. The ALTUS provides bed elevation and water level measurements with resolution of 0.2 mm and 20 mm respectively. For this study, the transducer was positioned 22 cm above the bed, with a sampling frequency of one measurement every fifteen minutes.

Thus, the altimeter data was processed to determine the distance to the seabed every fifteen minutes. The pressure record for each deployment was also analyzed and

evidences of tripod sinking were found and removed from the seabed variation record at 20 m tripod site (Be09). However, the pressure sensors at 30 m and 40 m sites were out of range during the deployments and therefore, possible tripod sinking episodes could not be identified. Thus, at 30 and 40 m depth, seabed deposition was not taken into account and seabed erosion was treated as minimum erosion.

After removing the sea level variation from the seabed variation record, the minimum distance between the sensor and the seabed was taken as a reference level to measure the seabed deposition/erosion events.

2.3.7 One-dimensional (vertical) sediment transport model

A 1D sediment transport model (Wiberg and Smith, 1983; Wiberg et al., 1994; 2002; Harris and Wiberg, 1997) was used to calculate suspended-sediment transport rates during resuspension events. The model represented the frictional momentum balance in the bottom boundary layer using an eddy viscosity profile enhanced by wave-current interaction. The 1D vertical model requires as input values of steady horizontal current velocity at a specific elevation (z), near-bottom wave-orbital velocity and associated period and direction and bed sediment characteristics.

The near-bottom (0.58 mab) current velocities recorded by the three tripod current meters and the calculated near-bottom orbital velocities (section 2.3.1) were used as input to the model at each site. The model calculates the wave shear velocity (U_{*w}), the current shear velocity (U_{*c}) and the nonlinear combined wave-current shear velocity (U_{*cw}). The total shear stress was then calculated using U_{*cw} and the water density (ρ) as $\tau_{cw} = \rho U_{*cw}$. The models calculates an eddy viscosity profile proportional to $U_{*cw}z$ in the wave boundary layer and the current stress velocity profile ($U_{*c}z$) in the mean current boundary layer.

The sediment size classes and fractions used in the model were based on the upper centimeter of samples collected at the tripod sites in the study period surveys. Critical shear stress and settling velocities for particles in each of the modeled sediment classes was calculated according to Soulsby (1997). Suspended sediment concentrations are computed for any specified number of size classes. The near-bed reference concentration is a function of the volume of sediment concentration of a bed, the resuspension parameter (γ_0) and the excess shear stress. A mean value of γ_0 =

0.004 was used for the computation based on profiles of suspended sediment concentration measured in the inner Ebro continental shelf (Guillén et al., 2002).

The Wiberg et al. (1994) model was modified by Harris and Wiberg (1997) to account for the changing size distribution at the bed surface during a resuspension event by modeling the upper 15 cm of the sediment bed as two layers: a superficial active layer that is well mixed and available for resuspension; and an underlying layer containing sediment that is inaccessible for resuspension. This active-layer depth is the depth on the seabed at which the critical shear stress and wave-current shear stress are equivalent.

The model calculates the bed size distribution as a function of depth below the bed surface as follows. At each time step the volume of sediment in suspension is calculated for every size class and removed from the active layer. Bed armoring is accounted for by limiting the volume of each size class suspended by the amount available within the active layer. Between steps any sediment in suspension is "redeposited" on top of the active layer in a fining upward sequence to simulate settling out of the water column.

2.3.8 Definition of sediment flux events

The measurements at site Be09 (20 m depth) provide the necessary information to identify sediment transport events and non-events intervals during the deployments from September of 2007 to June of 2008. Based on the observational data, sediment transport events were identified whenever the magnitude of the instantaneous sediment flux (fi) exceeded 1.5 g/m^2s and non-transport intervals as times when fi < 0.3 g/m^2s (background level). Hours with intermediate magnitude immediately preceding and following a sediment transport event were incorporated into that event. In addition, periods of fi > 1.5 g/m^2s separated for a period of fi < 0.3 g/m^2s not longer than 24h were considered the same event. In this manner, sediment transport events were extended to include both resuspension and river sediment supply events along with events of increased current activity.

3 Forcing conditions

The climatology of the NW Mediterranean sea displays seasonal variations in terms of storm passing frequency and intensity that play an important role over the delivery and the dynamics of sediment in the continental shelf. The time period of the present study comprised three seasons, from autumn 2007 to spring 2008, which showed distinct features between them. The purpose of this section is to describe the main hydrographic and hydrodynamic conditions during the study period to support the interpretation of sediment transport processes.

3.1 Wind and waves

The mean wind speed during the period that is considered here was 4.6 m/s, with the strongest winds (14.4 m/s) blowing from the northeast and associated to a storm event. Wind speeds higher than 12 m/s were reached during most of the storm episodes (Figure 3.1 A) with a blowing direction similar to the direction of wave propagation but slightly rotated (Figure 3.3 B1), i.e. NE-ENE in the majority of the storm events and few episodes of winds blowing from the SW. Although, about another 20% of the wind record felt into the third quadrant (Figure 3.3 B2), no more wind events of significantly increased strength and duration were associated to those wind directions.

The wave data between end of September 2007 and mid June 2008 showed a frequent but moderated wave storms in the inner continental shelf (Figure 3.1). During the study period, more than ten storm events were recorded with Hs and Tp over 2 m and 9 s, respectively, most of them coming from the ENE. Indeed, more than 35% of the wave direction record felt between the ENE and ESE directions and over about a 20% felt between S-SW directions (Figure 3.3 A1). The most energetic episode, between the 15th and 18th of December 2007, was characterized by the strongest storm recorded over the study period, a two peak wave storm with significant wave height (Hs) up to 3.47 m and peak period (Tp) about 11 s, followed by a minor second peak storm event (Hs > 2.5 m and Tp > 11 s) after less than 2 days of relatively calm conditions. Both storm events presented an eastern component in the direction of wave propagation (Figure 3.3 A1).

Figure 3.2 show the significant near-bottom wave orbital velocity (Ub_s) calculated for each tripod site depth using the recorded wave data. The maximum number of wave storm events and maximum Ub_s values occurred throughout the autumn months.

During this period, maximum bottom wave velocities higher than 80, 60 and 40 cm/s were obtained at Be09-20m, Be08-30m and Be07-40m sites, respectively. However, after two months of relatively calm conditions (from early January to early March 2008), it can be observed another period of significant increment on wave activity and frequency of storm events. During the spring months, maximum bottom wave velocities reached more than 60, 40 and 20 cm/s at 20, 30 and 40 m depth, respectively.

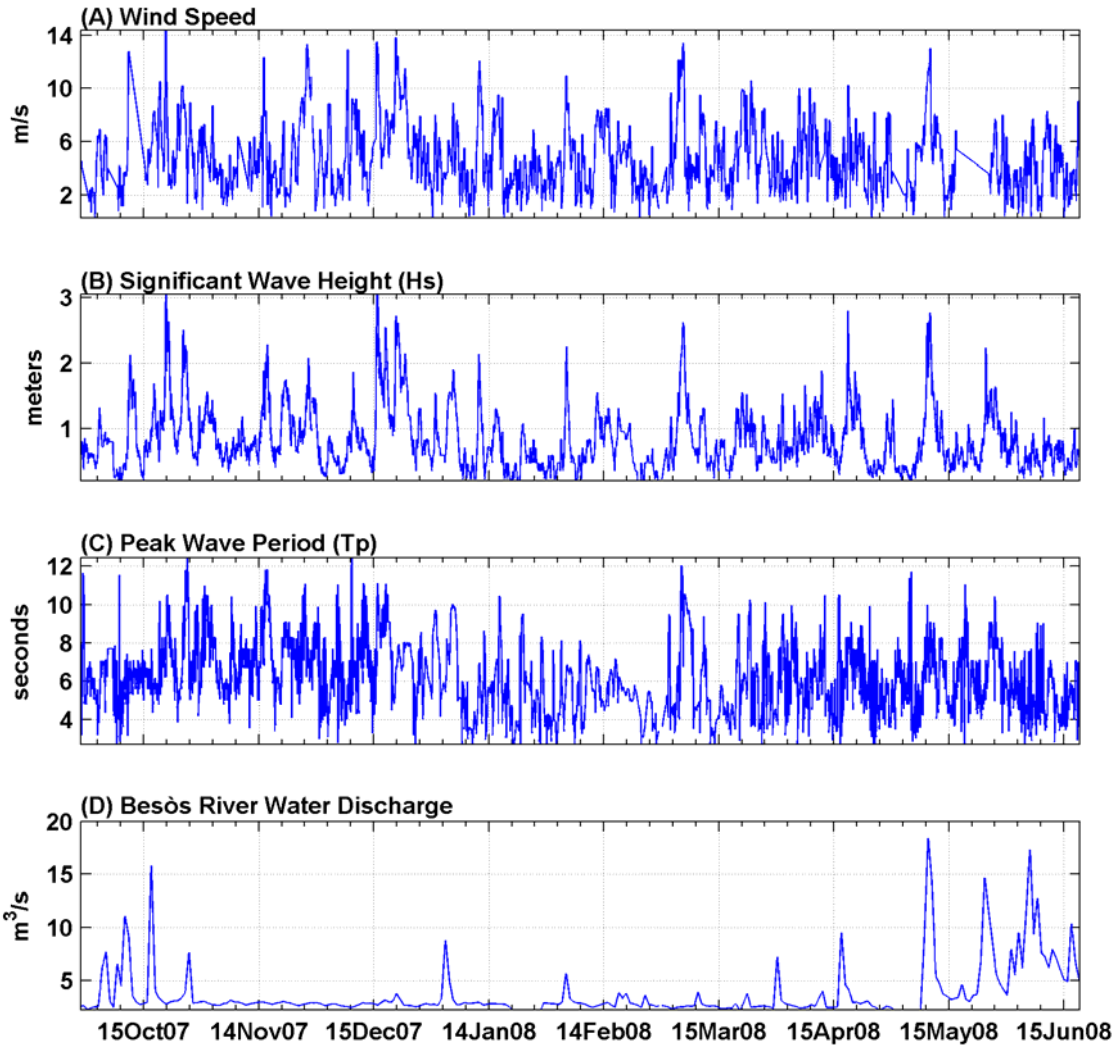

Figure 3.1 Wave, wind and river discharge conditions during the experiment, collected nearby the study area. (A) Wind speed at WANA model point 2066051; (B) and (C) wave data at WANA model point 2066051 calibrated with Llobregat buoy data; (D) water discharge at the Besòs River gateway.

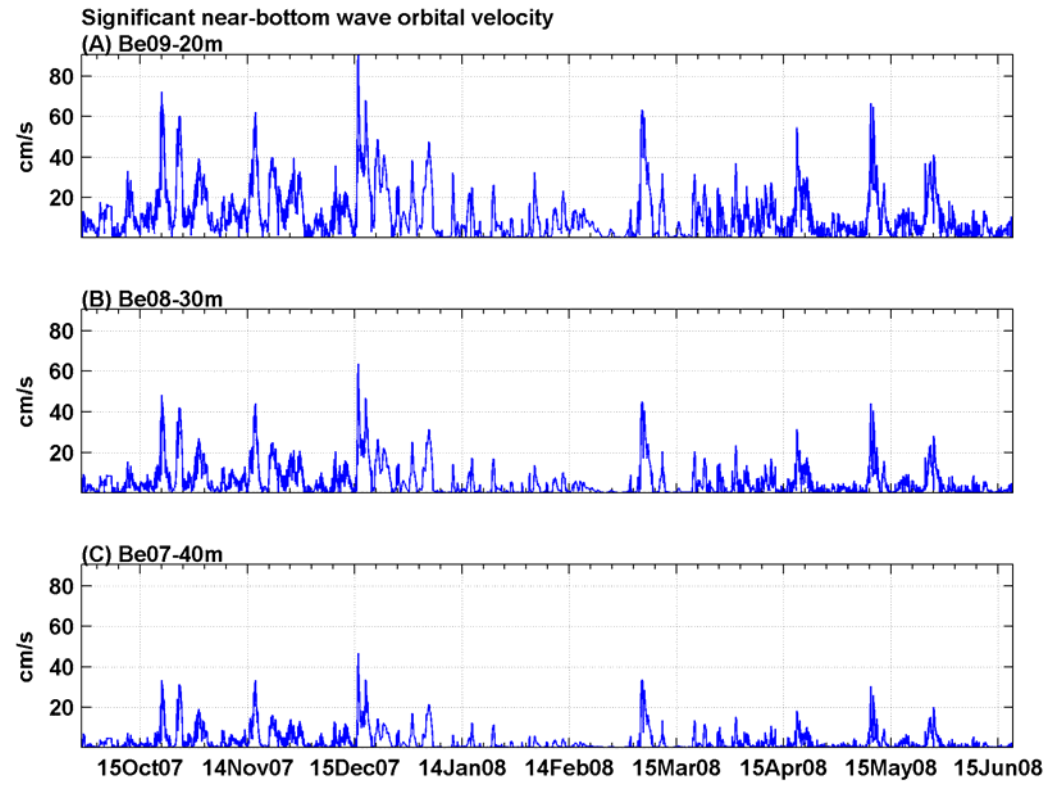

Figure 3.2. Time-series of significant wave orbital velocity at location (A) Be09-20m, (B) Be08-30m and (C) Be07-40m.

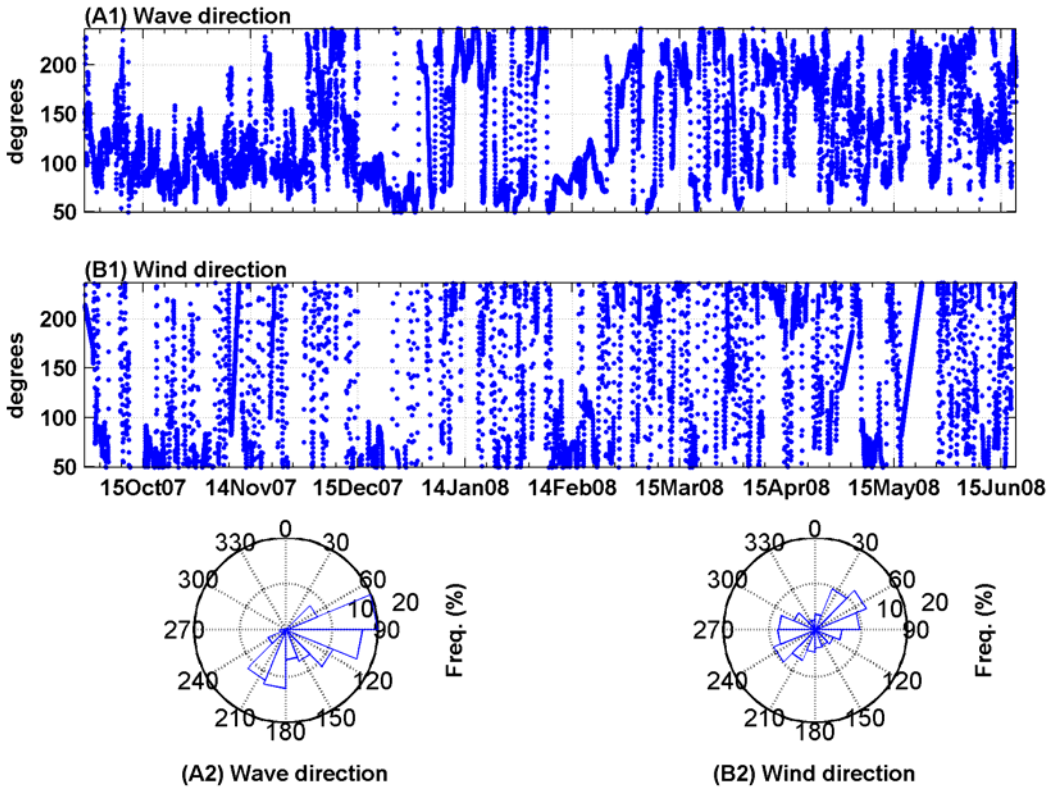

Figure 3.3. Time series of wave (A1) and wind (B1) directions at WANA model point 2066051 during the study period. (A2) and (B2) rose diagram of the relative frequency of the record of wave and wind direction, respectively.

Spectral analysis of significant wave orbital velocities showed important peaks at 15 and 5 days periods, approximately, and a minor peak in periods of 2-3 days (Figure 3.4 A). Dominant frequencies in wind velocities were obtained by applying spectral analysis after projection the wind velocity into across- and along-shelf directions. Firstly, higher power content was observed for the along-shelf wind velocity component (Figure 3.4 B2), which is in keeping with the above mentioned presence of higher velocities under NE or SW winds. In the along-shelf component, most of the energy was present in the low frequency band, with two peaks in periods of 15 and 4-5 days, but another additional peak was observed in the frequency band of approximately 1 day. Although across-shelf winds presented peaks in the same frequency bands than along-shelf winds but with lower power content, additional peaks in periods of 2-3 days were also observed (Figure 3.4 B1).

Therefore three different periods in terms of storm activity matched the natural seasons of the year. Thus, the period comprised between end of September 2007 and December 2007(autumn) was characterized by an intense frequency of northeaster-eastern storm passages with moderated intensity; between January and early March 2008 (winter), the wave activity and frequency were reduced significantly; and finally, from March to mid June 2008 (spring), specially between May and June 2008, another period of increasing wave activity took place, this time the storm events were from the S-SE and some SW, more moderated and less frequent than in the first period.

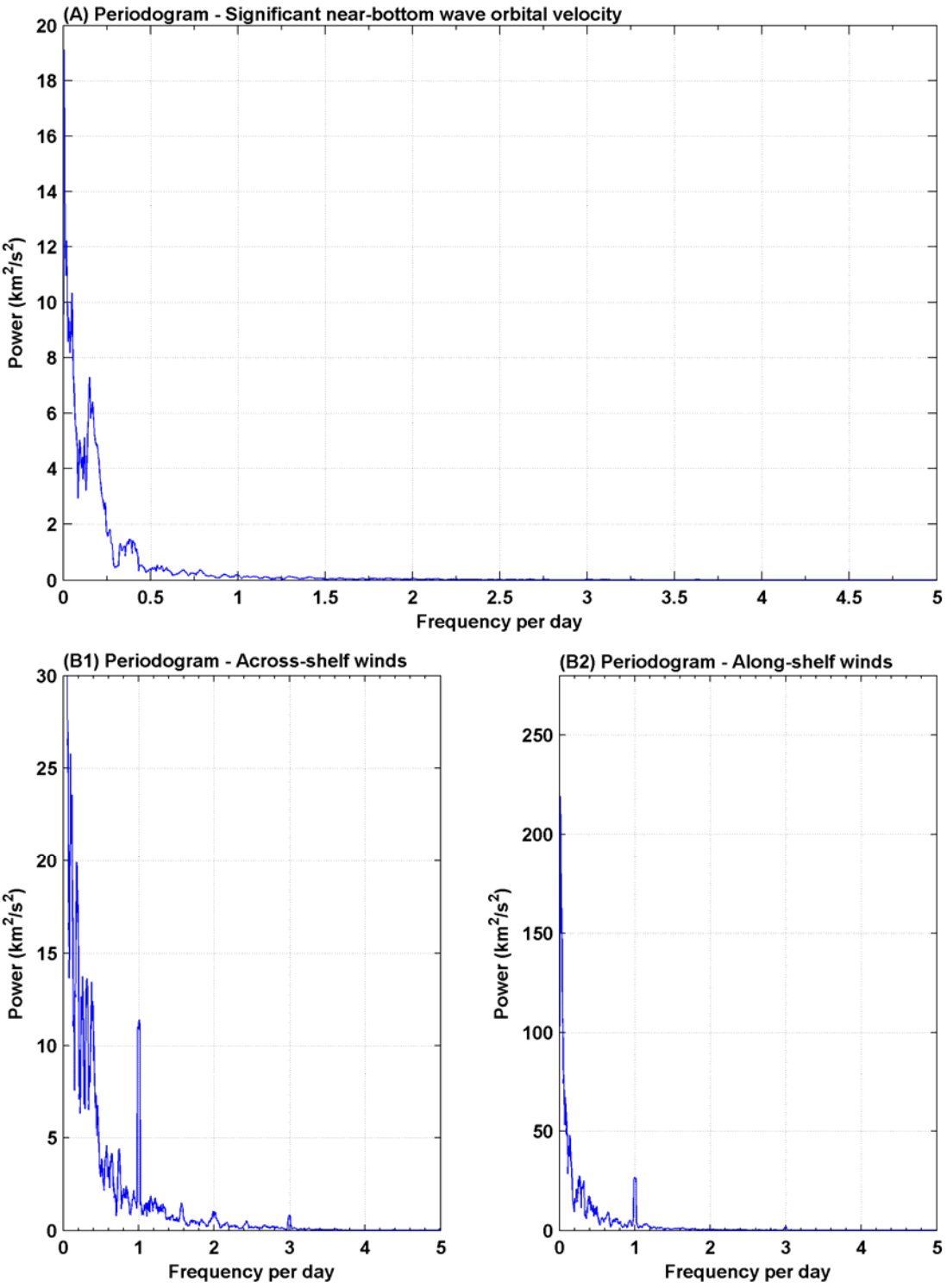

Figure 3.4. Spectral analysis of forcing agents time series. (A) Significant near-bottom wave orbital velocity, (B1) Across-shelf winds and (B2) Along-shelf winds.

3.2 Hydrography and water river discharge

The hydrographic transects conducted during the cruise SEDMET-I (28th of September 2007) correspond to the end of the summer stratified conditions of the water column, as shown in the temperature and density (sigma-0) sections (Figure 3.5 A). In the SSC sections it can be identified a well developed bottom nepheloid layer, with thickness around ten of meters and maximum concentrations higher than 3 mg/l.

In SEDMET-II and SEDMET-III (conducted by the end of November and end of February, respectively) the temperature, salinity and density sections evidence vertical mixing of the water column (Figure 3.5 B and Figure 3.6 A), which shows that the autumn and winter storm passages were capable of destroy the previous vertical structure. During both surveys the bottom nepheloid layer is well identified with maximum concentrations between 3 and 4 mg/l. However, the relatively high wave energy conditions during the November cruise survey developed a bottom nepheloid layer thickness around 20 m with concentration values of 1 mg/l reaching the surface.

The final situation of the study period, June 2008 (SEDMET-IV), corresponds to the onset of stratification, as shown in the sections of Figure 3.6 B. The bottom nepheloid layer is also well identified with maximum concentrations between 3 and 4 mg/l.

The hydrography of the studied zone is also modified for continental freshwater inputs, especially the Besòs river water discharges. The Besòs river water discharge record, shown in Figure 3.1 D, presented a typically episodic pattern with pulses of water discharge occurring mainly during autumn and spring seasons. Average river discharge during the period of study was 3.8 m^3/s with discharge peaks up to 15 m^3/s and 18 m^3/s in October 2007 and May-June 2008, respectively. In October 2007, the increments in river water discharge were characterized by short and fast water pulses accompanied by increments in wave activity. During spring 2008, river discharges lasted longer than in autumn 2007, especially the discharges of June 2008 that occurred under low energy wave conditions. The influence of the river discharge can be observed in the salinity and density sections taken at that time (Figure 3.6 B) where the stratification of the water column is disturbed in the onshore limit of the sections.

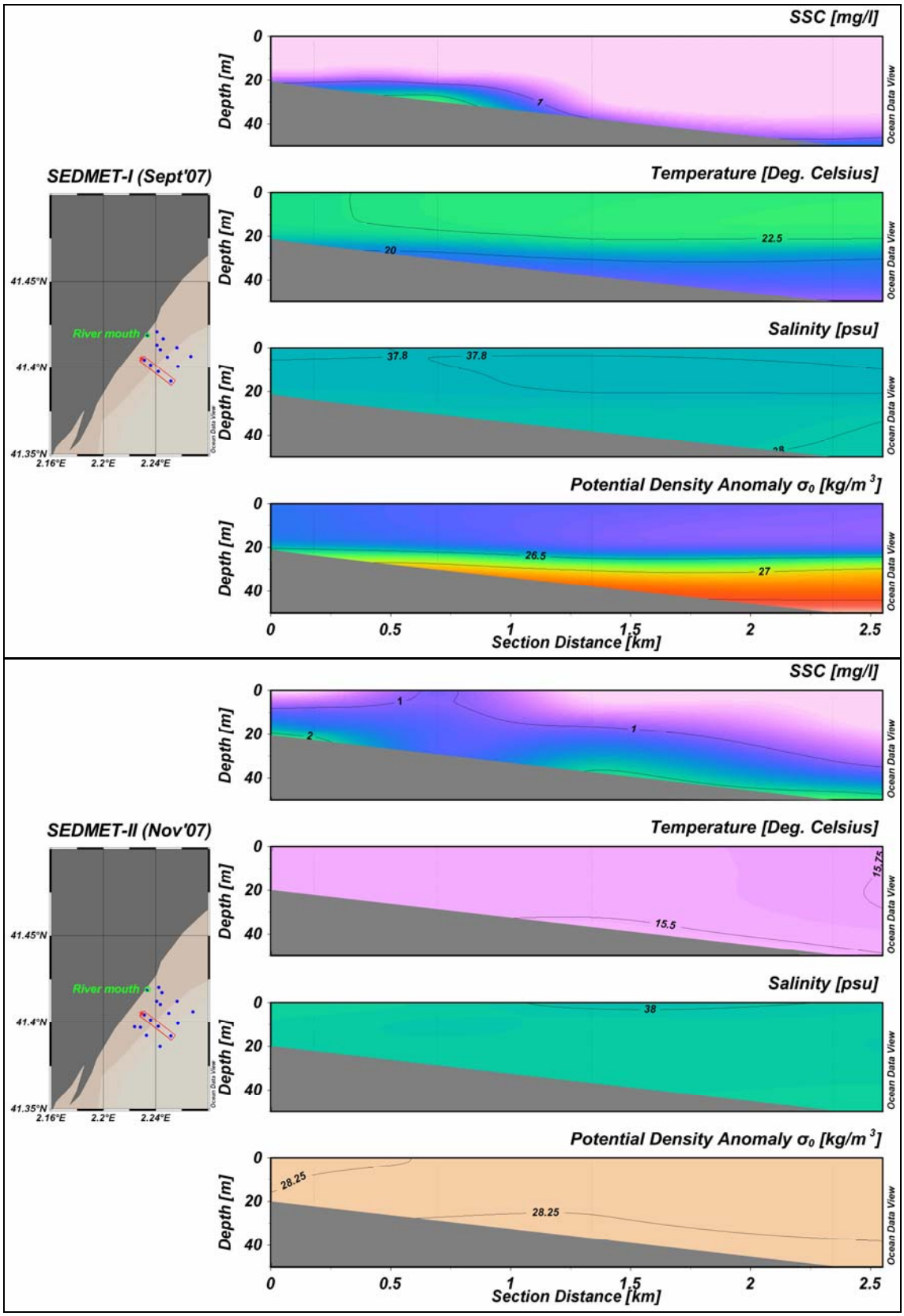

Figure 3.5. Across-shelf sections of temperature, salinity, SSC and density over the study area during (A) the SEDMET-I (September 2007) and (B) SEDMET-II (November 2007) cruises. The location of the stations is shown in the left map of each box.

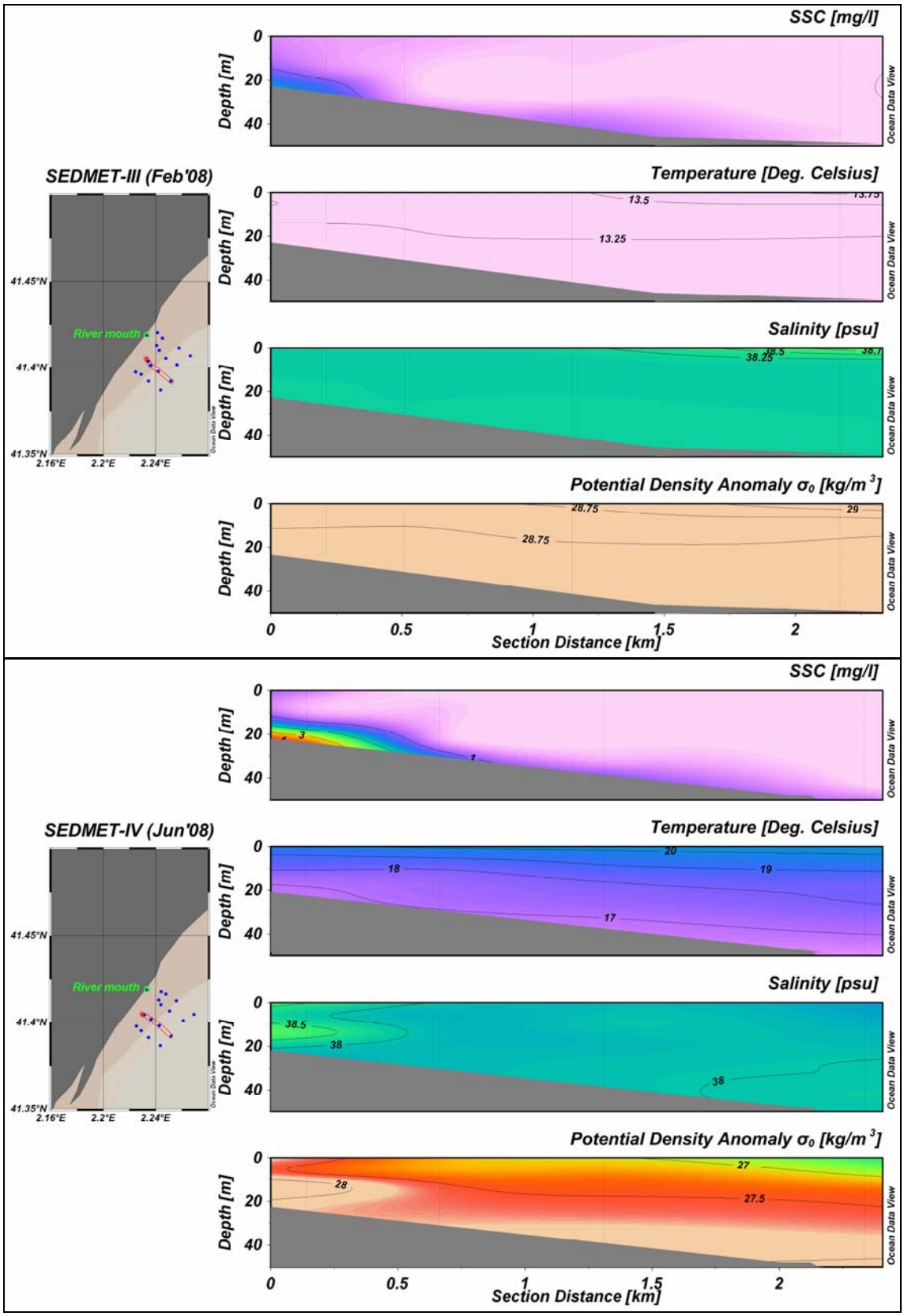

Figure 3.6. Across-shelf (lower box) sections of temperature, salinity, SSC and density over the study area during (A) the SEDMET-III (February 2008) and (B) the SEDMET-IV (June 2008) cruises. The location of the stations is shown in the left map of each box.

3.3 Near-bottom currents

Times series of current speed and current vectors fields measured at 0.58 mab from the Be09-20m, Be08-30m and Be07-40m sites are shown in Figure 3.7. Near-bottom current speed showed similar values at all sampling sites with an average about 7 cm/s. The highest near-bottom current speeds were associated with storm events on the inner shelf (Figure 3.1 and Figure 3.2) with peak values up to 27 cm/s at 20 and 30 m water depth (Figure 3.7 A1 and B1, respectively) and up to 32 cm/s at the deepest site (Be07-40m, Figure 3.7 C1). Both, current and wave activities were more energetic and frequent in autumn. The current direction was slightly variable among sampling locations (Figure 3.7 A2, B2 and C2). The dominant direction was NE – SW at Be09-20m site, following the orientation of the isobaths, during the three deployments. However, the dominant direction was NNE – SSW at Be08-30m and Be07-40m sites with 20º and 15º of rotation towards the north, respectively, and a major spread in the negative values of the u component especially at site Be08-30m.

The current speed and direction were transformed to along- and across-shelf components following the orientation of the isobaths at each site, with positive values towards the NE and offshore, respectively. The along- and across-shelf currents observed during the study period were variable in time with higher values in the along-shelf flow than in the across-shelf one (Figure 3.8). However, while the along-shelf current component flew towards approximately the same direction and reached similar values at all sites, the across-shelf component was spatially variable in magnitude and direction, highly affecting the resultant current velocity.

In the spectral analysis of current components shown in Figure 3.9, it can be observed the differences of the frequencies that dominate along-shelf and across-shelf components at the three locations. The higher power content in the along-shelf flow was basically reflected at lower frequencies, whereas at high frequencies (higher than 0.5 times per day, i.e. periods shorter than 2 days) both components showed a similar level of intensity. The along-shelf current at the three locations presented the highest energy for the frequency band corresponding to periods between 3 and 5 days, which was higher at the 20 m depth site decreasing offshore. Although, the across-shelf flow also presented a significant power content in this low frequency band, in this flow direction, the energy was higher at the 30 m depth site than at the two other sites. The spectral analysis also presented some energy content at higher frequencies, corresponding to periods around 1 day, which was detected only at 20 m and 30 m

depth in the across-shelf flow and at 20 m depth in the along-shelf one and decreased offshore.

In the along-shelf component, these low-frequency currents with fluctuations of 3-5 days reached more than 20 cm/s at all tripod locations between autumn and early winter (Figure 3.8). However, the across-shelf speed values were under 10 cm/s at 20 m depth (Figure 3.8 A1) and under 15 cm/s at 30 m and 40 m depth (Figure 3.8 B1 and C1, respectively).

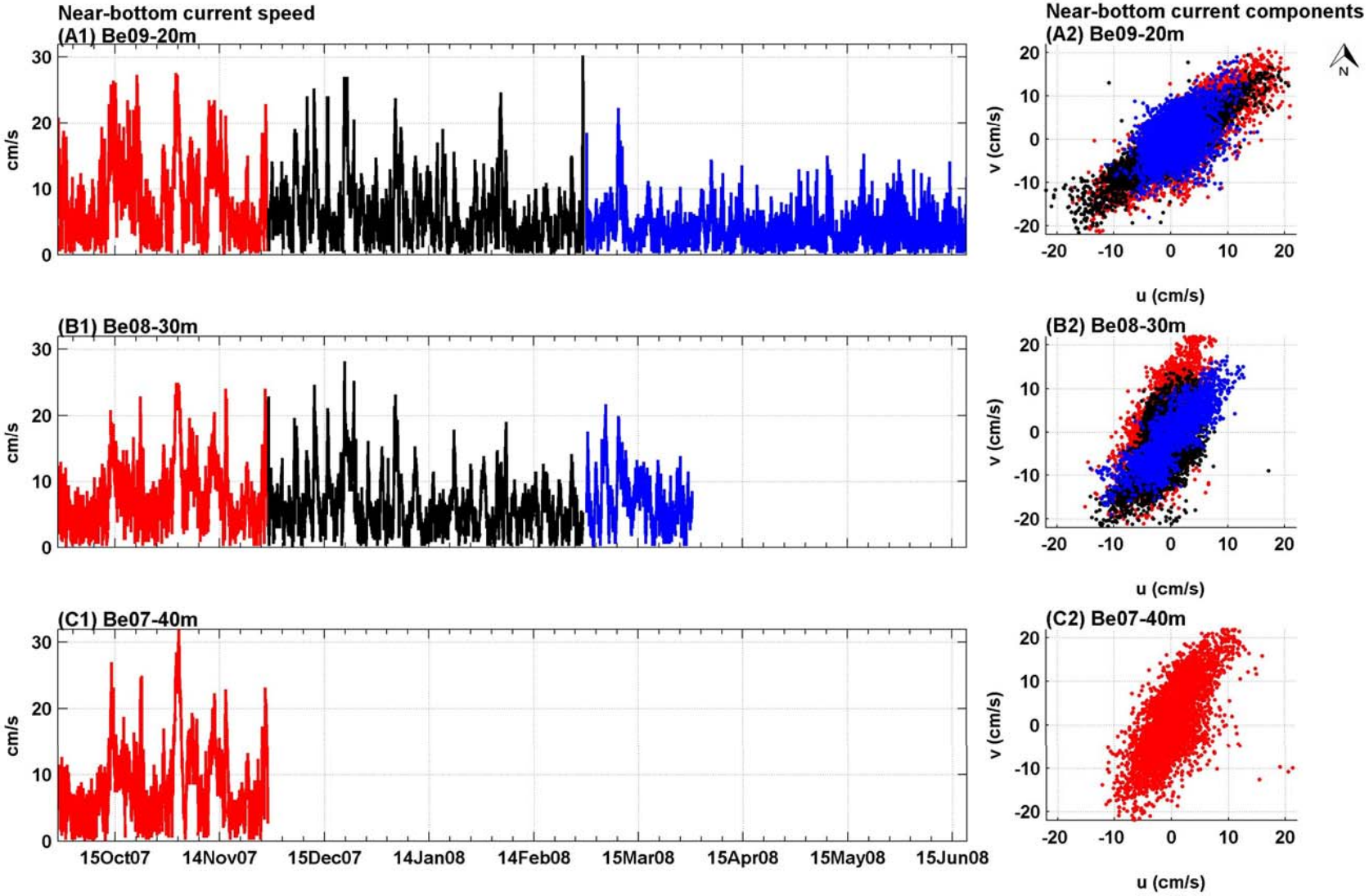

Figure 3.7. Time series of current speed during the study period (left boxes) and current components fields (right boxes) measured at 0.58 mab at the study sites (A1) and (A2) Be09-20m, (B1) and (B2) Be08-30m and (C1) and (C2) Be07-40m.

Progressive vector representing flow conditions during the recording period available for each site (Figure 3.8 A2, B2 and C2), also show the above-mentioned spatial variability of the current flow. At the end of the first deployment (end of red line in Figure 3.8), the along-shelf component dominated at 20 and 40 m depth with a virtual current displacement about 150 km towards NE but slightly offshore (53 km) and 60 km towards NE and slightly onshore (36 km), respectively. However, at 30 m depth the flow was directed mainly landward (about 121 km) ending at the same location in the along-shelf direction after some fluctuations.

Between November 2007 and March 2008 (black line in Figure 3.8), and specifically after the December 2007 eastern storm, an evident reversal in current direction determined the flow behavior in such a way that the virtual current displacements were mainly seaward at 20 m depth and southeastward (i.e. along-shelf) at 30 m depth. During this period, the main difference between both sites was related to an increment in the along-shelf current intensity at 30 m depth more than to prevailing currents of opposite directions as recorded in the previous period. At the 20 m site, the across-shelf virtual displacement was almost four times higher (59 km seaward) than the resultant along-shelf displacement (16 km towards SW) reversing the circulation pattern recorded during the previous period (Figure 3.8 A2). In the case of the 30 m site, the virtual displacement in the along-shelf direction was relatively high (267 km towards SW) compared to the across-shelf flow (96 km offshore) and specially respect to the previous period (Figure 3.8 B2).

From March to the end of the record (blue line in Figure 3.8), at the Be09-20m site, a notable change occurred in the intensity and direction of the current. The across-shelf current intensity increased progressively while the along-shelf current intensity decreased significantly along this period. In relation to the direction of the current, both along and across components showed a reversion in the flow direction, towards the NE and seaward, respectively.

Therefore, two different patterns were observed in the behavior of water fluxes in the inner shelf: One along autumn 2007, an strong along-shelf current dominated at Be09-20m and at the deepest site (Be07-40m) resulting in a virtual current displacement about 150 km towards the NE and about 100 km towards the NNE, respectively, whereas at the 30 m depth site (Be08-30m) the across-shelf component dominated during this period with a resultant virtual displacement of more than 100 km onshore. The other pattern, between late autumn 2007 to the end of the record, showed that the

across-shelf component dominated at 20 m depth with a resultant offshore direction about 100 km, while at 30 m depth the along-shelf component was much higher compared to the previous period which resulted in a major reversal in the current direction with a current virtual displacement towards SW and seaward.

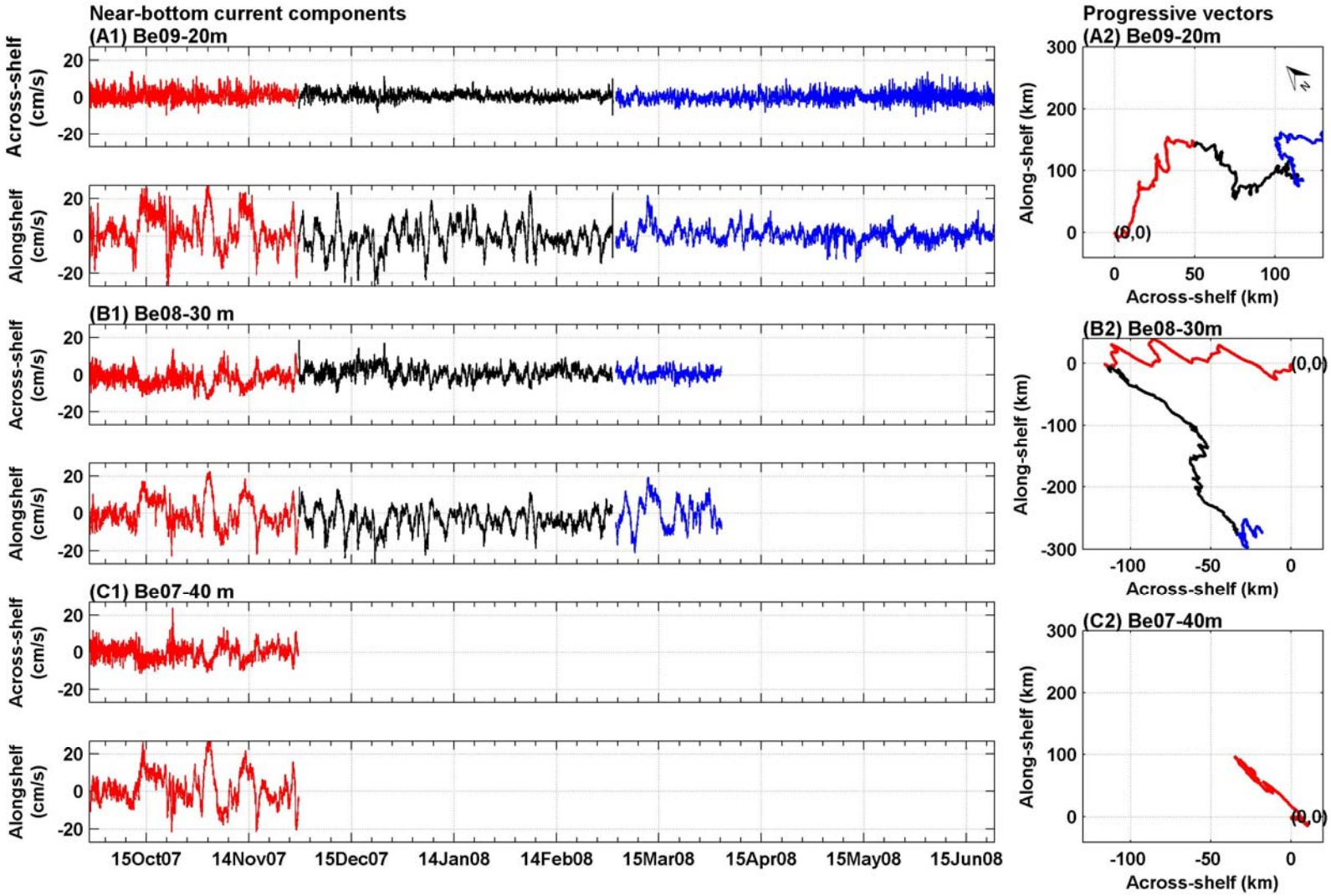

Figure 3.8. Times series of transformed across-shelf and along-shelf current components and the progressive vectors in those directions at (A1) and (A2) Be09-20m, (B1) and (B2) Be08-30m and (C1) and (C2) Be07-40m, respectively. Positive values are towards the NE in the along-shelf direction and offshore across the shelf.

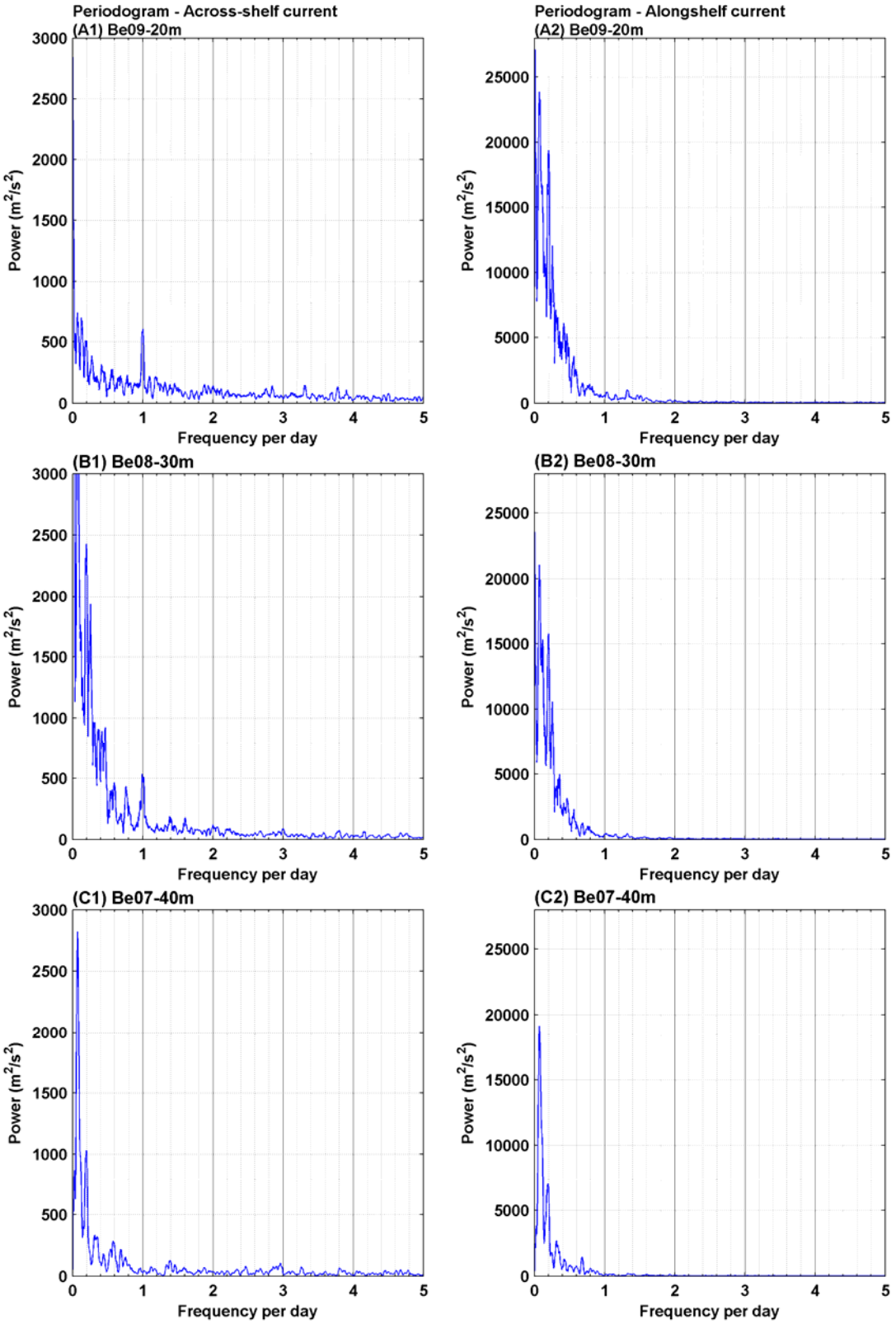

Figure 3.9. Spectral analysis of across-shelf (left boxes) and along-shelf (right boxes) current components. (A1) and (A2) Be09-20m location, (B1) and (B2) Be08-30m location and (C1) and (C2) Be07-40m location. Note different scales for the Y axis.

3.4 Processes affecting currents during the study period

The frequency spectra of the along-shelf and across-shelf currents show increasing energy in the low frequencies corresponding to periods over 3 days and 1 day (Figure 3.9). High energy were also observed in those frequency bands from the spectral analysis of the along- and across-shelf winds (Figure 3.4) suggesting that the wind regime controlled current fluctuations in a certain way during the study period. Wind velocities and near-bottom currents show correlation in times with increased current velocity. However, the occurrence of events with relatively high near-bottom currents under weak wind energy and the high current variability suggest that other processes may also control the current intensity and changes in current direction such as sea level gradients (Grifoll et al., 2012) and wave-driven currents (Lentz et al., 2008).

High current velocities were recorded under relatively high wind stress. The along-shelf current flowed mainly towards the SW during relatively high north-easterly winds (e.g. October and December 2007 storms) and toward the NE during winds blowing from the SW (February 2008 storm). This is consistent with the result obtained from Grifoll et al. (2012) on the Catalan inner-shelf which suggested that, under storm conditions, north-easterly winds generate a negative sea level gradient along the Catalan coast resulting in high SW along-shelf currents, while south-westerly winds reverse along-shelf current toward the northeast. Along-shelf winds also force cross-shelf circulation over the inner-shelf (Lentz, 2001). In this sense, northeastern winds were downwelling-favorable and the return flow generated an offshore current near the bottom in the across-shelf component, while southwestern winds favored upwelling and near bottom onshore flows. However, the across-shelf flow showed high variability and the correlation between down- and up-welling favorable winds and the direction of the across-shelf current was not as clear as in the along-shelf component. Fewings et al. (2008) suggested that cross-shelf winds can be more effective than along-shelf winds at driven across-shelf flows in the inner-shelf. Indeed, the high power content in the 1 cpd frequency band of the across-shelf winds and currents also suggests a contribution of diurnal breezes (cross-shelf winds) to the across-shelf near-bottom currents, specially during spring (May and June 2008) where the predominant winds are also associated with diurnal sea-breezes (Font, 1990).

During events characterized by relatively high currents unrelated with local winds other processes may contribute to the near-bottom flow. The importance of wave forcing to drive flow circulation over the inner-shelf has been proposed as an active mechanism

(Lentz et al., 2008). During events of high wave incidence angle, wave-driven flows can enhance the magnitude of along-shelf currents (16th and 20th of November 2007 and 4th of January 2008 events) or even, increase the seaward component of the near-bottom current (27th of May 2008), if waves propagate perpendicular to the coast. In addition, Grifoll et al. (2012) showed that during weak local winds, the along-shelf current flows toward southwest when the sea level gradient is positive associated with general dynamics of the NW Mediterranean. When the sea level gradient is negative, Grifoll et al. (2012) showed that the along-shelf current switches northeastward associated presumably with the excursion of water from the south. This mechanism could explain the relatively high northeastern currents during the 12th of October and 1st of November events, where the current speed reached values around 25 cm/s under relatively low wind and wave energy.

The along-shelf current variability was similar across-shelf, but the across-shelf current velocities observed at the inner-shelf sites frequently differed between each other (Figure 3.8). As a result, near-bottom flows varied not only in magnitude, but also in direction, meanly eastward in 20 m, onshore in 30 m and northeastward in 40 m of water, during early autumn, and offshore and southward means at 20 m and 30 m water depth, respectively, during the period comprised between end of November 2007 and January 2008 (Figure 3.8). This pattern suggest a flow convergence between 20 and 30 m water depths after the sequence of events occurred in early autumn and a net flow offshore after late autumn and winter in the across-shelf component of near-bottom currents. The spatial variability of near-bottom currents across the shelf can be explained by the relatively importance of wind and wave forcing depending on water depth. Through the inner-shelf, as the water depth increases, the circulation is dominated first by wave forcing, cross-shelf wind forcing and then along-shelf wind forcing (Lentz et al., 2008; Fewings et al., 2008).

4 Sediment characteristics

Seabed granulometry and physical properties play and important role for understanding sediment dynamics in response to the oceanographic conditions. With this aim, this section presents the grain size and porosity measurements taken in the sediment samples collected during the experiment (sediment cores, sediment grabs and sediment traps) and their temporal evolution and spatial distribution in the study area. Near-bottom suspended sediment concentration (SSC) is also presented to describe the sediment response to the forcing conditions and water fluxes introduced in the previous section. Here we discuss the controlling factors of SSC across the inner shelf.

4.1 Bottom sediment variability

The bottom sediment analyzed in the continental shelf of Barcelona, between 20 and 60 m isobaths, was mainly composed of mud with a percentage of sand increasing towards the coast and to the river mouth. Considering their relative abundance in the sediment, three modal granulometric fractions were identified in the study area: very fine sand (63-125 μm), medium to fine silt (8-31 μm) and clay (< 4 μm). The down-core logs of grain size and porosity analysis for all the cores sampled in September 2007 during the SEDMET-I cruise are shown in Figure 4.2 and Figure 4.3.

At 20 m depth (Be09-20m site), the sand fraction dominated the upper 10 cm with a median grain size between 80 and 100 μm. The lower 10 cm was mainly sandy mud with 70-80 % of mud (silt + clay) content and a 20-30 % of sand. This distribution indicated a coarsening trend towards the surface with a sharp gradient in the upper 10 cm. The porosity was lower in the upper 10 cm than in the lower part of the core that presented a peak around 10-12 cm depth decreasing smoothly towards the core base.

In most of the cores sampled at 30 m water depth (Be08-30m in Figure 4.2 and Be21-30m, Be03-30m and Be22-30 m in Figure 4.3), the grain size presented a coarsening trend towards the surface, with a percentage of mud (silt + clay) around 90 % (median grain size of 10 μm) at the lower part, and between 70 and 80 % (median grain size of 25-35 μm) in the surface layer of the cores. However, this trend was not linear and most of the cores presented a sharp change around 10-15 cm core depth: the site closest to the river mouth (Be21-30m) presented a median grain size maximum peak of 140 μm at 11 cm core depth. While the Be08-30m and Be03-30m cores presented a minimum grain size at 10 cm (10 μm) and 15 cm (5 μm), respectively. At all 30 m depth

sites, the porosity trend to increase towards the surface, with some fluctuation along the core depth, reaching values between 0.65 and 0.75. Therefore, along the 30 m isobath, the median grain size averaged 30 μm at the surface and 10 μm at the bottom of the core, with differences along the core depth, especially at the one sampled closest to the river mouth (Be21-30m core). The porosity content was about the same order of magnitude with values fairly constants towards the base of the cores, except for the core sampled at the tripod site Be08-30m (close to the old pipeline) where around the 10 cm depth the porosity increases 0.12 towards the surface.

Finally, at the cores sampled at 40 and 50 m water depths, the mud (silt + clay) fraction dominated the sediment column with a percentage around 90 % with slightly changes in the median grain size and porosity, mostly in the upper centimeters of the cores. The bottom sediment properties display spatial variability across and along the shelf. In terms of across-shelf gradients, the median grain size increase with decreasing water depth. The porosity, however, behave in an opposite way increasing in water depth, specially, between 30 and 40 m isobaths. Along-shelf differences in bottom sediment properties were noted basically near the Besòs river mouth. The median grain size at the closest location (Be21-30m in Figure 4.3) was more than 140 μm at some layers of the core whereas where towards the south the median grain size fluctuated slowly with values between 30 and 15 μm. The porosity was quite similar between all sites along the 30 m isobath but slightly lower closest to the river mouth and at the Be08-30m tripod site (Figure 4.3 and Figure 4.2, respectively).

The bottom sediment spatial variability can also be observed in the mud content and median grain size distribution maps interpolated from grab sediment samples taken during the October 2007 and April 2008 monitoring surveys (Figure 4.1). The general pattern is an offshore increasing of the mud content that is modified near the river mouth. The median grain size distribution shows an area under the influence of the river sediment supply and an onshore coarsening gradient, more pronounced the further from the river mouth.

In Figure 4.1, a temporal coarsening trend of the bottom sediment is also appreciable between October 2007 and April 2008. In detail, Figure 4.4 shows the temporal variability, along the experiment, of the median grain size and porosity at the three tripod locations. Changes in grain size and porosity ranged from the surface to at least 8 cm at 20 m water depth and to at least 10 cm at 30 and 40 m water depths. At 20 m depth, the main change in the grain size distribution was a decreasing in median grain

size between September and November 2007, with a maximum vertical gradient in November 2007. Median grain size trended to a coarsening towards the end of the record (June 2008) ending in a uniform layer of 8 cm in thickness, in the fine sand fraction. In general, the variability of the porosity during the study period at that depth behaved opposite to the variability of the median grain size, decreasing with coarsening, but increasing with decreasing sediments grain size. Regarding to the 30 m site, there was a coarsening trend of the 2-3 surface centimeters from November 2007 to February 2008, ending in a finer quasi-uniform median grain-size distribution in the sediment column at the end of the study period (June 2008). Changes in porosity are associated to those changes in the median grain size increasing with decreasing sediment grain size. No major changes in grain size and porosity were observed at the deepest site because the grain size variability moves at very finer sediment range. However, the observed trend was also a coarsening towards the end of the record (June 2008) where the small patches of clayey sediment detected in previous sampling surveys disappeared.

Those changes in grain size and porosity described from the sediment cores and from the grabs showed a high spatial and temporal variability of the seabed. Changes in the sediment properties were observed to at least 8 cm depth of the sediment cores sampled at 20, 30 and 40 m water depth. This variability appears related to the seabed response to the forcing conditions occurred during the experiment as main changes in grain size and porosity were observed after periods of high wave and current energy.

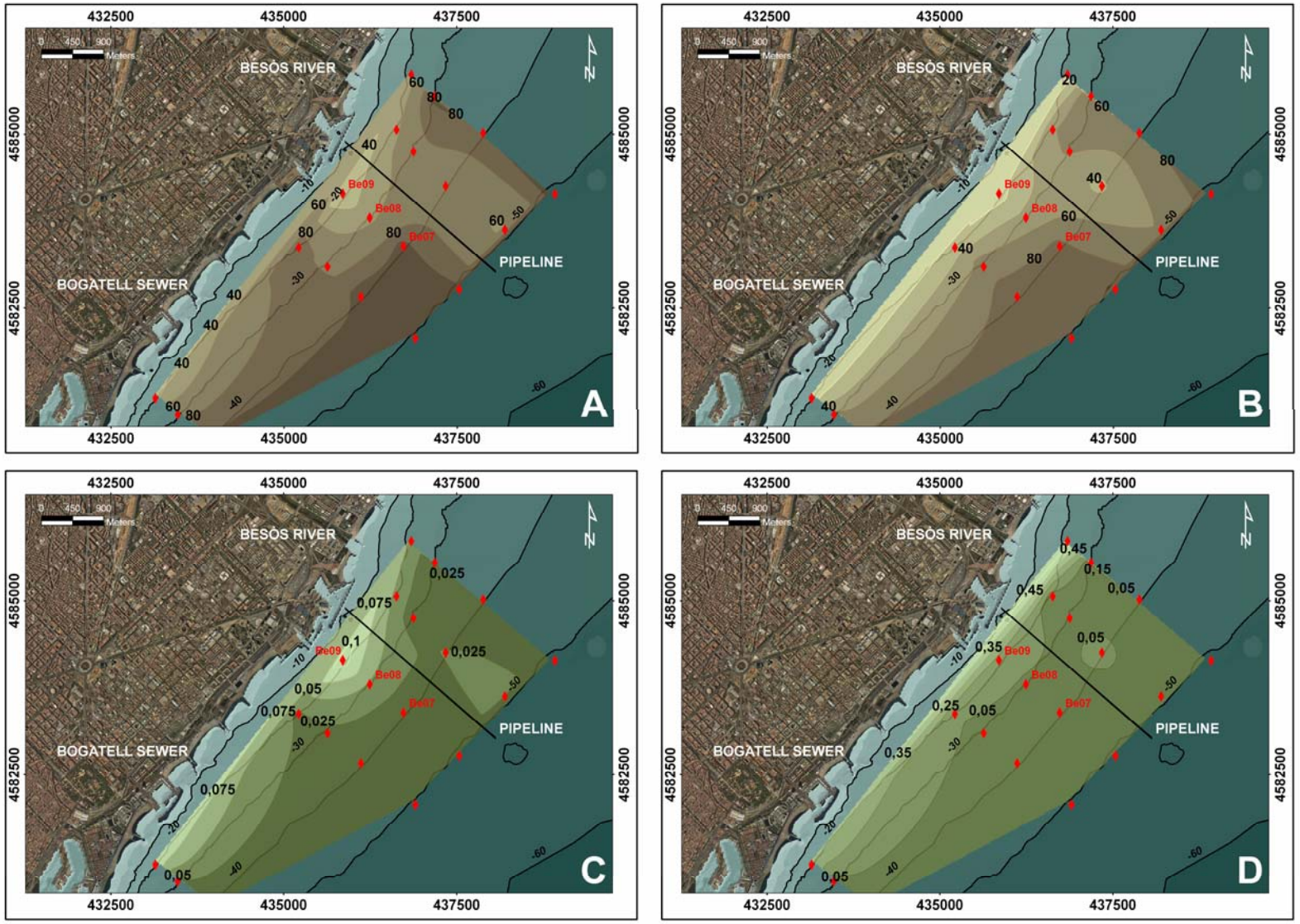

Figure 4.1. (A) and (B) Mud content (%) and (C) and (D) median grain size of the superficial bottom sediment from Barcelona continental shelf. Red diamonds correspond to the surface sediment samples (grabs) taken in October 2007 monitoring survey (A and C) and April 2008 monitoring survey (B and D). The black lines correspond to the bathymetry of the study area. The maps projection is UTM zone 31N datum ED50.

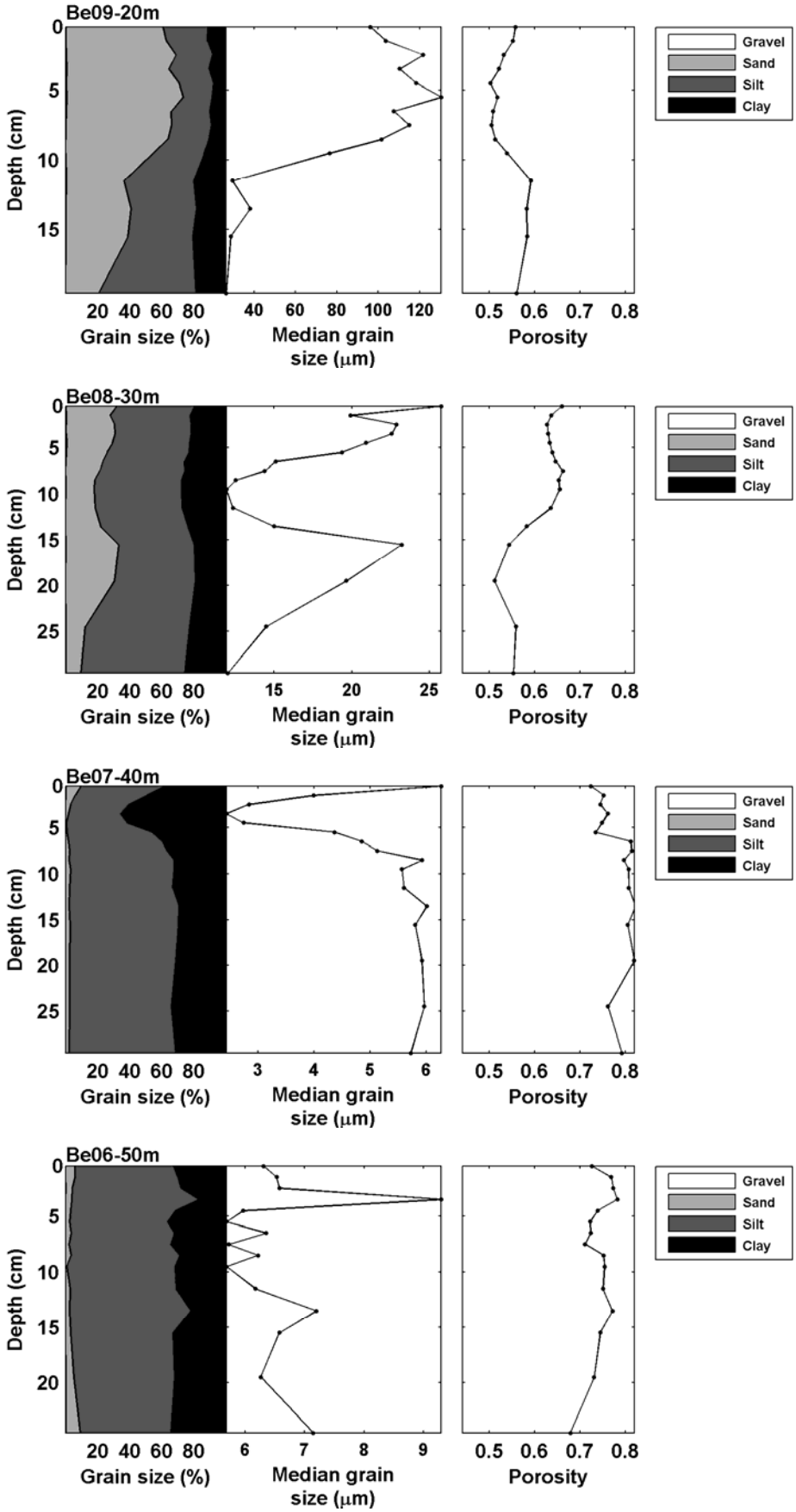

Figure 4.2. Down-core logs of grain size, porosity and organic and inorganic carbon content of the studied sediment cores taken in the tripods transect in September 2007. See location at Figure 2.5.

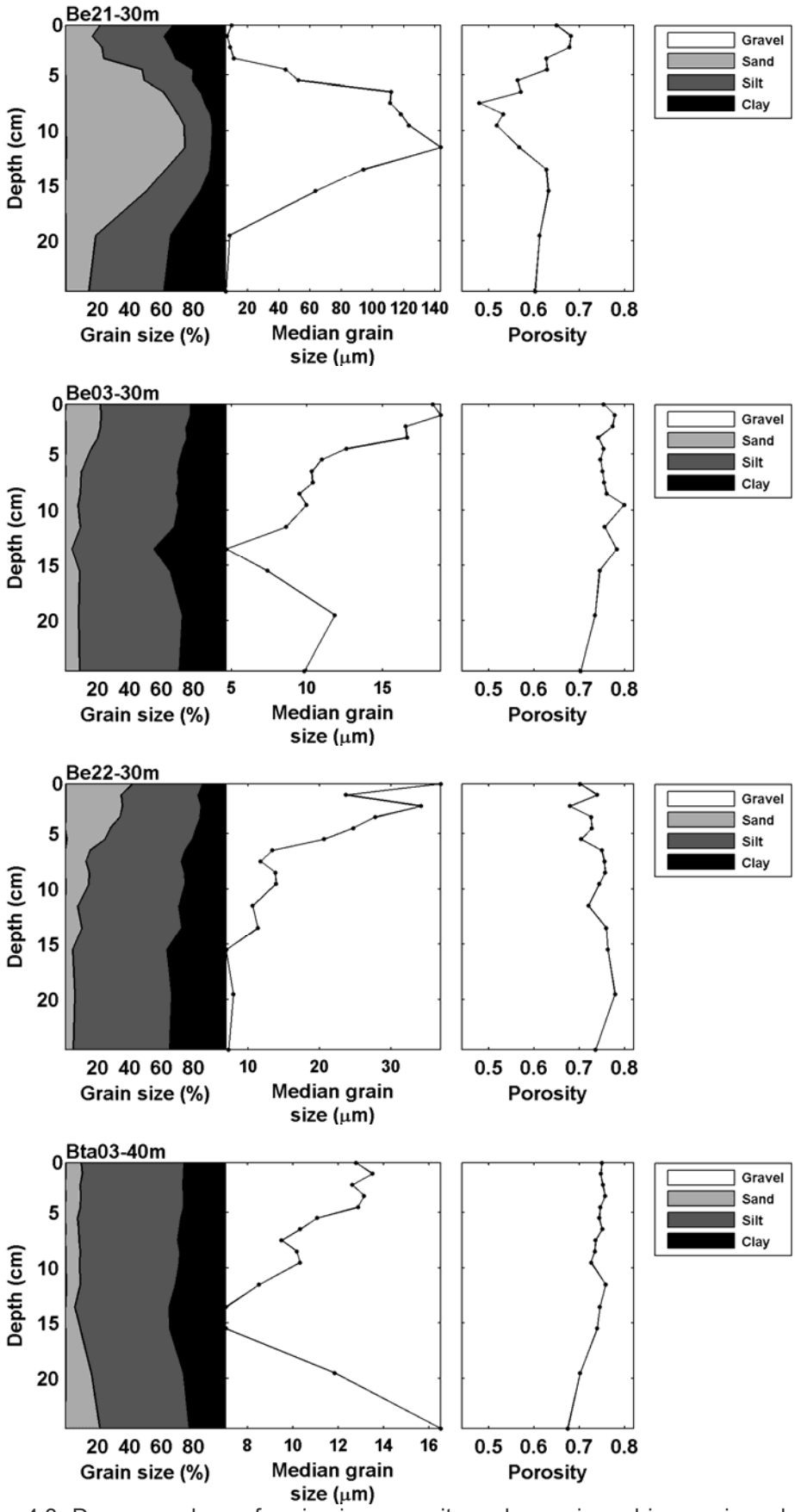

Figure 4.3. Down-core logs of grain size, porosity and organic and inorganic carbon content of the studied sediment cores taken at 30 m and 40 m depth in September, 2007. From north to south. See location at Figure 2.5.

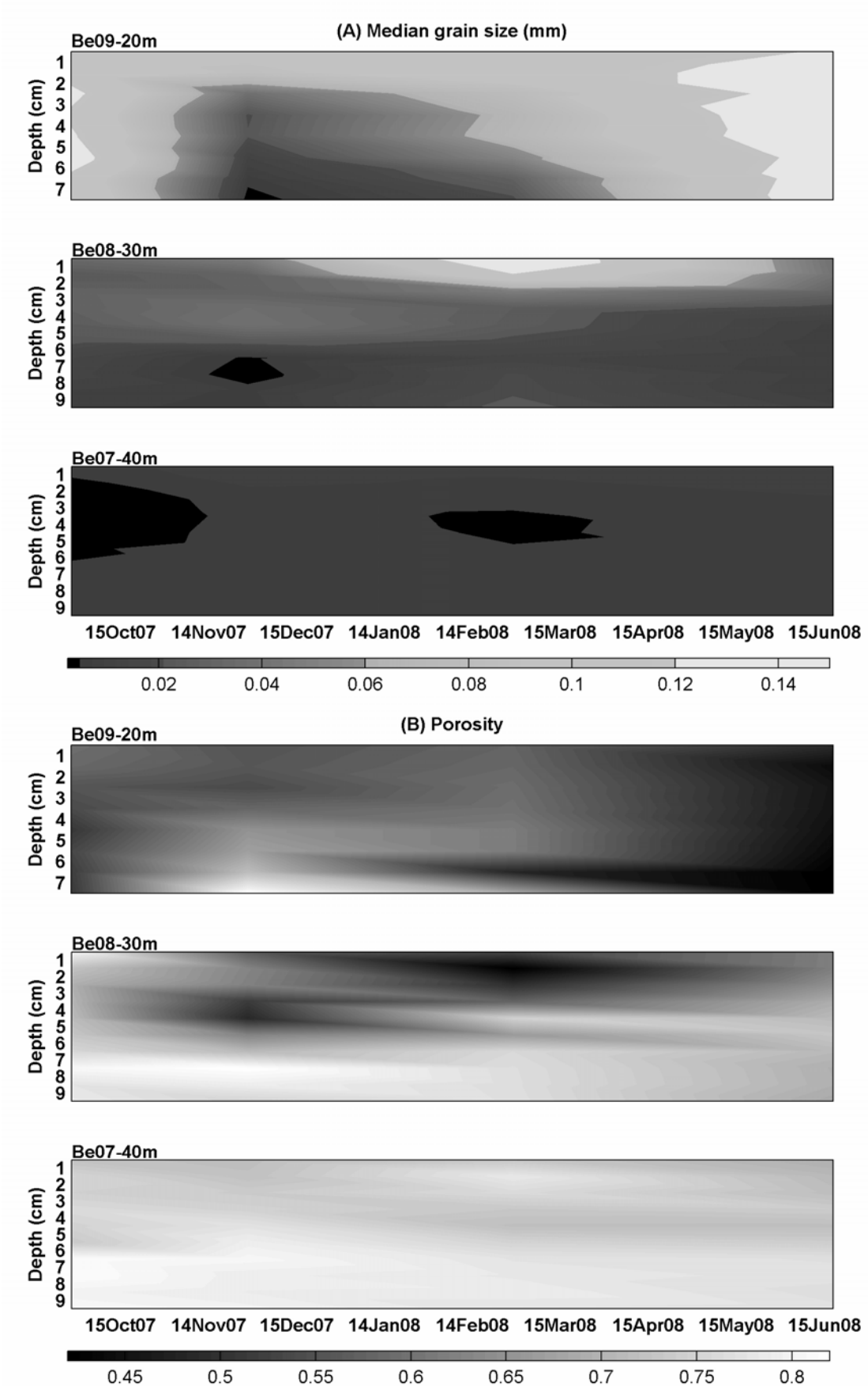

Figure 4.4. Temporal variability of (A) median grain size (d50 in mm) and (B) porosity between 0 and 10 cm depth of the cores sampled at 20, 30 and 40m water depth (Be09-20m, Be08-30m and Be07-40m sites) from figure top to bottom.

4.2 Particulate matter downward fluxes

Total downward fluxes collected by the traps during the deployment decreased with increasing water depth with mean values around 350 g/m^{2}d, 230 g/m^{2}d and 200 g/m^{2}d between 20 and 40 m isobaths. Many of the peaks of total mass flux were coincident in time at the different sites. Although in general terms, the total downward flux decreased with depth along the study period, there was a clear temporal variability in the amount of downward fluxes collected by the traps with a period of similar downward fluxes at 20 m and 30 m water depth. At 20 m depth, the maximum near bottom downward flux occurred between the 26th of October and the 1st of November 2007 with maximum values of 1100 g/m^{2}d. At that time, at 30 m water depth (Be08-30m site) the maximum downward flux was about 500 g/m^{2}d while the maximum flux collected by the trap took place between December 2007 and January 2008 coinciding with the strongest recorded storm (the 15th to 18th of December episode). During this episode, the traps collected 620 g/m^{2}d and 550 g/m^{2}d at the 20 m and 30 m depth sites, respectively. At 40 m depth (Be07-40m site) the maximum flux event coincided with the same period of the Be09-20m site with a maximum downward flux of 363 g/m^{2}d.

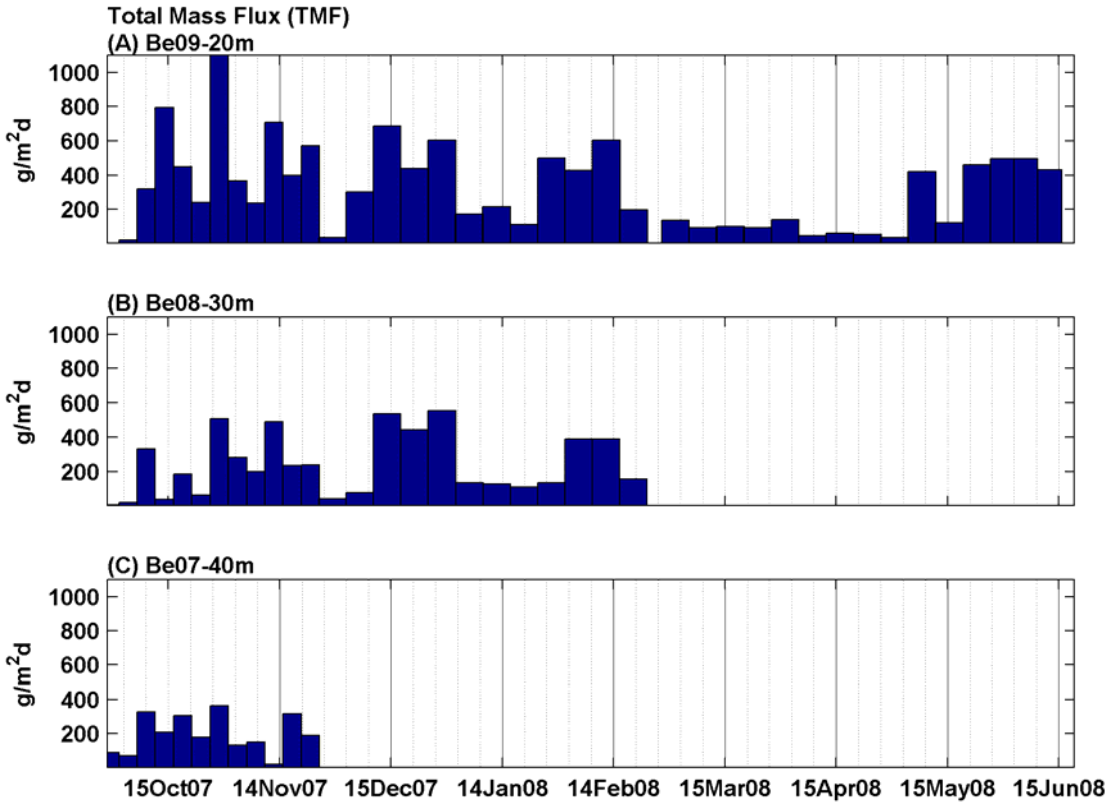

Figure 4.5. Bar graphs illustrate the time series of total mass fluxes of particulate matter for each sediment trap during the study period: (A) Be09-20m trap at 20 m water depth, (B) Be08-30m trap at 30 m depth and (C) Be07-40m trap at 40 m water depth.

The temporal variability of median grain size in the traps sediment samples (Figure 4.6) showed a coarsening trend from clay to very-fine sand between October and late December 2007 at both sites, 20 and 30 m depth, corresponding with the most energetic period in terms of storm activity. After that, the suspended sediment samples at 20 m depth showed some fluctuations in the median grain size distribution coinciding with times of relatively increasing of wave and current intensities. However, in the samples available from that time at the 30 m site the median grain size decreased sharply and no fluctuations were observed.

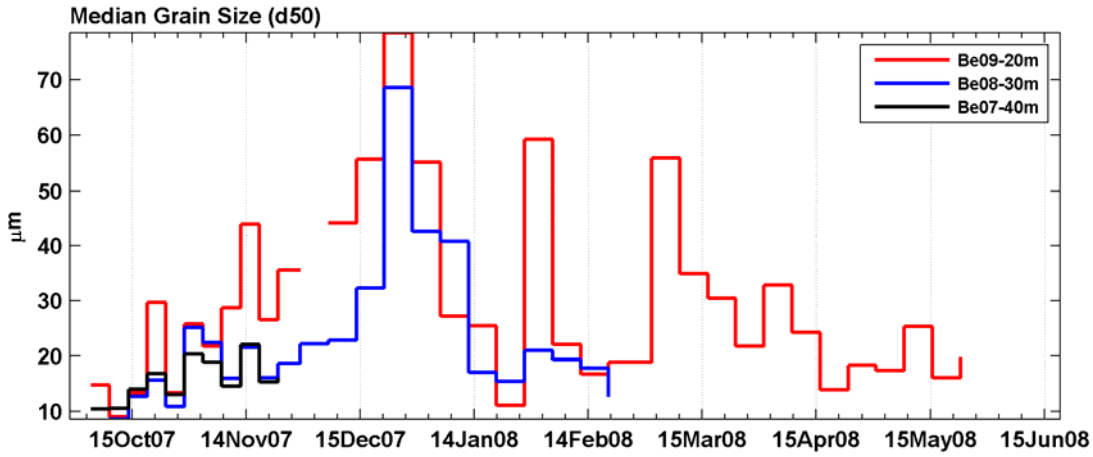

Figure 4.6. Temporal variability of the median grain size (d50 in µm) of the trap samples collected at the tripod sites (Be09-20m, Be08-30m and Be07-40m) during the experiment.

4.3 Near-bottom suspended sediment concentration and shear stress

The near-bottom suspended sediment concentration (SSC) and shear stress during the recording period also showed a high temporal and spatial variability. Across the shelf at 0.53 mab, the SSC reached values up to 90 mg/l at 20 m, up to 70 mg/l at 30 m water depth and up to 35 mg/l at 40 m water depth during autumn 2007 and winter 2008 (Figure 4.7, Figure 4.8 and Figure 4.9, respectively). However, the maximum of SSC at the 20 m water depth site was recorded at mid May, during a period of relatively increase in wave and river activity (Figure 3.1), when the SSC reached about 140 mg/l at the 20 m depth site. Although in general terms, the near-bottom SSC decreased with depth, there were two events with SSC values equal or even higher at 30 m than at 20 m depth. Both events occurred between December 2007 and January 2008, the first one, classified as the strongest recorded storm (the 15th to 18th of December episode), generated an increment of SSC about 70 mg/l at 30 m depth while at 20 m the concentration values were about 40 mg/l.

Wave induced stress dominated over that caused by currents at all sites (Figure 4.7, Figure 4.8 and Figure 4.9), with wave shear velocity (U_{*w}) generally 2 or 3 times larger than the current shear velocity (U_{*c}). The bed shear stress averaged 0.11 N/m^2, 0.04 N/m^2 and 0.03 N/m^2 but reached as high as 2.1 N/m^2, 1.3 N/m^2 and 0.6 N/m^2 at 20 m, 30 m and 40 m water depth sites, respectively. Along the study period, wave and current shear velocities decreased with increasing depth across the shelf, but current shear velocities were about the same magnitude at 30 m and 40 m isobaths.

As observed in previous sections, three different periods can be also identified analyzing the variability of the SSC and shear stress along the experiment: A first period of high frequency of SSC peaks corresponding to relatively high shear stresses during autumn and early winter; a second period of lower near-bottom suspended sediment concentration under fair-weather conditions with intermittent increments in shear stress and; a third period, from early May 2008 to end of the recording period, of relatively high near-bottom SSC associated with an increase in wave activity but especially in river discharge.

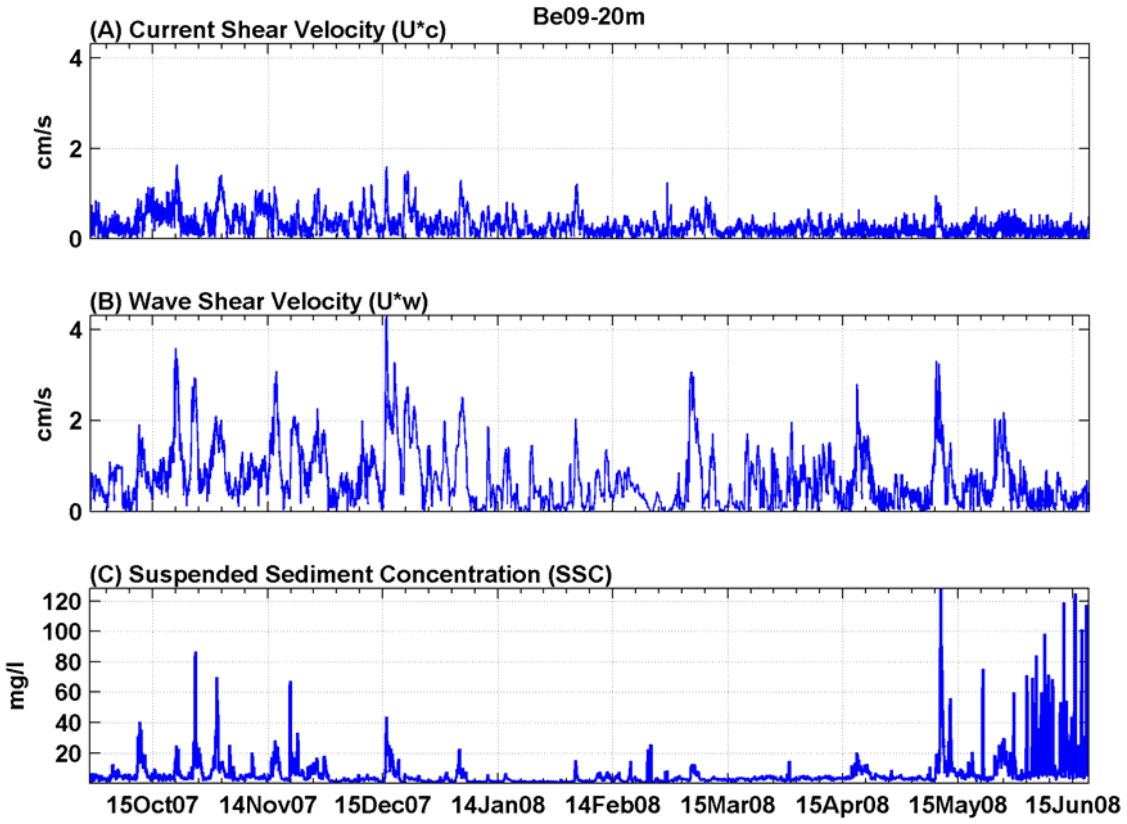

Figure 4.7. Time series of (A) current shear velocity, (B) wave shear velocity, and (C) SSC at 20 m depth (Be09-20m site).

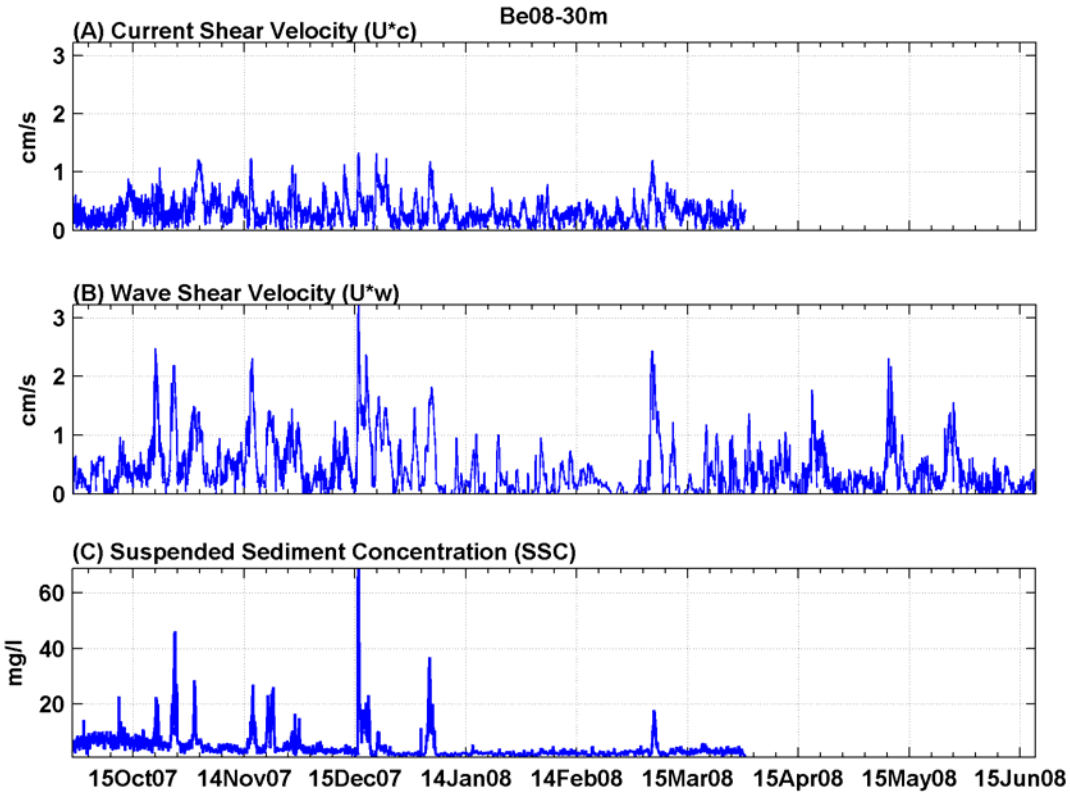

Figure 4.8. Time series of (A) current shear velocity, (B) wave shear velocity, and (C) SSC at 30 m depth (Be08-30m site).

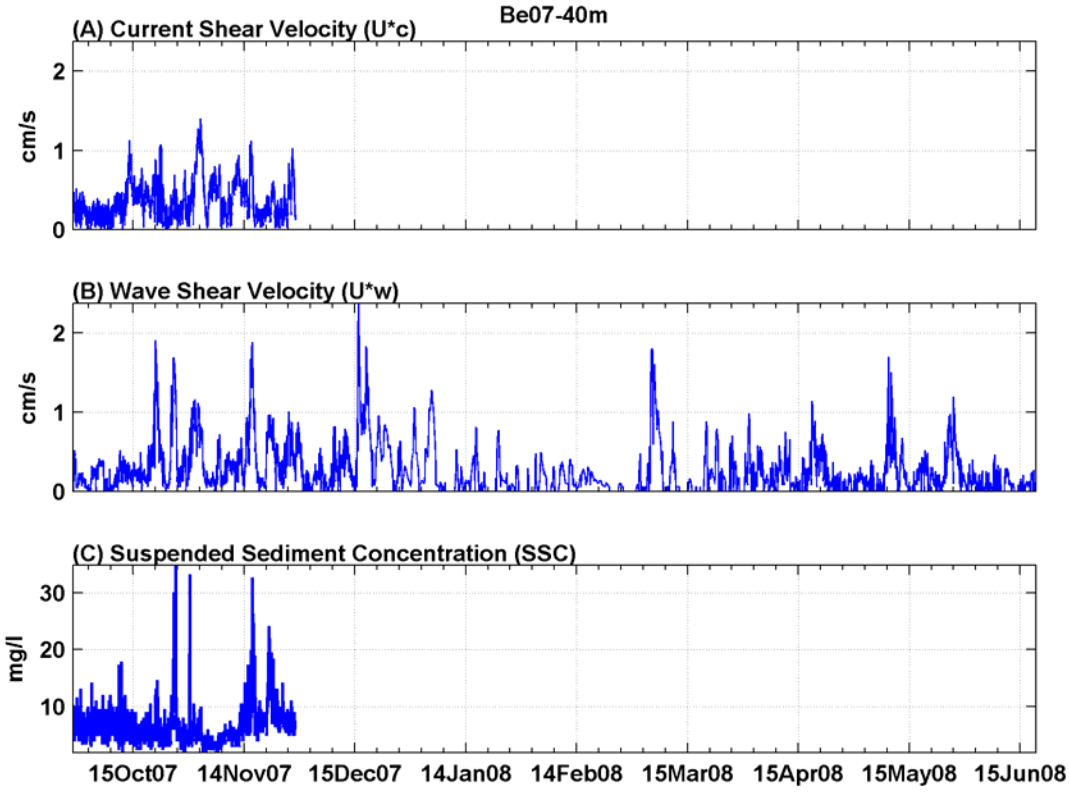

Figure 4.9. Time series of (A) current shear velocity, (B) wave shear velocity, and (C) SSC at 40 m depth (Be07-40m site).

4.4 Factors controlling SSC

River sediment inputs and bed shear stresses change seabed texture (grain size, sorting, grading) modifying the availability of fine-grained sediment on the seabed and therefore, the SSC during resuspension events. In this sense, Guillén et al., (2006) analyzed sediment flux observations from the inner shelf offshore of the Têt River in the Gulf of Lions. They showed the influence of the formation of flood-derived deposits (ephemeral layers) previously to a storm passage that enhanced bottom sediment erodibility and SSC respect to other storms because of the higher porosity and water content of the fresh sediment. Conversely, shear stresses preferentially resuspend finer-sediment leaving a coarser layer of sediment at the bed surface that prevents the flow from suspending underlying fine sediment ("bed armouring"; Wiberg et al., 1994) and limiting sediment availability and SSC during resuspension events.

During the study period, increases of suspended sediment concentration at all tripod sites are consistent with higher bed shear stresses, with SSC peaks close to the peak of the storms (Figure 4.7, Figure 4.8 and Figure 4.9). The importance of surface gravity waves in shelf sediment flux has been reported by many studies (e.g., Cacchione et al., 1995; Sherwood et al., 1994), so this association is not unexpected and it is indicative of resuspension of bed sediment induced by the wave shear stress. However, the current shear velocity during periods of high SSC were not as different as other times when there was an increment in current shear velocity but not in SSC and therefore, resuspension was not associated to the current shear stress.

In the other hand, the relatively high river discharge during May and June 2008 induced a period of a significant increment in SSC not associated to high shear stresses (Figure 4.7). This association of near-bottom suspended sediment concentration and river discharge suggests that riverine sediment reached directly the seabed at least at 20 m water depth registering values of SSC three orders of magnitude above the background level and therefore, the formation of a temporal bottom nepheloid layer at this location.

When wave storms and river floods occurred at the same time, the additional sediment discharged from the river can increase the suspended sediment concentration near the bottom (Ogston et al., 2000; Fan et al., 2004). Early autumn and some spring events during which wave storms coupled with increased river water discharge reached higher values of SSC than during other events with similar wave energy conditions but without

simultaneous river discharge. Indeed, the maximum SSC at 20 m water depth was recorded during the highest river water discharge coupled with one of the most energetic storm of the experiment (10^{th} – 15^{th} of May 2008).

In many cases, the comparison between bed shear stress and the SSC during waves events reveals a lack of proportionality suggesting that the conditions of the bottom sediment previous to resuspension were different between events. From the sequence of events occurred between October 2007 and January 2008 at 20 m water depth can be derived that the Besòs river delivered riverine sediment into the shelf that conditioned directly or indirectly the SSC during intermixed and subsequent wave storm events. Waves and river inputs increased SSC up to 90 mg/l during October 2007 probably leaving a deposit of fresh sediment in shallow waters (ephemeral layer). During the subsequent storms occurred in November 2007, the SSC reached values higher than expected considering wave conditions (around 70 mg/l) because the higher erodibility of the flood-derived storm deposits generated during preceding events. The December 2007 and January 2008 waves storms were much more energetic but the SSC was less of 50 mg/l presumably because all the fine particles in shallow areas had already been winnowed by the preceding storms. This interpretation is consistent with the downward fluxes and grain-size variability of the suspended sediment collected by the sediment traps (section 4.2). During the October and November 2007 events, total downward fluxes at 20 m water depth registered their maximum of the study period with a median grain-size around 30-40 μm. During December 2007 and January 2008 events, the median grain-size was much larger (around 60-80 μm) but the downward fluxes were lower than the preceding period indicating a lower bottom sediment erodibility during resuspension events. Therefore, the chronology of the events on the shelf plays a crucial role in SSC, since small storm events can produce larger SSC depending on the sequence of previous flood and storm event.

Although riverine sediment inputs and bed shear stresses decrease with increasing water depth during the study period, the influence of these processes was also observed at deeper areas of the inner shelf (Be08-30m and Be07-40 m sites). Changes in the textural characteristics of the bottom sediment occurred at least 8 cm below the water-sediment interface, at the three tripods sites (section 4.1). The across shelf gradient in critical shear stress was then modified and therefore, the availability of resuspendable sediment. The mean critical shear stress of the bottom sediment median grain size was estimated in 0.142 N/m^2 for the 20 m water depth site, 0.094 N/m^2 for the 30 m site and 0.031 N/m^2 for the 40 m site. At the beginning of the study

period, the offshore gradient in critical shear stress was estimated in -0.13 mPa/m and -0.08 mPa/m between 20 m and 30 m and 30 m and 40 m isobaths, respectively, with similar values in November 2007 and June 2008 (Figure 4.10). However, the coarsening of the surface layer observed at 30 m depth (section 4.1) in February 2008 reduced drastically the estimated offshore gradient in critical shear stress of the bottom sediment between 20 m and 30 m water depth sites. This suggests that the December 2007 and January 2008 storms removed fine-grained sediment from the 30 m water depth presumably because the limitation of fine-grained sediment at shallow areas. This is consistent with the higher values of SSC and downward sediment fluxes recorded at this depth compared to the values obtained at 20 m water depth during the same events. Therefore, the across shelf variation of sediment availability (i.e. critical shear stress gradients) also plays an important role in SSC, since the same storm produce larger SSC in deeper waters depending on the availability of resuspendable sediment across the inner shelf.

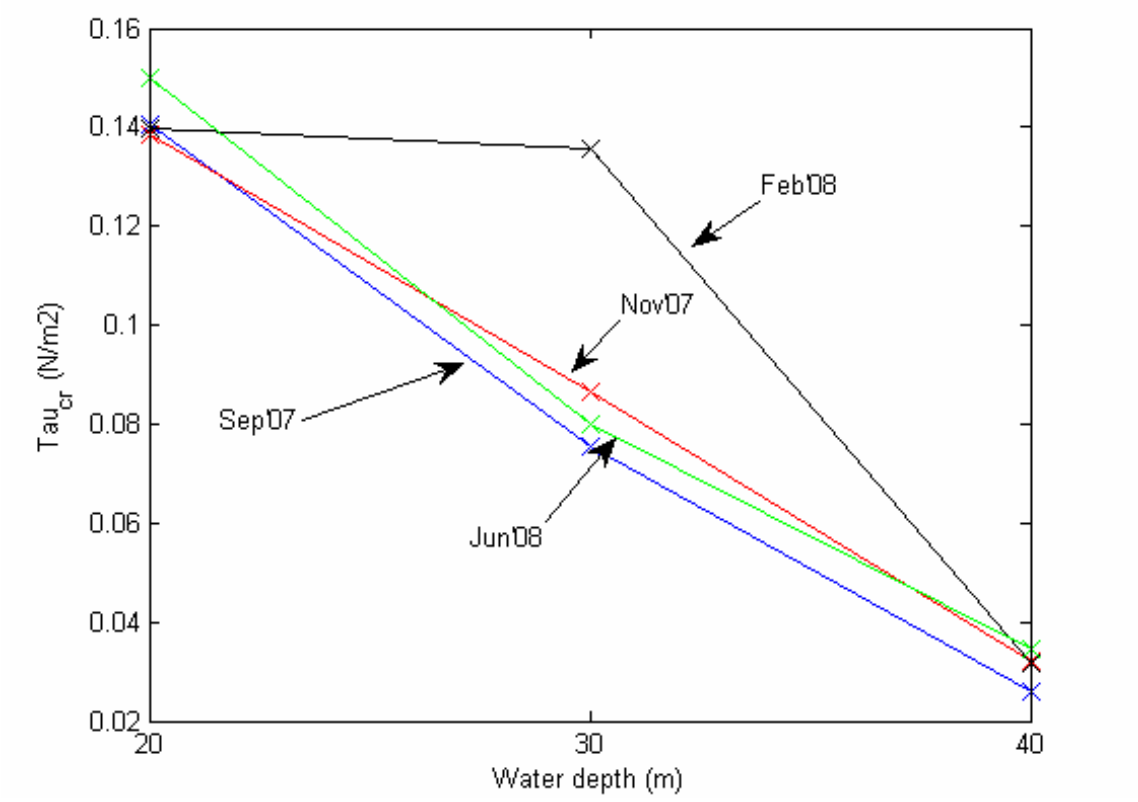

Figure 4.10. Temporal variability of the across-shelf critical shear stress estimated for median grain size of sediment samples from the inner-shelf off Barcelona.

5 Patterns of sediment transport

The observations analyzed in previous sections show the episodic characteristics of wave storms, increments in river discharge and near-bottom currents in the Barcelona inner shelf and suggest that near-bottom suspended sediment concentration (SSC) was induced by resuspension produced by relatively large waves and sediment inputs by the Besòs River. These mechanisms placed sediment into the water column which were transferred by currents to other areas of the shelf.

This section discusses near-bottom sediment fluxes in terms of temporal and spatial variability in the study area during the period comprised between September 2007 and June 2008 (Table 5.1). In addition, the applied 1D shelf sediment transport model used to estimate the concentration of sediment in suspension and sediment transport during resuspension events (Wiberg et al., 1994) is correlated against observed SSC during the study period at 20 and 30 m water depth. In particular, the most significant resuspension event from the study period is accurately analyzed in order to validate the estimation of vertically integrated sediment fluxes during a resuspension event in the inner-shelf off Barcelona. Near-bottom sediment transport rates across the inner shelf are then addressed from observational and modeled data with the aim of understanding sediment transport gradients and erosion/deposition patterns across the inner continental shelf of Barcelona.

5.1 Near-bottom sediment fluxes

In order to address sediment transport patterns in the area under study, sediment flux events and non-events intervals were defined from the sediment magnitude flux calculations using the current and SSC measurements at site Be09-20m (see criteria in section 2.3.4). Fourteen sediment flux events were identified between September 2007 and June 2008 (Figure 5.1). These included eight sediment transport events during autumn 2007, two events during winter 2007-2008 (January – February 2008) and four events during spring 2008 (May –June 2008). Note that event A and H were divided into two sub-events due to the occurrence of significant changes in the hydrodynamics during the events (Table 5.2).

During the study period, the magnitude of the instantaneous near-bottom sediment flux reached maximum values of 15, 14 and 4.5 g/m^2s at 20 m, 30 m and 40 m water depths, respectively (Figure 5.1). In general, the magnitude of the instantaneous

sediment flux decreased offshore, except in events H and I (December 2007 and January 2008 storms) when it was higher at 30 m than at 20 m water depth. Mean and net near-bottom sediment fluxes during the three deployments are shown in Table 5.1. The mean sediment flux was higher during the first deployment (September – November 2007). To compare between the three locations, the mean sediment flux from September to November 2007 was 584 mg/m^{2}s at the 20 m site, 462 mg/m^{2}s at 30 m water depth and 473 mg/m^{2}s at 40 m water depth. The mean along-shelf near-bottom flux was higher than the across-shelf flux at all recording sites, specially at shallow water (Table 5.1), with an across/along relation increasing offshore. In addition, the percentage of the along-shelf transport represented a 77 % of the total near-bottom sediment transport occurred in autumn when the majority of the defined events occurred, 44 % during winter and 58 % during spring when less energetic processes controlled the near-bottom sediment transport at the 20 m isobath. This implies that along-shelf sediment fluxes were controlled by the largest storms, whereas across-shelf fluxes also occurred as the sum of less energetic processes.

Sediment flux events at 0.58 mab represented the 54 % of the total sediment flux along the study period. The contribution of the events, however, differed along each season, which represented the 70 %, 34 % and 53 % in autumn, winter and spring, respectively. This is roughly proportional to the number of events in each season. During autumn a high frequency of moderate eastern wave storms, moderate river discharge and greater current magnitude characterized the near-bottom sediment flux events (events A to H). Two moderate storm (events I and J) occurred in winter and two river discharge combined with two southern wave storms (events K, L, M and N) in spring , contributed to the total near-bottom sediment flux.

In autumn 2007, near-bottom sediment fluxes decreased with increasing depth as a result of the offshore decrease in wave shear stress, current speed and SSC. The instantaneous sediment flux reached values one order of magnitude higher than the background level (12 g/m^{2}s – event D) at the shallowest site (Be09-20m), while at 30 m and 40 m water depths the instantaneous flux was under 5 g/m^{2}s. At the end of autumn and beginning of winter 2007-2008, the excess of shear stress, the SSC and the current speed increased offshore. Under these conditions, the magnitude of the sediment flux was higher at 30 m depth than at 20 m during most of the storms, with peak values of 14 g/m^{2}s and 9 g/m^{2}s (event H_1 and I, respectively).

Spring 2008 was characterized by a notable increment in river discharge that lasted more than one month. The near-bottom sediment flux reached the maximum of the study period at 20 m water depth with values of 15 g/m^{2}s during event K. After this event, wave and current energy decayed and the sediment flux was induced mainly by the high SSC associated to the river discharge (events L, M and N).

	Sept - Nov 2007			Nov 2007 - Feb 2008		Feb 2007 - June 2008
Near-bottom fluxes in mg/m^{2}s	**20 m**	**30 m**	**40 m**	**20 m**	**30 m**	**20 m**
Mean alongshelf flux	530	376	401	178	223	203
Mean across-shelf flux	158	223	203	50	114	138
Mean flux	584	462	473	192	260	269
Net flux	106	117	45	53	180	17
Net flux direction (º)	94	256	38	104	111	90

Table 5.1. Near-bottom sediment fluxes in mg/m^{2}s at the tripod locations during the three surveys.

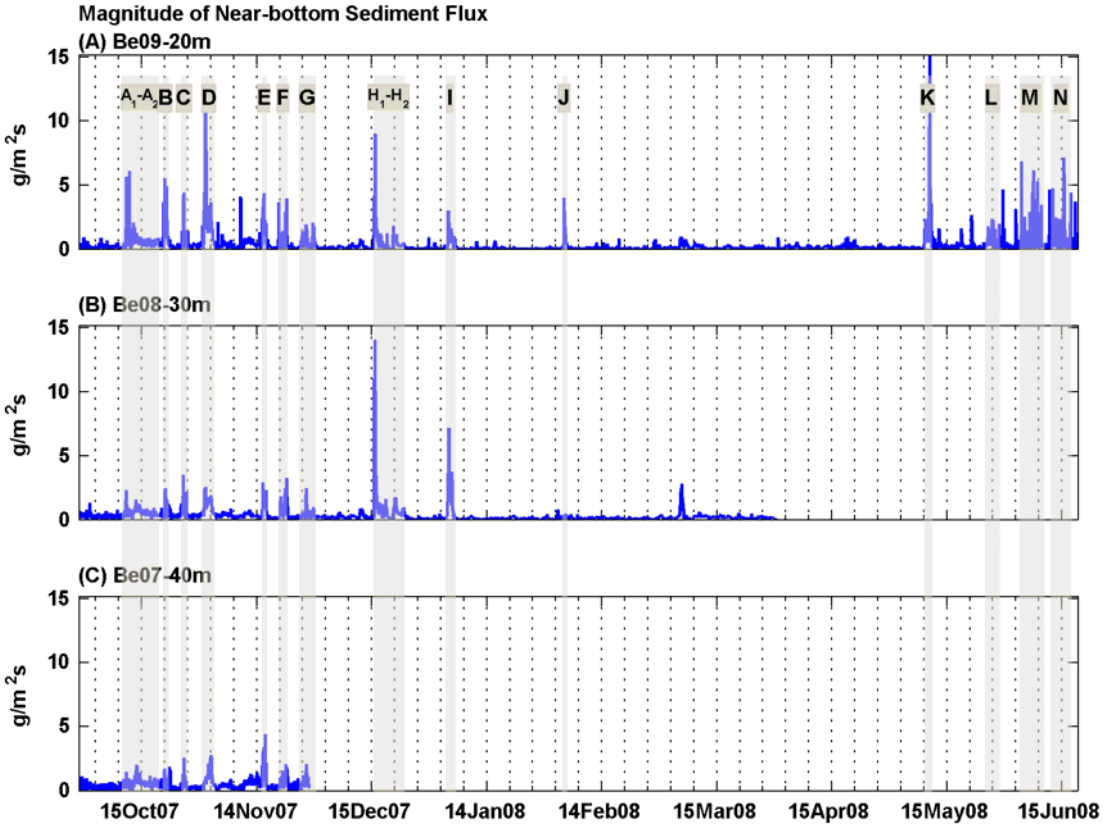

Figure 5.1. Time series of the magnitude of sediment flux near the bottom at the three tripod locations. (A) Be09-20m at 20 m depth, (B) Be08-30m at 30 m depth and (C) Be07-40m at 40 m depth. Letters indicated the selected sediment fluxes events defined at site Be09-20m.

Event	Date: Start / Peak	Duration (h)	Sediment flux (g/m2s)	Ub (cm/s)	Wave dir	River water dis. (m3/s)	SSC (mg/l)	Current (cm/s)		Wind (m/s)	
								Speed	Dir	Speed	Dir
A_1	11-oct-07 00:18	29	*1.7*	*15.7*	*96º*	*4.3*	*16.7*	*10.5*	*128º*	*10.0*	*43º*
	11-oct-07 21:18		**6.1**	**33.0**	**82º**	**9.1**	**44.3**	**17.6**	**220º**	**11.1**	**46º**
A_2	12-oct-07 05:38	194	*0.6*	*10.0*	*100º*	*4.7*	*5.4*	*12.7*	*49º*	*6.3*	*56º*
	12-oct-07 23:58		**2.1**	**27.1**	**101º**	**15.8**	**22.2**	**26.1**	**43º**	**10.4**	**44º**
B	20-oct-07 18:38	35	*1.7*	*48.5*	*78º*	*2.8*	*10.5*	*16.5*	*180º*	*6.3*	*69º*
	21-oct-07 07:38		**5.6**	**72.4**	**77º**	**2.8**	**21.3**	**24.1**	**213º**	**14.4**	**59º**
C	25-oct-07 19:38	36	*0.9*	*38.6*	*88º*	*5.8*	*26.3*	*3.3*	*143º*	*5.8*	*68º*
	26-oct-07 07:38		**4.4**	**60.3**	**76º**	**7.7**	**92.3**	**8.8**	**232º**	**8.8**	**30º**
D	31-oct-07 12:58	72	*2.4*	*24.0*	*100º*	*2.8*	*16.6*	*16.2*	*43º*	*4.6*	*49º*
	01-nov-07 00:58		**12.3**	**39.5**	**132º**	**2.9**	**78.0**	**27.6**	**56º**	**8.7**	**32º**
E	16-nov-07 01:38	29	*2.0*	*45.0*	*95º*	*2.9*	*19.1*	*10.3*	*202º*	*4.5*	*69º*
	16-nov-07 12:18		**4.4**	**62.2**	**92º**	**3.0**	**27.5**	**21.1**	**217º**	**8.3**	**9º**
F	20-nov-07 09:58	56	*0.8*	*29.8*	*98º*	*3.0*	*15.9*	*5.0*	*175º*	*3.0*	*217º*
	22-nov-07 10:38		**3.9**	**40.0**	**87º**	**3.0**	**33.7**	**15.0**	**221º**	**7.5**	**202º**
G	26-nov-07 00:18	90	*0.7*	*24.3*	*100º*	*2.9*	*8.5*	*7.7*	*103º*	*6.9*	*77º*
	27-nov-07 16:58		**1.8**	**39.8**	**83º**	**3.0**	**11.6**	**22.9**	**216º**	**13.3**	**37º**
H_1	15-dec-07 15:38	93	*1.0*	*43.4*	*89º*	*3.0*	*13.0*	*5.9*	*167º*	*7.3*	*52º*
	15-dec-07 22:58		**9.1**	**91.0**	**87º**	**3.0**	**48.9**	**24.1**	**224º**	**13.5**	**60º**
H_2	20-dec-07 16:38	74	*0.5*	*34.1*	*84º*	*3.1*	*3.5*	*14.2*	*222º*	*10.3*	*58º*
	21-dec-07 11:58		**1.8**	**49.1**	**109º**	**3.1**	**7.8**	**27.0**	**217º**	**13.8**	**86º**
I	03-jan-08 17:18	61	*0.8*	*32.6*	*104º*	*3.7*	*8.0*	*10.2*	*187º*	*5.4*	*264º*
	04-jan-08 08:18		**3.0**	**47.8**	**55º**	**6.1**	**24.1**	**23.8**	**219º**	**8.9**	**351º**
J	03-feb-08 22:37	21	*1.3*	*21.6*	*205º*	*4.8*	*6.9*	*18.5*	*49º*	*8.9*	*250º*
	04-feb-08 03:17		**4.0**	**32.5**	**191º**	**5.7**	**15.8**	**24.6**	**51º**	**10.9**	**202º**
K	09-may-08 12:39	48	*2.3*	*40.1*	*129º*	*15.0*	*36.2*	*7.6*	*208º*	*8.8*	*79º*
	10-may-08 23:38		**15.2**	**66.6**	**131º**	**18.4**	**145.9**	**15.0**	**201º**	**13.0**	**78º**
L	25-may-08 22:19	86	*0.6*	*23.6*	*121º*	*7.2*	*15.5*	*3.9*	*168º*	*4.1*	*227º*
	27-may-08 10:18		**2.4**	**41.3**	**111º**	**11.8**	**29.0**	**12.3**	**182º**	**7.7**	**241º**
M	03-jun-08 19:39	157	*0.6*	*3.1*	*171º*	*10.6*	*17.5*	*3.4*	*158º*	*3.6*	*159º*
	04-jun-08 07:59		**6.9**	**13.6**	**150º**	**17.3**	**83.8**	**12.9**	**143º**	**7.7**	**240º**
N	12-jun-08 04:39	129	*0.7*	*1.9*	159º	*6.7*	*20.5*	3.8	113º	*3.4*	*164º*
	15-jun-08 13:59		**7.2**	**5.2**	**212º**	**10.4**	**119.1**	**14.1**	**53º**	**7.2**	**222º**

Table 5.2. Characteristics of sediment flux events at 20 m water depth from September 2007 to June 2008. Italic and bold numbers correspond to mean and maximum values, respectively.

5.2 Evaluation of a 1D Sediment transport model

Using measured hydrodynamic times series as model inputs to calculate the suspended sediment concentration and verified at a reference level against tripod turbidity measurements allowed the evaluation of the model procedure. The model runs were performed with the times series from Be09-20m and Be08-30m sites.

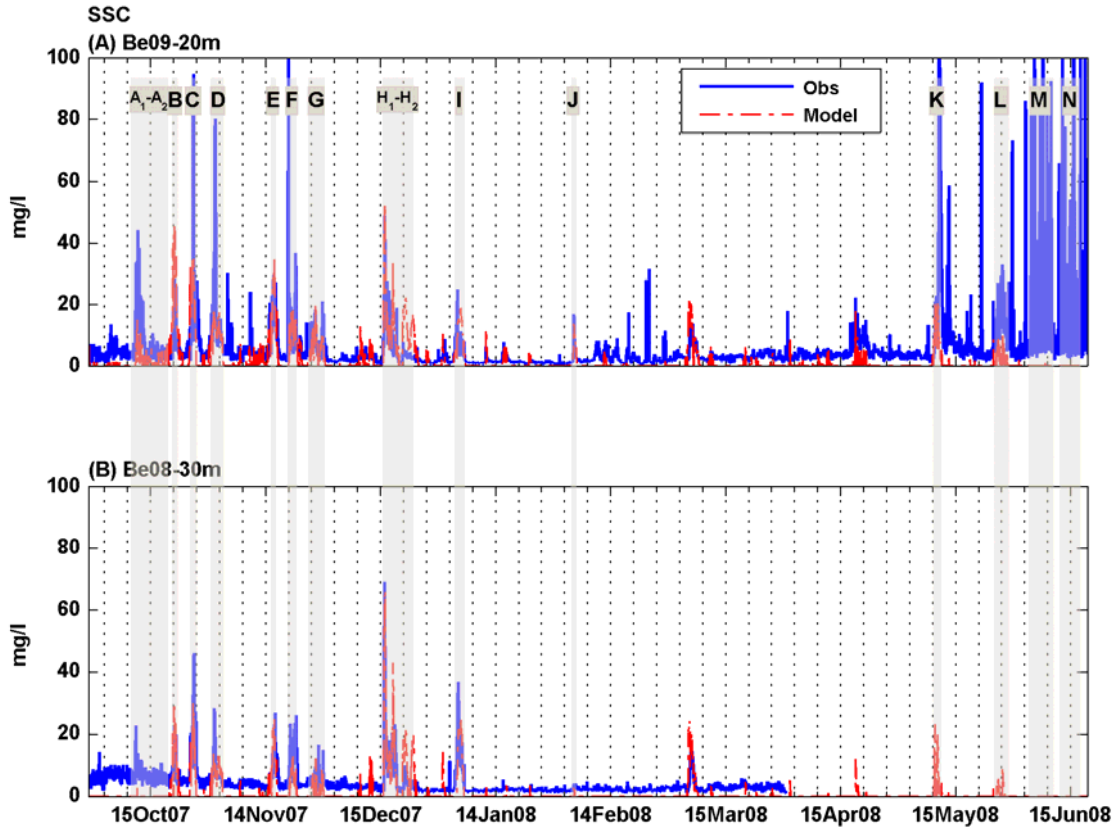

Figure 5.2. Model evaluation of observed (blue) and calculated (red) SSC at 0.53 mab at sites (A) Be09-20m and (B) Be08-30m.

In terms of resuspension events frequency and relative magnitude between events, the model performed very well and agreed with the observational data. At all tripod locations, the highest frequency of modeled suspended sediment concentration occurred during autumn 2007 as observed. In general terms, observed and modeled SSC were about the same order of magnitude along the study period. The model clearly capture the most significant resuspension event during the measurement period (event H_1) at both sites, also capturing the higher value of SSC at 30 m water depth respect to the shallower site. The subsequent resuspension events occurred until March 2008 (events H_2, I and J) were also capture and agreed strongly with the observational data.

However, during some events of increased SSC associated to increments in shear stress, model results were slightly low compared to measurements (e.g. events A, D and G). Additionally, there were also observations of elevated SSC that did not correspond to elevated bed shear stresses (e.g. M and N at Be09-20m), but coincided with periods of elevated river water discharge. Therefore, it is evident that the model does not adequately reproduces all observations and that these discrepancies may be

partially related with seasonal and eventual changes in bottom sediment properties no detected during the sediment sampling interval. These changes were usually associated to either advection of SSC resuspended elsewhere, changes during and after a storm event or riverine inputs.

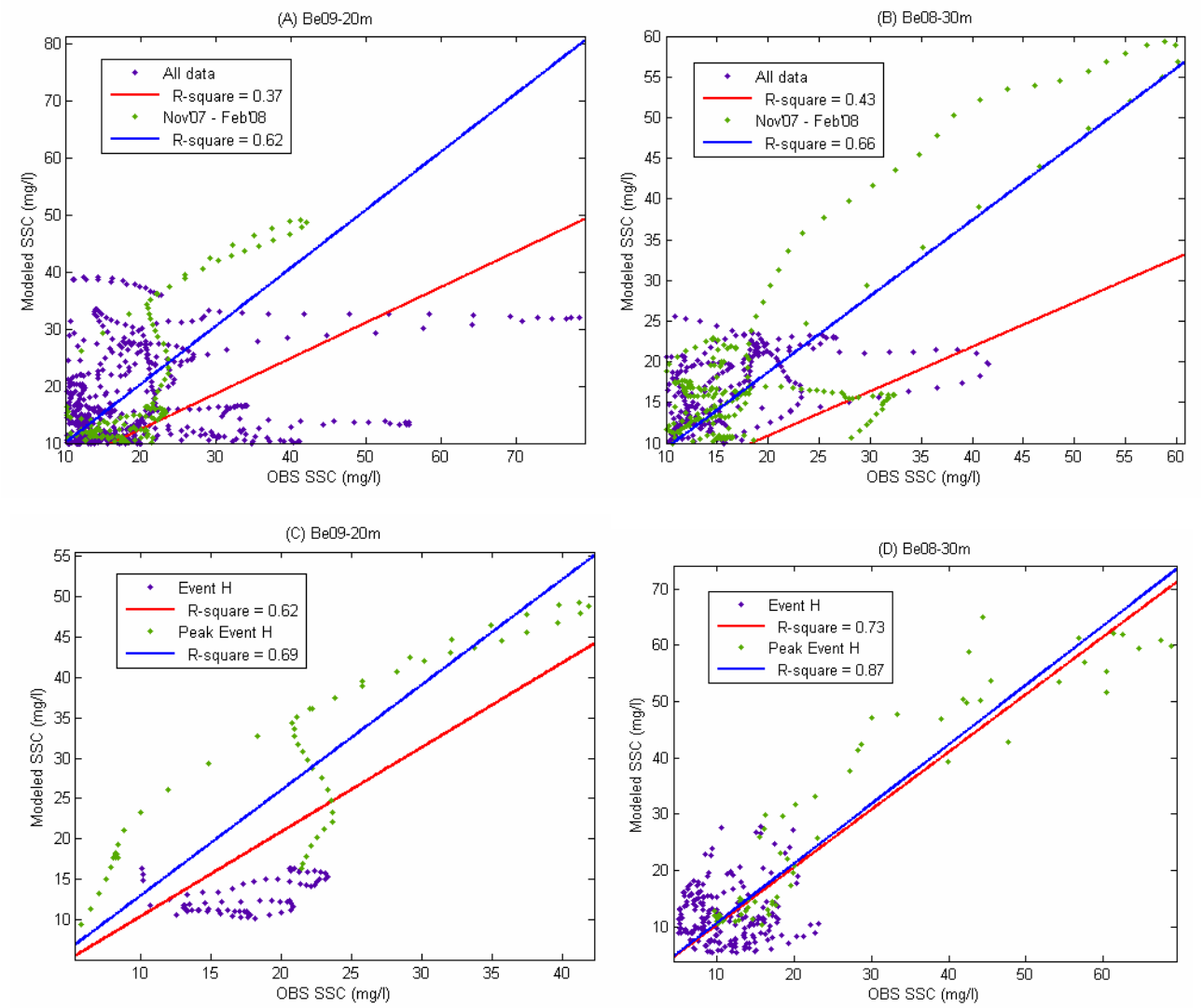

Figure 5.3. Correlation forced to zero between observed data (after removing background levels) and model results: (A) and (B) along the study period and between December 2007 and February 2008 at Be09-20m and Be08-30m, respectively; and (C) and (D) for the December 2007 storm and at the peak of the event at Be09-20m site and Be08-30m site, respectively.

The correlation between observed and modeled SSC (after removing background levels) obtained along the entire study period reflects a better model performance at the 30 m water depth site than the obtained at the 20 m site, with correlation coefficients (R^2) of 0.43 and 0.37, respectively, and improves when using data from periods of negligible river influence with R^2 values of 0.62 at the 20 m water depth site and 0.66 at the 30 m site (Figure 5.3 A and B). Therefore, the model better performed during periods without river discharge and when farther the site from sediment sources (late autumn and winter and 30 m depth, respectively) as it is assumed that most of the SSC is due to resuspension. It is intriguingly that the model fits better at 30 m than 20 m water depth, in spite of bottom sediment changes were higher at the deeper site (Figure 4.4 and Figure 4.10). It is hypothesized that changes in sediment properties were better captured with the scheduled sampling interval at the 30 m water depth site than at the other site probably because the influence of river inputs and shear stresses decreased offshore and changes in the bottom sediment properties were less frequent in deeper than in shallow waters.

The correlation obtained between observed and modeled SSC during Event H at both sites (Figure 5.3 C and D) improved respect the one obtained from the longer time series presented above. Accounting all data during event H, the correlation coefficients were 0.62 and 0.73 at 20 m and 30 m water depths, respectively, reaching values of 0.69 and 0.87 if only the first storm was compared (Event H_1). These correlation coefficients show fair agreement between observed and modeled SSC during event H. The observed discrepancies occurred, especially, during the second storm (Event H_2) where the model overpredicted the SSC, in absence of external sediment inputs. This fact suggests that seabed sediment properties varies during a storm event. In this sense, the model simulates SSC as non-cohesive material whose availability is limited by the thickness of an active layer. However, event H_1 underwent erosion at both sites (see Figure 5.6) and probably more cohesive sediment were exposed during and after this resuspension event and the seabed became more difficult to erode.

The temporal and spatial (in the vertical) variability of sediment properties in the inner shelf has been demonstrated in a number of studies during last few decades. These studies showed that grain size distribution and porosity changes as a result of the contribution from known sediment sources or regional supply or for the wave-energy affecting the bottom sediment during storms (e.g. Wheatcroft and Borgeld, 2000; Harris and Wiberg, 2002; Guillén et al, 2005; 2006; Stevens et al., 2007; Law et al., 2008; Ferré et al., 2010; Bever et al., 2011). Data from sediments grain size and porosity

taken on the inner shelf showed that sediment characteristics varies temporally and spatially in the inner shelf off Barcelona as well (see 4.1). A continuous control of bottom and suspended sediment grain size is then required if an accurate evaluation of the SSC and sediment fluxes is to be achieved. Nonetheless, the good agreement between observed and modeled SSC during event H, specially during the first storm (event H_1), gives a fair validation to estimate near-bottom sediment fluxes and vertically integrated suspended sediment fluxes during a resuspension event in the inner shelf off Barcelona.

Therefore, the results obtained during event H_1 were accounted for the analysis of sediment dynamics in the following section. The vertical profiles of model suspended sediment concentration, current speed and the sediment flux components during event H_1 are shown in Figure 5.4. The SSC was lower at the 20 m than at the 30 m isobath over 10 meters above bottom (mab) except for the lower 0.20 m (Figure 5.4). The current magnitude through the lower 10 m of water column was slightly higher at 20 m water depth than at the deeper site. However, the across-shelf component at 20 m water depth displayed a change in the sing in the profile, offshore up to 7 mab but onshore between 7 and 10 mab (Figure 5.4). Consequently, the estimated vertically integrated total sediment flux during the peak of the event H_1 was higher at 20 m than at 30 m water depth with values of 4000 and 3800 g/m^2s, respectively, although the observed and modeled suspended sediment flux at the reference level was higher at the deepest site.

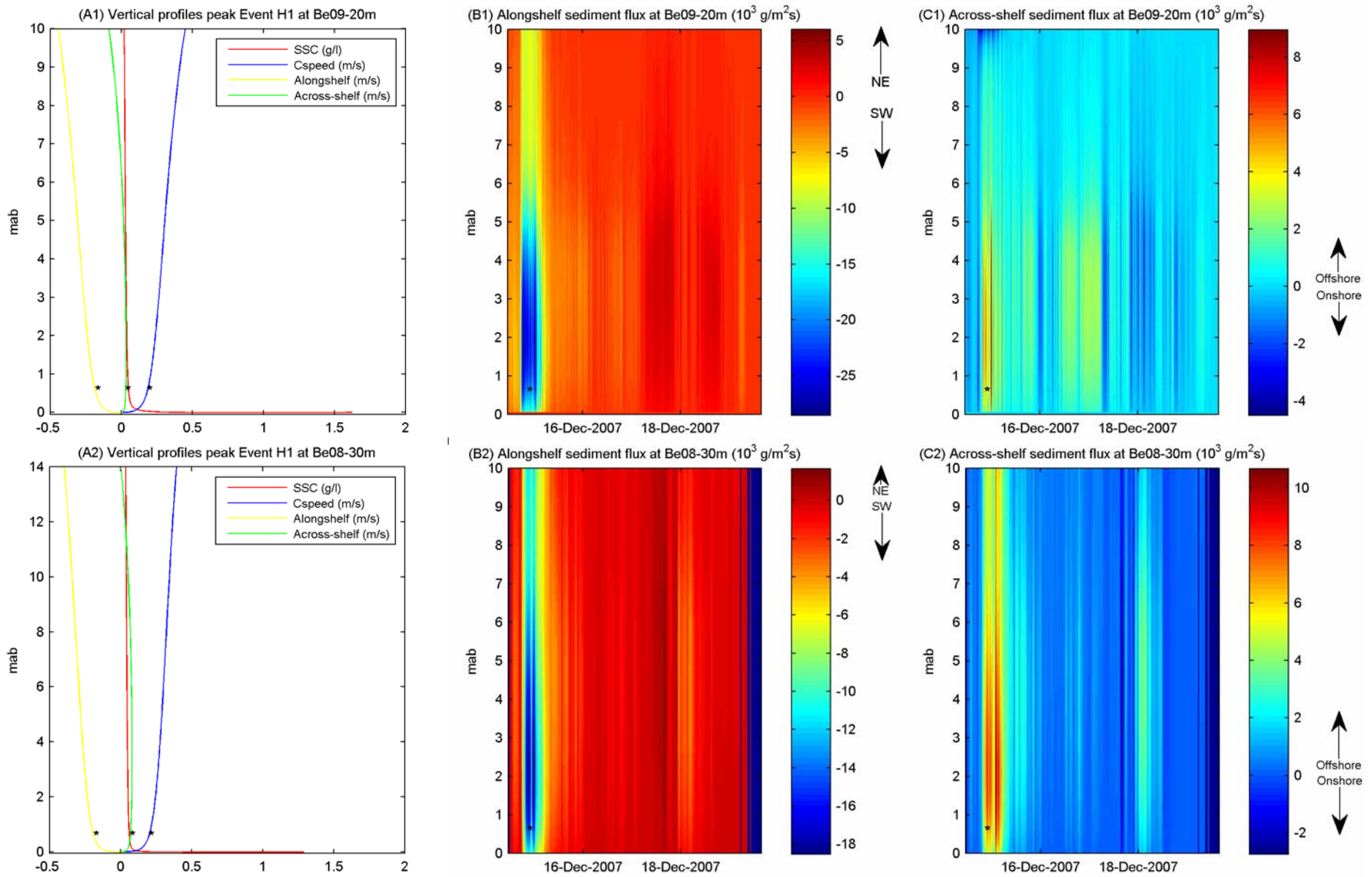

Figure 5.4. Model profiles of SSC, current speed and components at Event H1 peak (A1 and A2) and along-shelf (B1 and B2) and across-shelf (C1 and C2) sediment fluxes during Event H1 at 20 m and 30 m water depth, respectively. * Reference level during the peak of Event H1.

5.3 Sediment dynamics across the shelf

Fluctuations in the across-shelf component of the current velocity combined with across-shelf gradients in bed shear stress can produce a net drift of sediment on – offshore. Across the shelf, divergences and convergences of sediment flux depend on the across-shelf gradient in wave energy and the direction of the across-shelf current but also on the availability of suspendable sediment across the shelf which the combined effect lead to net erosion or deposition of the seabed (Harris and Wiberg, 2002).

Altimeter data collected during the deployments showed the seabed to be very dynamic, with significant bottom sediment erosion coinciding with periods of increased wave and current activity (Fig 3.1 and 3.8, respectively). Although the seabed at both, 20 m and 30 m water depth sites, underwent a net sediment erosion over the study period, the net seabed variation was higher at 30 m (Figure 5.6 B) than at 20 m water depth (Figure 5.6 A), with an erosion of about 10 cm and 4 cm, respectively. In terms of event-scale changes, differences in sediment erosion/deposition were also evident between the two sites. Two major seabed erosion events were recorded at 30 m isobath during this period, an erosion event of more than 6 cm associated to the most energetic episode of the record (Event H_1) and a second event of more than 3 cm (Event I). At 20 m depth, the variation recorded at the same time was a deposition of a 3 cm layer which was rapidly eroded and an erosion event of 2 cm, respectively, although this site presented more dynamism in terms of frequency of erosion/deposition events along the study period.

In the inner shelf off Barcelona, the sediment transport was mainly directed towards the southwest (along-shelf) during the study period (Figure 5.5), however, the seaward component was considerably relevant and favored the segregation of coarse and fine sediment from the nearshore towards deeper areas. Nonetheless, noticeable differences in sediment transport patterns were observed across the inner shelf. Near-bottom sediment transport at 20 m water depth was mainly offshore, while in deeper parts of the inner shelf the along-shelf component dominated the sediment transport. This is consistent with previous studies carried out in the area that located a mud belt between 30 m and 60 m water depths shifted southwestward (Checa et al., 1988; Palanques and Diaz, 1994; Liquete et al., 2007).

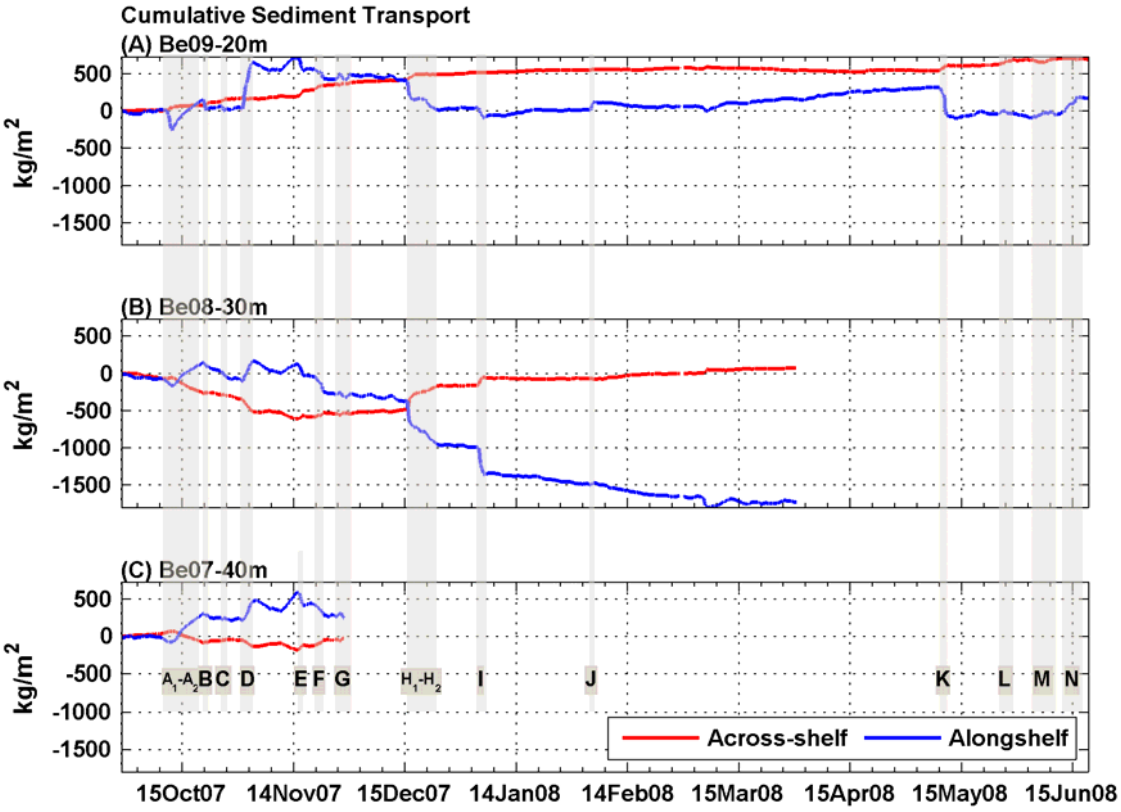

Figure 5.5. Along-shelf and across-shelf cumulative sediment transport near the bottom for the recording period at (A) Be09-20m site, (B) Be08-30m site and (C) Be07-40m site. Positive values are towards the NE in the along-shelf direction and offshore, across the shelf. Letters inside the plots represent the selected events.

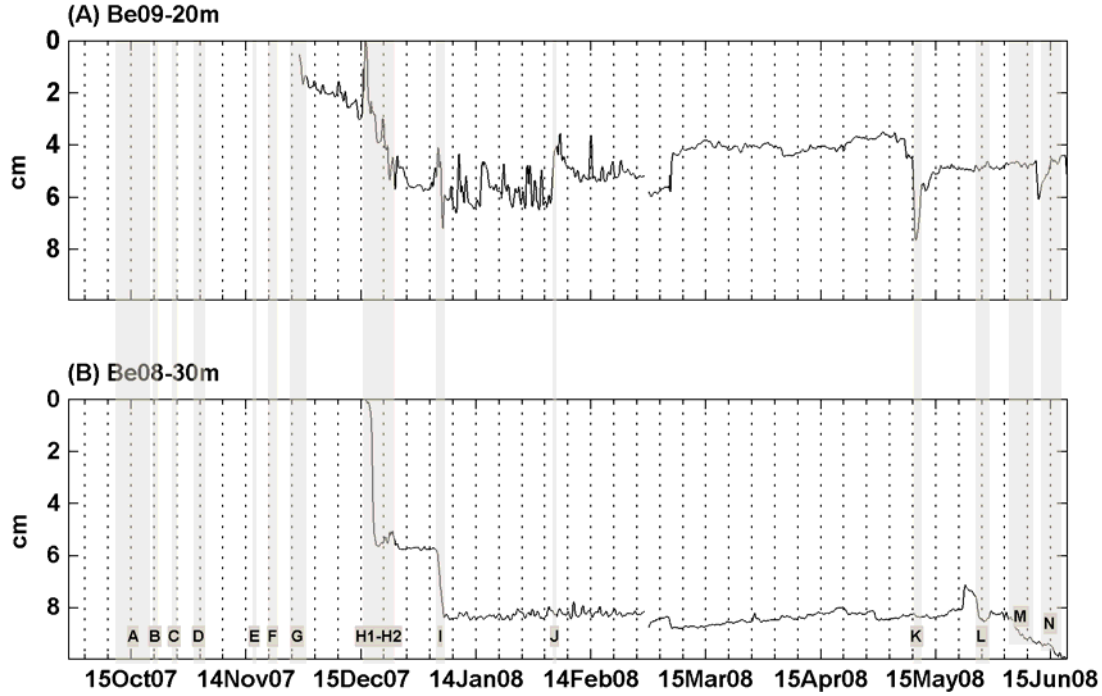

Figure 5.6. Seabed evolution at (A) Be09-20m and (B) Be08-30m sites. Letters inside the plots represent the selected events.

During the study period, near-bottom sediment transport intensity at 20 m water depth mainly depended on the availability of fine-sediment to be resuspended, while in deeper parts of the inner shelf fine sediment was most of the time available and the near-bottom sediment transport intensity was only controlled by waves and currents. The availability of resuspendable fine-sediment during autumn 2007 was conditioned directly or indirectly by the Besòs river inputs that deposited fresh river-derived sediment in shallow waters (ephemeral layers). The combined action of wave and current energy resulted in a convergence of the flux between 20 m and 30 m water depths, preventing the spread of the riverine sediment, which was trapped mostly shallower than 30 m water depth. During subsequent events (e.g. C, D and E), waves, river inputs and currents increased near-bottom sediment fluxes more than expected considering wave conditions because the higher erodibility of the river-derived storm deposits generated during preceding events. The more energetic waves during event E probably caused the erosion of the storm-derived deposit and transported part of it from the nearshore across the shelf. The subsequent events (G and H) were much more energetic however the estimated sediment transport was relatively lower than the obtained during previous events presumably because most of the fine particles in shallow areas had already been winnowed by the preceding storms. The net near-bottom sediment transport during this period was 650 kg/m^2 mainly offshore (80º) at the 20 m isobath, 550 kg/m^2 mainly onshore (285º) at the 30 m isobath and 300 kg/m^2 toward the NE (39º) at the 40 m isobath (Figure 5.5). Therefore, this pattern of near-bottom sediment transport would suggest an accumulation zone shallower than 30 m water depth between events A and D. This would be supported by a layer of finer sediment between 3 and 8 cm below seabed observed at the 20 m depth core (see section 4.1). However, during events E and G, without riverine inputs and offshore directed currents dominating across the entire inner shelf, most of the river-derived fine sediment in shallow waters was winnowed to deeper areas.

The most significant transport event of the late autumn and winter period (Event H_1) resulted on a net near-bottom suspended sediment transport of 260 kg/m^2 mainly southwestward and slightly offshore (205º - SSW) and 465 kg/m^2 southwestward and offshore (192º - S) at 20 and 30 m water depth, respectively (Figure 5.5). For the same event, the model estimated adequately the net near-bottom sediment transport in 312 kg/m^2 toward the SSW (211º) and 493 kg/m^2 toward the S (191º), respectively and estimated a cumulative vertically integrated sediment transport of 123000 kg/m^2 at 20 m water depth which 120000 kg/m^2 are transported southwestward and 30000 kg/m^2 offshore, while at 30 m water depth, a total of 160000 kg/m^2 is decomposed into

140000 kg/m^2 southwestward and 80000 kg/m^2 offshore. Therefore, accounting the whole resuspension event, the along-shelf and across-shelf cumulative transport was also lower at 20 m than at 30 m water depth, specially in the across-shelf direction where the sediment transported during the event was 2.5 times higher at the deepest site. Consequently with observations and modeling, a 6 cm layer was eroded at 30 m water depth during this event (Figure 5.6). This erosion occurred because, as previously described in other areas (Harris and Wiberg, 2002), an offshore flow becomes erosive across the shelf where the flow first encounters fine-grained sediment. At 20 m water depth, the seabed level displayed smaller variations (< 1 cm erosion) denoting moderate across-shelf gradients of sediment transport at the shallower inner shelf (Figure 5.6). In late autumn then, fine sediment was limited at shallow areas when the strongest storm of the period occurred and its effect was greater at deeper areas of the inner shelf due to the location of resuspendable sediment, reversing the sing of the across shelf gradient in sediment transport. Similar behavior was observed during the subsequent events occurred in late autumn and early winter (H_2 and I) eroding the seabed at 30 m water depth preferentially (about 3 cm during event I) until the across shelf gradient in critical shear stress decreased again between 20 m and 30 m water depths (Figure 4.10). At that time, the gradient in sediment transport smoothed across the shelf. In the last even occurred in winter (event J), sediment transport rates were again higher at the shallower site and the seabed variation was more intense at shallow waters becoming depositional, with a deposit of 2 cm at 20 m water depth versus few millimeters at the 30 m water depth site (Figure 5.6). The resulting net near-bottom sediment transport at that time was therefore, 500 kg/m^2 and 1500 kg/m^2 mainly southwestward and offshore (200º- SSW) at the 20 m and 30 m water depth sites, respectively, transporting sediment toward deeper areas of the shelf but mainly southwestward at 30 m water depth.

In spring 2008, the conditions during sediment transport events were different and the resulting net sediment transport and seabed erosion were lower than occurred during autumn and winter. In May 2008, river intensity increased and two moderate southeastern storms were recorded together with offshore prevailing currents at the beginning of the increment in the water discharge. The first storm (Event K) eroded a 1.5 cm layer at 20 m water depth and hardly affected the seabed at 30 m water depth; conversely to the second storm (Event L) that only eroded the seabed at the deeper site (about 1 cm - Figure 5.6), which was partially deposited previously to the storm, under low energy conditions. The two subsequent events (M and N) were related with the high riverine inputs under low wave energy conditions, but the observed sea bottom

changes were unrelated with these events. However, a continuous erosion was observed at 30 m water depth during the last two weeks of the deployment. The mechanisms responsible of the sediment accumulation previous to event L and the erosional trend at 30 m water depth during the final period of deployment remain unclear. It is hypothesized that the presence of a thermocline can play a role. Typically in this zone the thermocline begins to be generated close the surface in March-April and deepening progressively. A thermocline associated with a high near bottom SSC was located around 30 m water depth at June 2008 (Figure 5.7). Previous studies have reported the occurrence of internal waves on Mediterranean shelves such as the Ebro continental shelf (Puig et al., 2001), the Adriatic Sea (Puig et al., 2007) and the Llobregat prodelta (Urgeles et al., 2011) and the potential role in resuspending and transporting sediments where the seasonal thermocline intersects with the seabed. On the other hand, the sedimentation event probably occurred when the thermocline intersect the sea bottom shallower than 30 m. In that conditions, resuspended sediment associated to the thermocline could be thereafter transported offshore and deposited by the prevailing offshore currents. During the spring events, the cumulative net sediment transport was 150 kg/m^2 towards the NE and offshore (90º-E) at 20 m water depth and at the end of the study period 650 kg/m^2 were transported offshore and about 100 kg/m^2 along-shelf towards the southwest at that site.

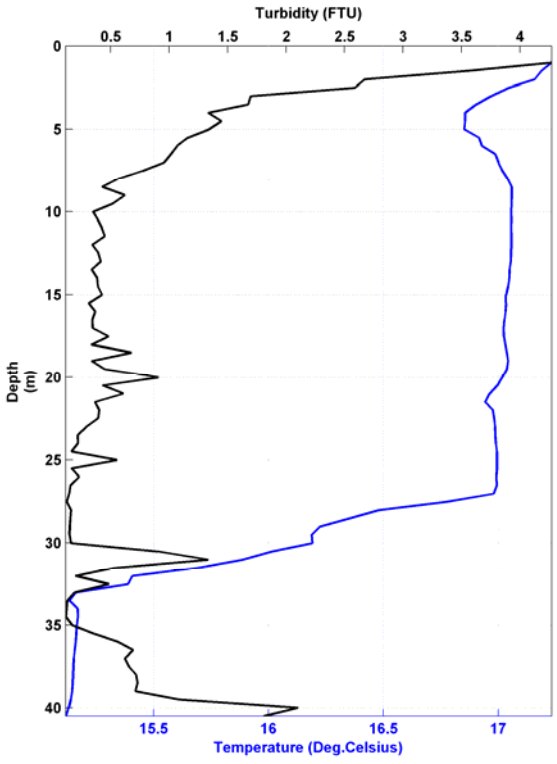

Figure 5.7. CTD profile of temperature and turbidity in June 2008 waters at the Be08-30m site.

6 Heavy metal pollution in sediments

This section focuses on the evaluation of the associated heavy metal contamination in the settling particulate matter and the surface bottom sediment across the inner continental shelf off Barcelona. Mean fluxes and mean concentrations were estimated as time-weighted mean fluxes and flux-weighted mean concentration, which is equivalent to what had been collected by a single cup during the entire deployment period.

6.1 Distribution and pollution levels of heavy metals

The impact of anthropogenic heavy metals in the Barcelona inner shelf is represented by maps constructed from the metals levels evaluated for the fine-grain fraction (Figure 6.1). These maps show sources of pollution and degree of dispersion. The most contaminated sediment accumulates southwestward from the Besòs River and the Bogatell sewer along the inner shelf and there is a decreasing gradient of metal contamination towards deeper areas. In the inner shelf, the maximum heavy metal contamination associated to the Besòs river is located around the tripod sites, specially between Be09-20m and Be08-30m (Figure 2.1 and Figure 6.1).

The mean concentrations of Cr, Pb, Cd, Cu, Zn and Hg in the Besòs River suspended and in the settling particulate matter and bottom sediment at the three tripod sites, are summarize in Table 6.1. Mean concentration values from most of the heavy metals analyzed were higher at the Besòs River suspended sediment than the values obtained at the tripod sites for both settling particulate matter and bottom sediment. At all tripod sites, concentration of heavy metals in the settling particulate matter were about the same order of magnitude of those analyzed from the bottom sediment samples taken at the same locations. In general, contents of heavy metals were higher at sites Be09-20m and Be08-30m than at Be07-40m site in both settling particulate matter and bottom sediment (Table 6.1 and Figure 6.1).

Mean heavy metals concentrations presented in Table 6.1 were compared with their natural concentration levels obtained from unpolluted bottom sediment samples taken in the Northwestern Mediterranean Sea (section 2.2.5). The comparison allowed to calculate the enrichment factor of those heavy metals and to evaluate the pollution levels affecting this littoral environment. The results obtained are shown in Table 6.2. In the study area, the higher ratios of metal contamination in relation to natural levels

were found in the Besòs River suspended sediment for all the selected heavy metals except for Hg. Conversely, Hg produced the highest impact in the inner shelf settling particulate matter and bottom sediment, with more than 20 times its natural level, reaching more than 30 times at the Be08-30 m site bottom sediment. Hg presented a level of contamination 3 times higher than the other pollutants in the inner shelf. However, the other metals levels were still very high in the area under study.

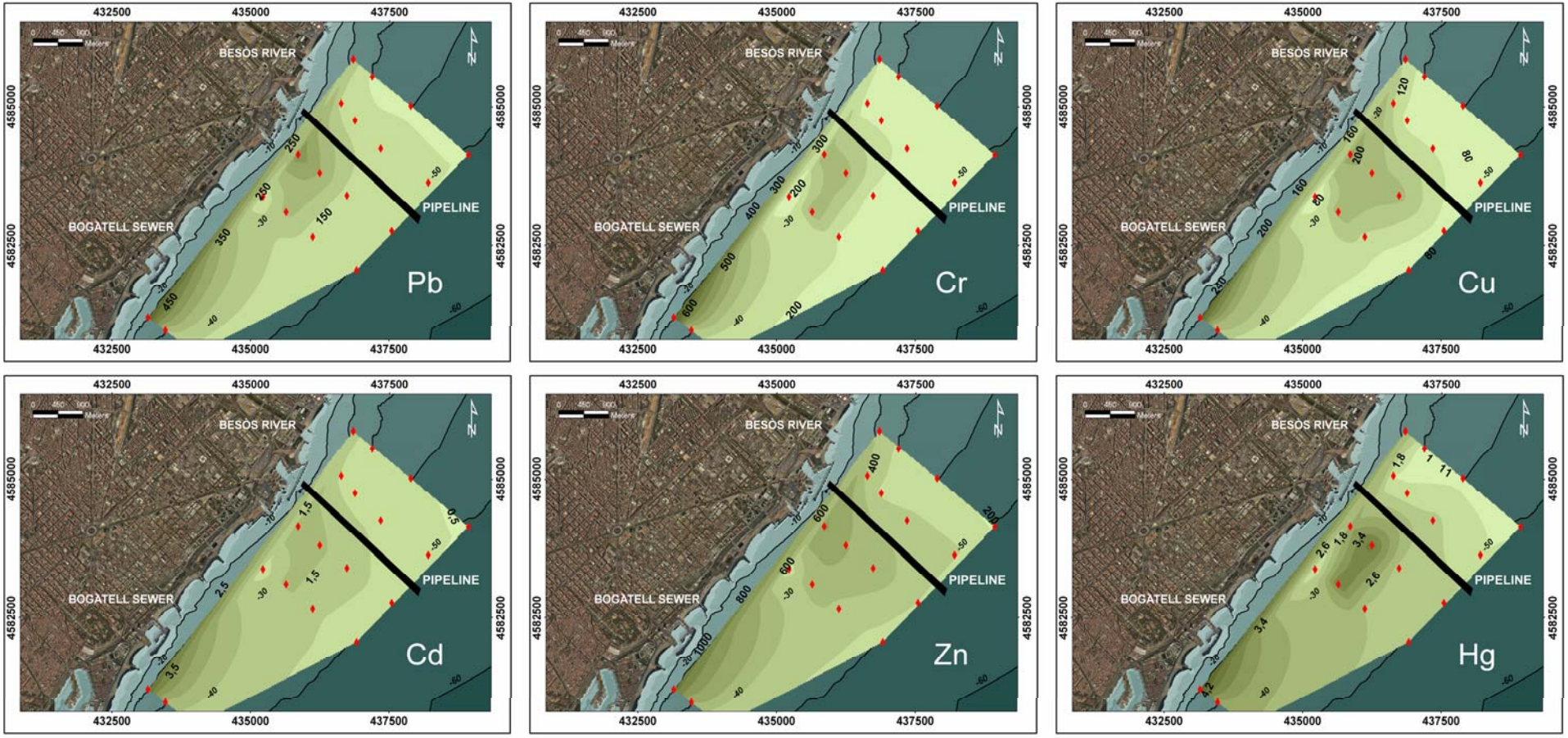

Figure 6.1. Maps showing the surface distribution of the most important heavy metal contaminants in the fine fraction of the bottom sediment sampled in October 2007. Metal concentrations are expressed in ppm.

	PPM in Suspended Sediment (SS) and Settling Particulate Matter (SPM)				PPM in Bottom Sediment		
	Besòs river SS	Be09 (20m) SPM	Be08 (30 m) SPM	Be07 (40m) SPM	Be09 (20m)	Be08 (30 m)	Be07 (40m)
Cr	506.6	169.2	185.8	183.7	270.0	303.5	209.2
Pb	255.6	130.2	123.4	109.2	256.9	234.6	153.1
Cd	3.5	1.3	0.9	0.7	1.6	2.0	1.3
Cu	323.4	107.4	105.4	109.6	161.2	150.0	149.7
Zn	1832.3	327.0	312.5	322.3	594.2	488.7	529.7
Hg	0.7	1.7	1.9	1.6	2.1	2.7	1.6

Table 6.1. Mean concentration of heavy metals in the Besòs River suspended sediment and settling particulate matter and bottom sediment of the three tripod locations in September 2007.

	EF in Suspended Sediment (SS) and Settling Particulate Matter (SPM)				EF in Bottom Sediment		
	Besòs river SS	Be09 (20m) SPM	Be08 (30 m) SPM	Be07 (40m) SPM	Be09 (20m)	Be08 (30 m)	Be07 (40m)
Cr	7.9	2.7	3.0	3.0	4.4	4.9	3.4
Pb	8.0	4.1	3.9	3.4	8.0	7.3	4.8
Cd	20.7	7.7	5.6	4.0	9.5	11.8	7.6
Cu	12.9	4.3	4.2	4.4	6.4	6.0	6.0
Zn	21.6	3.9	3.7	3.8	7.1	5.8	6.3
Hg	10.1	24.1	26.9	22.9	29.8	38.7	22.6

Table 6.2. Enrichment Factor of the mean concentration of heavy metals in the Besòs River suspended sediment and settling particulate matter and bottom sediment of the three tripod locations in September 2007.

6.2 Temporal variability of heavy metals concentrations

The temporal variability of main heavy metals concentrations in the Besòs River suspended sediment and in settling particulate matter and bottom sediment in the inner shelf sites are shown in Figure 6.2, Figure 6.3 and Figure 6.4, respectively. Most of the heavy metals analyzed (Cr, Cd, Pb, Cu and Zn) showed a similar trend in time in the Besòs River sediment and also in the inner shelf settling particulate matter and bottom sediment. However, Hg concentrations in the Besòs River sediment and together with Cd concentrations in the inner shelf settling particulate matter followed independent patterns.

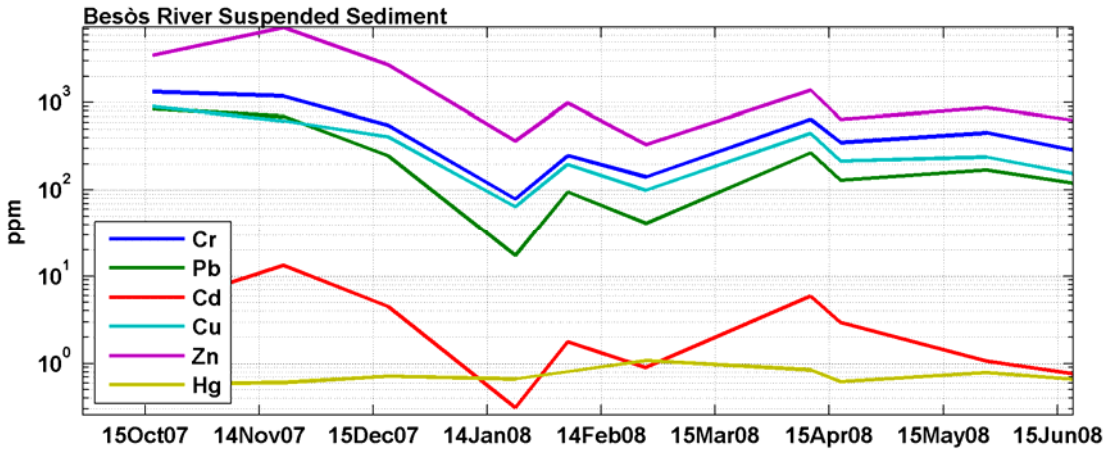

Figure 6.2. Temporal variability of heavy metals concentration in the Besòs River suspended sediment during the study period.

In the inner shelf, heavy metals concentrations in the settling particulate matter samples were considerably lower than in the river suspended sediment being most of the fluctuations under one order of magnitude (Figure 6.3). As mentioned before, concentrations of Cr, Pb, Cu and Zn in settling particulate matter sediment followed a similar trend while Hg and Cd values changed differently along the study period. At 20 m depth, Cr, Pb, Cu and Zn concentrations reached their maximum in December of 2007 dropping slowly after some fluctuations from that time to March of 2008 and increasing again to June of 2008 (Figure 6.3 A). In general, those pollutants followed a similar pattern between them and across the shelf during the time that samples were available.

In the surface bottom sediment sampled at the tripod sites, heavy metals concentration changed moderately in time compared with their fluctuations in the settling particulate matter sediment. Across the shelf, concentrations of heavy metals in the bottom sediment varied with depth. At 20 m water depth (Be09-20m site - Figure 6.4 A) all analyzed heavy metals, except Hg, increased from October to June of 2008. At that site, Hg concentrations decreased in December of 2007 but peaked also in March of 2008 decreasing in June of 2008. In the bottom sediment at 30 m water depth (Figure 6.4 B), Cr, Pb, Cu, Zn and Cd concentrations fluctuated along the study period: increasing to November of 2007 and decreasing from that time to June of 2008. However, Hg concentrations at site Be08-30m, dropped and rocketed in March of 2008 and in June of 2008, respectively. Finally, concentration values of all analyzed heavy metals, at 40 m water depth (Be07-40m site - Figure 6.4 C), decreased between October and November 2007 and between March and June 2008 but increased between December 2007 and March 2008 peaking at that time.

In general, there was a correlation between most analyzed heavy metals river inputs and concentrations in the inner shelf sediments. In both river sediment and inner shelf settling particulate matter sediment, heavy metal concentrations increased during autumn coinciding with wave and current energetic conditions and water discharge events; decreased during the dry winter season; and finally, raised moderately during spring, a period of relatively increment in river water and sediment inputs. The surface bottom sediment record also reflected changes along the study period, however those changes were dilated in time and varied with water depth.

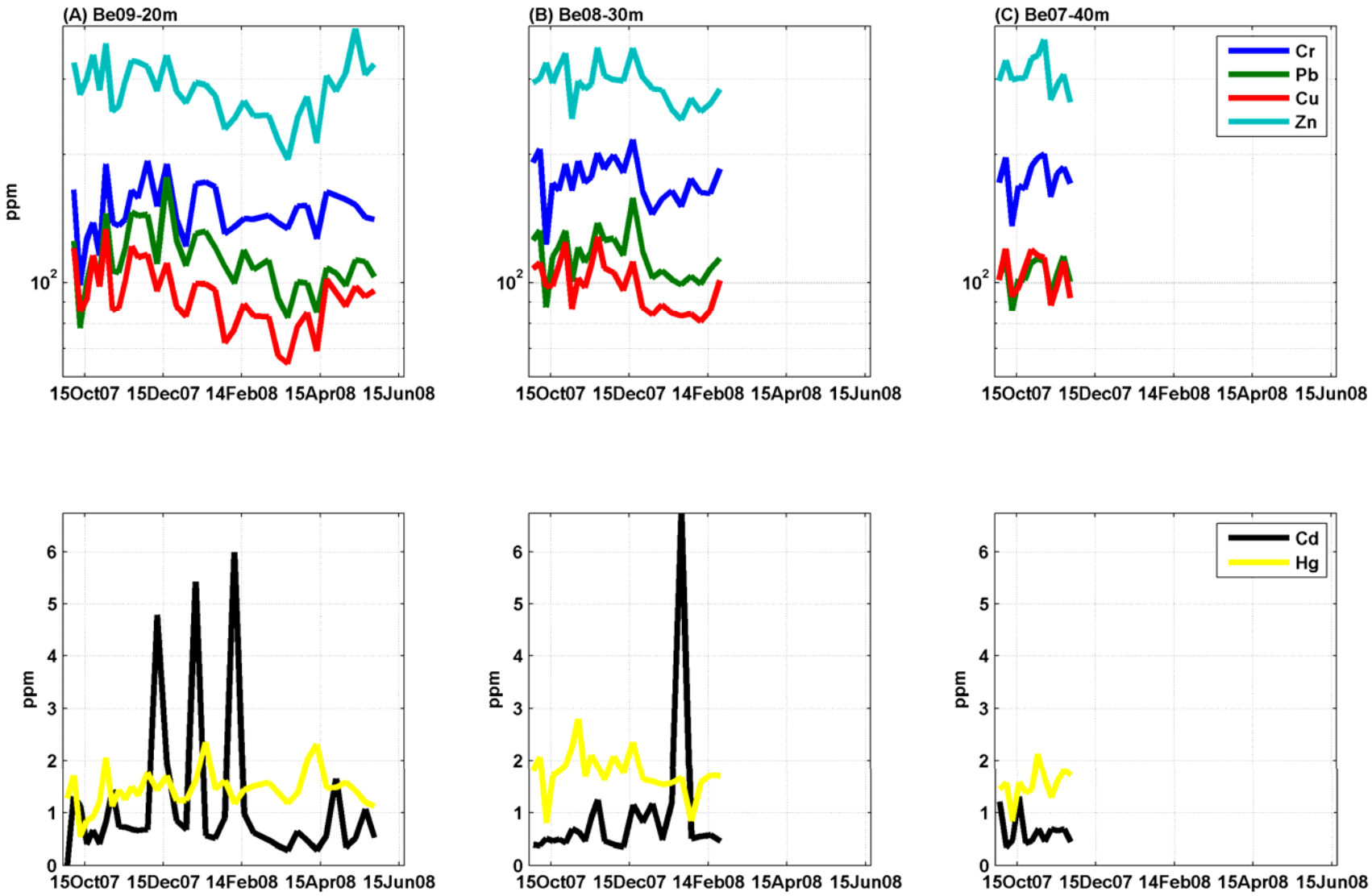

Figure 6.3.Temporal variability of heavy metals concentration in the settling particulate matter during the study period at A) Be09-20m site, B) Be08-30m site and C) Be07-40m site.

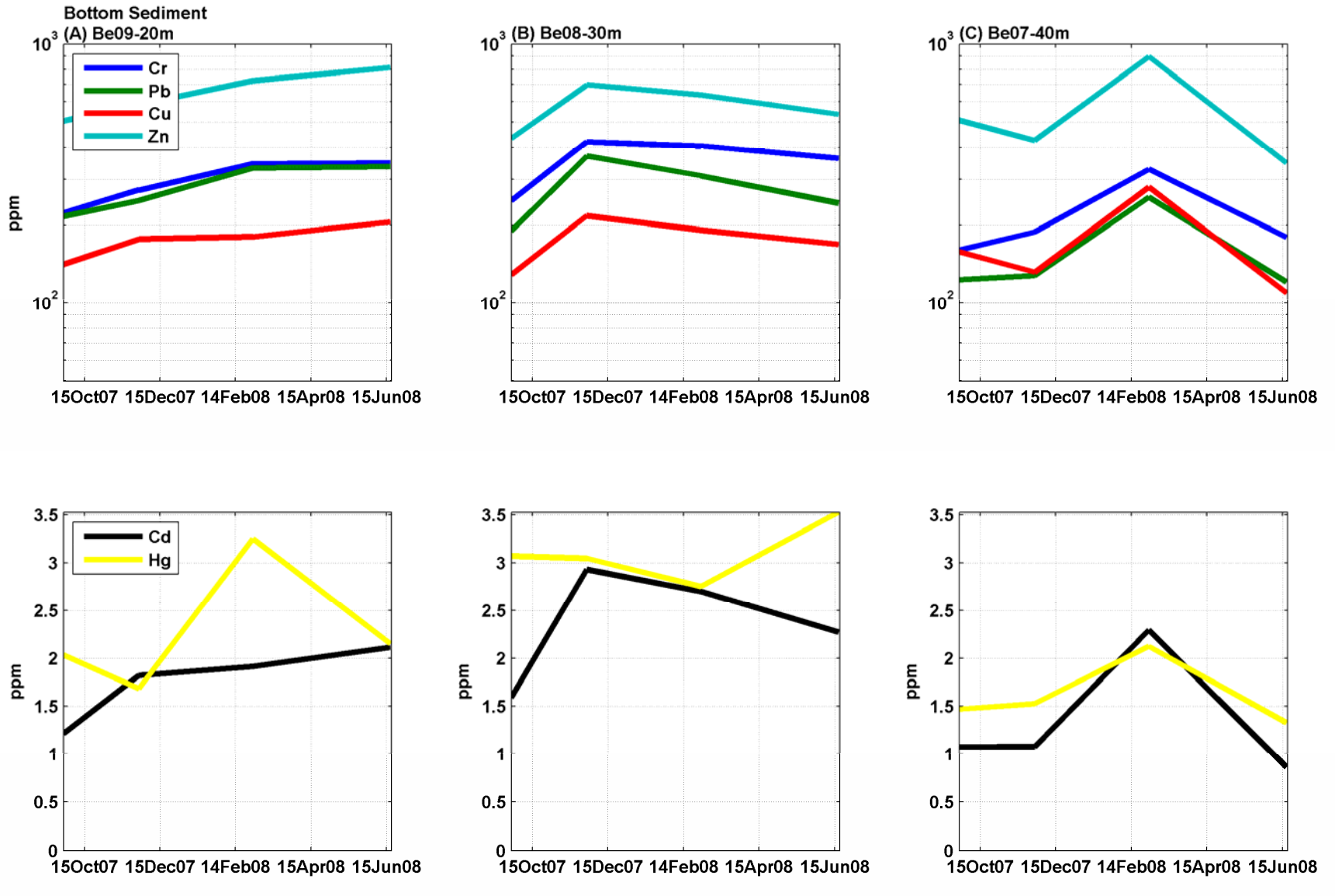

Figure 6.4.Temporal variability of heavy metals concentration in the bottom sediment during the study period at A) Be09-20m site, B) Be08-30m and C) Be07-40m.

6.3 Implications for the fate of heavy metals in the inner shelf off Barcelona

The higher contamination of shelf sediment is usually found associated to big coastal cities and the mouths of contaminated rivers. Accumulation of waste on the shelf depends on the balance between waste discharge and current dispersal. These currents are weak on average in shelves of epicontinental and semi-enclosed seas such as the Mediterranean Sea. This favors the accumulation of contaminated solids in nearshore areas around the discharging sources of these seas. This situation was observed in continental shelf such as the Gulf of Lions (Roussiez et al., 2006; Radakovitch et al., 2008), the Ebro continental shelf (Palanques et al., 1990) and the continental shelf off Barcelona (Palanques and Díaz, 1993; 1994; Puig et al., 1999). Palanques and Diaz (1994) found that the most important sources of contaminants in the northern Barcelona continental shelf were the Besòs River, the Bogatell sewer and the old pipeline of the Besòs waste treatment plant (see Figure 2.1 for location). This heavy metal contamination showed an along-shelf pattern of distribution affecting mainly the sediments of the inner Besòs prodelta, decreasing gradually southward and more sharply seaward from the river mouth. Our observations agreed well with these results (section 6.1) although it can be observed a general decreasing in heavy metals levels respect to previous studies. In the study area, the most contaminated sediment accumulates southwestward from the river and sewer mouths along the inner shelf decreasing offshore (Figure 6.1). The most affected area associated to the Besòs river influence was located around the tripod sites, specially between 20 m and 30 m water depths decreasing offshore. However, a temporal variability was observed along the study period which changed the across shelf gradient of heavy metal contamination. As a result of the high affinity between metals and fine particles, distribution of anthropogenic metals in coastal systems is mainly affected by the same dynamics as fine sediment. Therefore, it is expected that fine sediment dynamics derived from the observations in the inner-shelf off Barcelona could explain the distribution and fate of heavy metals in this region.

The metal content in the suspended sediment of the Besòs River near the river mouth indicates that there is a high temporal variability associated with increments in the water river discharge that enhance the concentration of heavy metals in the river suspended sediment. However, values of heavy metals contents were always above their natural levels along the study period (Figure 6.2). During the study period, the maximum heavy metals contents in the suspended sediment of the Besòs river, except

for Hg, were found in Autumn 2007, when events of increase water discharge took place (Figure 6.2). In the inner shelf, SPM and most of the associated heavy metals responded to a similar behaviour than river suspended sediment along this period, specially at 20 and 30 m water depths, with increments in SPM and heavy metal concentrations during increased river discharge (Figure 6.4). Although, the metal concentrations of the SPM in the inner-shelf sites were much lower than those of the river suspended sediment. Therefore, an apparent direct association between river discharges and suspended heavy metals reaching the inner shelf occurred during this period. This association was expected as fine sediment and associated heavy metals tend to accumulate at the river bed during low river flow conditions and are mostly resuspended and transported toward the sea when the water discharge increases during river floods (Puig et al., 1999). As a result, during high river discharges heavy metals are removed and discharged onto the Barcelona inner-shelf and their contents increased in the bottom sediment at both sites (Figure 6.3). Indeed, fine river-derived sediment and therefore, associated heavy metals, accumulated shallower than 30 m at the beginning of the season which was transported offshore during late autumn and winter events.

Riverine inputs decreased at the end of autumn and were low during winter 2008. At that time, Cr, Pb, Cu and Zn contents decreased in river suspended sediment and in SPM in the inner-shelf sites. The high near-bottom sediment fluxes occurred at 20 m and 30 m sites transported fine grained sediment southwestward and offshore. This offshore flux partially accumulated around 40 m water depth which can explain the increment of heavy metal contents at that depth (Figure 6.4). That implies that only during high wave and current energy the anthropogenic contamination, previously deposited in the shallow inner-shelf, reached deeper areas. Thus, river sediment inputs during autumn events presumably reached the outer part of the inner-shelf later than their discharge into the nearshore by the Besòs River.

However, Hg and Cd followed a different pattern denoting that other factors controlled their concentration in the inner-shelf. Roussiez et al. (2006) found that the silt fraction likely regulated the accumulation of anthropogenic Cd in the vicinity of rivers discharging in the Gulf of Lions. This association can be applied in our study area since the grain size sediment collected by the traps during Cd concentration peaks were higher than 50 μm, specially at the 20 m site, during winter resuspension events (Figure 4.6). Hg concentrations, though, showed a more dispersed pattern along the

inner-shelf with clear background contamination levels and increasing concentrations associated to increments of the clay fraction in bottom sediment (Figure 6.4).

The suspended sediment discharge along spring events, differing from those occurred in autumn, presented lower concentrations of SPM and therefore, heavy metal concentration in river suspended sediment decreased respect to the previous period. Differences in the inputs of suspended sediment and associated heavy metal contamination levels between these two periods of increased river discharged could be related to the type and duration of the discharge events. In Autumn 2007, events of river discharge were shorter and more episodic than during spring events when Besòs river discharged quasi-continuously during one month. During high and long river water discharges, anthropogenic metals transported by the river are probably mixed by large amounts of non-contaminated riverine sediment eroded in its drainage basin, which dilute the metal contamination transferred to the shelf. However, heavy metal contents in SPM and bottom sediment slightly increased at 20 m water depth during this period probably because the river discharge occurred in conjunction with low wave and current energy conditions which favor the deposition of fine riverine sediments and associated contamination in shallow waters.

Consequently, riverine sediments and associated heavy metals inputs depended not only on the amount of water discharge by the river but also on the conditions of the discharge and the receiving waters. Thus, during high but short river discharges, contents of heavy metals were higher than during longer discharges as fine sediment and associated heavy metal accumulated in the bed river which are eroded and discharged into the sea at the beginning of the storm but diluted with unpolluted eroded sediment if the water discharge last longer. In addition, if the discharge occurs under high wave and current conditions, SPM and associated heavy metals could be retained in shallow waters or transported offshore depending on the magnitude and direction of the currents. However, if the discharge occurs under low energetic conditions riverine sediments and associated contaminants are probably deposited in shallow waters. The resulting sediment transport and its variability across the shelf, produced a deposition of heavy metals contaminants in an along-shelf path at 20 m water depth and transferred partly offshore. At 30 m depth, most of the sediment and associated heavy metals were transported southwestward and only under the strong storms the sediments and associated heavy metals were transferred seaward toward the 40 m water depth site and to deeper waters.

7 Conclusions and further research

The observations and modeling of sediment dynamics across the inner-shelf off Barcelona provide a better understanding of sedimentary processes mainly in relation to the sediment delivered for small rivers and the dispersion by waves and currents. The contribution of the Besòs River discharges, the effect of waves and currents with or without simultaneous river discharges and how these processes varied across the shelf gave some clues of the pattern of sediment dynamics across the shelf and seabed evolution between Autumn 2007 and Spring 2008. During the study period, sediment dynamics in the inner-shelf off Barcelona was a good example of multi-event sediment transport across a Mediterranean continental shelf affected by the discharges of a “small” contaminated river that despite its size had an appreciable influence in continental shelf dynamics and the fate of anthropogenic heavy metals.

The importance of “small” Mediterranean river systems in the transference of sediment from the continent to the sea is shown. The observed events of river discharge introduced sediment to the coastal area increasing the magnitude of the downward sediment flux and the suspended sediment concentration near the bottom. During these events, evidences of the formation of ephemeral sediment layers were found, which increased the availability of fine sediment on the seabed to interact with resuspension and transport processes and changed bottom sediment properties. When events of increased river discharge occur in conjunction with high wave activity (“wet storms”), the magnitude of downward sediment fluxes and near-bottom suspended sediment concentration increase due to the combination of riverine inputs and wave sediment resuspension. Additionally, the chronology of the events on the shelf also plays a crucial role in sediment dynamics and bed evolution, since small storm events produce larger suspended sediment concentration and transport rates depending on the sequence of previous flood and storm events.

Most near-bottom suspended sediment transport on the inner shelf occurred during major storm events. The along-shelf sediment transport was higher than across-shelf at the inner shelf during storm events. However, the net across-shelf sediment transport was higher than along-shelf at shallow waters (20 m) because along-shelf transport was compensated by events of opposite transport direction. At 30 m water depth, most of the sediment was transported along-shelf towards the southwest and only during the most energetic storms there was an offshore transport.

Changes in the availability of fresh-fine grained sediment and in the across-shelf current component can modify sediment flux gradients and lead to zones of preferential accumulation or erosion. The across-shelf sediment flux magnitude decreased offshore when fresh-fine-grained sediment was available across the shelf. When fine grained bottom sediment has been winnowed from shallow areas (20 m water depth) and deposited offshore (30 m water depth), sediment fluxes and seabed erosion were higher offshore because the excess of the critical shear stress and sediment availability increased. The seabed erosion reached 4 and 10 cm at 20 and 30 m water depth respectively. It is also hypothesized that the concentration of internal waves energy in the intersection between the thermocline and the seabed also generated an area of preferential erosion.

The modeled SSC adequately reproduced observations along the entire study during periods of negligible river influence as it was assumed that most of the SSC was due to resuspension. The good agreement between observed and modeled SSC during a resuspension event gives a fair validation to estimate vertically integrated suspended sediment fluxes during a resuspension event in the inner shelf off Barcelona. The observed discrepancies between observations and model suggest that seabed sediment properties varied in response to sediment inputs from nearby sources, advection and changing hydrodynamic conditions during resuspension events. Therefore, a continuous control of bottom and suspended sediment grain size is then required if an accurate evaluation of the SSC and sediment fluxes is to be achieved.

River inputs and storm events redistribute not only sediment but also all the associated contamination, such as heavy metals, which concentration and dispersion depend both on the amount of river water discharge and on the conditions of the discharge and the receiving waters. During high but short river discharges, contents of heavy metals are higher than during longer discharges. Fine sediment and associated heavy metals accumulate in the river bed and are mainly eroded and discharged to the sea at the beginning of the event but become depleted during long events. In addition, during relatively high waves and currents conditions, riverine inputs are dispersed on the continental shelf but during low energy events and between events the discharge of heavy metals from the Besòs River accumulates in the inner-shelf. This heavy metal contamination shows an along-shelf distribution pattern affecting mainly the sediments of the inner Besòs continental shelf, decreasing gradually southward and more sharply seaward from the river mouth. The most contaminated sediment is accumulated southwestward from the river along the inner shelf. The metals levels decrease

offshore. Our observations about heavy metal distribution on the inner shelf agree well with previous studies, although also show a temporal decreasing trend of the heavy metals levels in the study area.

This thesis has provided greater insight into sediment dynamics of “small” Mediterranean high contaminated river systems from an observational and modeling approach. However, the high variability observed along the study period and the relatively short data set used to analyze sediment dynamics in this region leave to the necessity of a long-term approach to assess the reprensentativity of the observed sediment transport pattern. In this sense, the validation of the 1D sediment transport model achieved in this thesis can support further studies of sediment dynamics using available long-term wave data if a previous statistical current data set is obtained. In addition, any future modeling approach must be subject to an extensive analysis of the variability of the bottom sediment properties.

8 References

Added, A., Fernex, F., and Mangin, J.P. (1980). Répartition des oligo-elements métalliques dans les sédiments marins devant l'embouchure du grand Rhône. Diverses modalités de transports. V^{es} Journées Eud. Pollutions, Cagliari, CIESM, 53-44.

Agència Catalana de l'Aigua (Generalitat de Catalunya). – Xarxa de control: Consulta de l'aigua i el medi (CDAM). Estació Mar-desembocadura-Sant Adrià del Besòs- del Besòs. http://mediambient.gencat.net/aca/ca/xarxes_de_control.jsp.

Allison, M.A., Kineke, G.C., Gordon, E.S. and Goñi, M.A. (2000). Development and reworking of a seasonal flood deposit on the inner continental shelf off the Atchafalaya River. Continental Shelf Research, Volume 20, Issue 16, Pages 2267–2294.

Alonso, B. and Maldonado, A. (1986). Metales pesados en la plataforma continental del delta del Ebro: influencia antropogénica y procesos sedimentarios. In El Sistema Integrado del Ebro: Cuenca, Delta y Medio Marino, ed. M. Marifio. Gnificas Hermes, Madrid, 389-415.

Amos, C.L., Feeney, T., Sutherland, T.F. and Luternauer, J.L. (1997). The stability of fine-grained sediments from the Fraser River delta. Estuarine, Coastal and Shelf Science 45, 507–524.

Amos, C.L., Bergamasco, A., Umgiesser, G., Cappucci, S., Cloutier, D., DeNat, L., Flindt, M., Bonardi, M. and Cristante, S. (2004). The stability of tidal flats in Venice Lagoon—the results of in-situ measurements using two benthic, annular flumes. Journal of Marine Systems 51, 211–241.

Bever, A.J., McNinch, J.E. and Harris, C.K. (2011). Hydrodynamics and sediment-transport in the nearshore of Poverty Bay, New Zealand: Observations of nearshore sediment segregation and oceanic storms. Continental Shelf Research, Volume 31, Issue 6, Pages 507–526.

Baut-Ménard, P. and Chesselet,R. (1979). Variable influence of the atmospheric flux on the trace metal chemistry of oceanic suspended matter. Earth Planetary Science Letters, 42, 399-411.

Bourrin, F., Friend, P.L., Amos, C.L., Manca, E., Ulses, C., Palanques, A., Durrieu de Madron, X. and Thompson, C.E.L. (2008). Sediment dispersal from a typical Mediterranean flood: The Têt River, Gulf of Lions. Continental Shelf Research, Volume 28, Issue 15, Pages 1895–1910.

Butman, C.A., 1986. Sediment trap biases in turbulent flows: Results from a laboratory flume study. Journal of Marine Research 44 (3)., 645–693.

Cacchione, D.A., Drake, D.E., Kayen, R.W., Sternberg, R.W., Kineke, G.C. and Tate, G.B (1995). Measurements in the bottom boundary layer on the Amazon subaqueous delta. Marine Geology 125, 235-257.

Canals, M., Puig, P., Durrieu de Madron, X., Heussner, S., Palanques, A., and Fabres., J. (2006). Flushing submarine canyons, Nature, 444, 354–357.

Checa, A., Díaz, J.I., Farrán, M., Maldonado, A., 1988. Sistemas deltaicos holocenos de los ríos Llobregat, Besòs y Foix: modelos evolutivos transgresivos. Acta Geol. Hisp. 23, 241–255.

Coastal Monitoring Station of Barcelona (ICM – CSIC). http://elb.cmima.csic.es/elb/.

Cros, L. and García-Rey, J. (1980). Contenido en mercurio de los sedimentos marinos cercanos a la desembocadura del río Besós y de un colector de aguas residuales de Barcelona. Investigación pesquera, 44, 331-336.

Csandady, G. T. (1981). Shelf circulation cells. Philosophical Transactions of the Royal Society, London, A302, 515-30.

Deloffre, J., Lafite, R., Lesueur, P., Verney, R., Lesourd, S., Cuvilliez, A., and Taylor, J. (2006). Controlling factors of rhythmic sedimentation processes on an intertidal estuarine mudflat — Role of the turbidity maximum in the macrotidal Seine estuary, France. Marine Geology, Volume 235, Issues 1–4, Pages 151–164.

Dever, E.P., Dorman, C.E. and Largier, J.L. (2006). Surfece boundary-layer variability off Northern California. Deep Sea Research, Part II, 53, 2887-2905.

Drake, D.E. and Cacchione, D.A. (1985). Seasonal variation in sediment transport on the Russian River shelf, California. Continental Shelf Research, 4, 495-514.

Drake, D.E. and Cacchione, D.A. (1989). Estimates of the suspended sediment reference concentration and the resuspension coefficient from near-bottom observations on the California shelf. Continental Shelf Research 9, 51–64.

Duedall, I.W., Ketchum, B.H., Park, P.K. and Kester, D.R. (1983). Global input characteristics and safes of ocean dumps, industrial and seawaste ocean. In Industrial and Sewage Wastes in

the Ocean, ed. I.W. Duedall, B.H. Ketchum, J.M. Capuzzo, P.K. Park & D.R. Kester. John Wiley and Sons, New York, 3-45.

Durrieu de Madron, X., Ferre´ , B., Le Corre, G., Grenz, C., Conan, P., Pujo-Pay, M., Buscail, R., Bodiot, O., 2005. Trawling-induced resuspension and dispersal of muddy sediments and dissolved elements in the Gulf of Lion (NW Mediterranean). Continental Shelf Research 25, 2387–2409

Einsele, G., Overbeck, R., Schwarz, H.U. and Unsold, G. (1974). Mass physical properties, sliding and erodibility of experimentally deposited and differently consolidated clayey muds. Sedimentology 21, 339–372.

Eisma, D. (1981). Suspended matter as a carrier for pollutants in estuarios and the sea. In: Marine Environmental Pollution 2. Dumping and mining, ed R.A. Geyer. Elsevier Scientific Publishing Company. Amsterdam, Oxford, New York, pp. 281-292.

Eisma, D. (1993). Suspended matter in the Aquatic Environment. Springer-Verlag. Berlin, 315pp.

Fan, S., Swift, D.J.P., Traykovski, P., Bentley, S., Borgeld, J.C., Reed, C.W., Niedoroda, A.W. (2004). River flooding, storm resuspension, and event stratigraphy on the northern California shelf: observations compared with simulations. Marine Geology, 210, 17-41.

Ferré, B., Guizien, K., de Madron, X.D., Palanques, A., Guillén, J., Gremare, A. (2005). Fine-grained sediment dynamics Turing a Sorong storm event in the inner-shelf of the Gulf of Lion (NW Mediterranean). Continental Shelf Research, 25, 2410-2427.

Ferre, B., Sherwood, C. R. and Wiberg, P. L. (2010). Sediment transport on the Palos Verdes shelf, California. Continental Shelf Research, Volume 30, Issue 7, 761-780.

Fewings, M., Lentz, S.J. and Fredericks, J. (2008). Observations of cross-shelf flow driven by cross-shelf winds on the inner continental shelf. J. Phys. Oceanogr., 38, 2358–2378.

Flexas, M.M., Durrieu de Madron, X., García, M.A., Canals, M. and Arnau, P. (2002). Flow variability in the Gulf of Lions during the MATER HFF experiment (March–May 1997). Journal of Marine Systems 33–34, 197–214.

Font, J. (1990). A comparison of seasonal winds with currents on the continental slope of the Catalan Sea (northwestern Mediterranean). Journal of Geophysical Research, 95 (C2), 1537-1545.

Font, J., García-Ladona, E. and Górriz, E.G. (1995). The seasonality of mesoscale motion in the Northern Current of the western Mediterranean: several years of evidence. Oceanol. Acta, 18, 207-219.

Frignani, M., Frascari, F., Quarantoto, G. and Poleti, R. (1978). Traces of heavy metals in the Adriatic Sea sediments of the Italian coast from Pesaro to the Po delta. G. GeoL, 43, 2145.

Geyer, W.R., Hill, P., Milligan, T., Traykovski, P. (2000). The structure of the Eel River plume during floods. Continental Shelf Research, 20, 2067-2093.

Gibbs, R.J. (1973). Mechanisms of trace metal transport in rivers. Science, 180, 71-72.

Giró, S. and Maldonado, A. (1985). Análisis granulométrico por métodos automáticos: tubo de sedimentación y Sedigraph. Acta Geològica Hispànica, 20, 95-102.

Grifoll, M., Aretxabaleta, A. L., Espino, M. and Warner, J. C. (2012). Along-shelf current variability on the Catalan inner-shelf (NW Mediterranean). J. Geophys. Res., 117 (C9).

Guillén, J., Palanques, A., Durrieu de Madron, X., Nyffeler, F. (2000). Field calibration of optical sensors for measuring suspended sediment concentration in the western Mediterranean. Scientia Marina, 64 (4), 427-435.

Guillén, J., Jiménez, J.A., Palanques, A., Gràcia, V., Puig, P., Sánchez-Arcilla, A. (2002). Sediment resuspension across a microtidal, low-energy inner shelf. Continental Shelf Research, 22, 305-325.

Guillén, J., Jiménez, J., Palanques, A., Puig, P., Gràcia, V. (2005). Bottom sediment variability in the active layer of the inner shelf. Journal of Coastal Research, 21 (3), 482-496.

Guillén, J., Bourrin, F., Palanques A., Durrieu de Madron X., Puig P. and Buscail R. (2006). Sediment dynamics during wet and dry storm events on the Têt inner shelf (SW Gulf of Lions). Marine Geology, 234 (1–4), 129–142.

Gómez J., Espino, M., Puigdefabregas, J., Jerez, F. (2005). Xarxa d'Instrumentació Oceanogràfica i Meteorologica de la Generalitat de Catalunya (XIOM). Boies d'onatge dades obtingudes l'any 2004. Informe Técnico.

Harris, C.K. and Wiberg, P.L. (1997). Approaches to quantifying long-term continental shelf sediment transport with an example from the Northern California STRESS mid-shelf site. Continental Shelf Research, 17 (11), 1387-1418.

Harris, C.K. and Wiberg, P.L. (2001). A two-dimensional, time-dependent model of suspended sediment transport and bed reworking for continental shelves. Computers and Geosciences, 27, 675-690.

Harris, C.K. and Wiberg, P.L. (2002). Across-shelf sediment transport: Interactions between suspended sediment and bed sediment. Journal of Geophysical Research, 107 (C1).

Hendrickson, J. and MacMahan, J. (2009). Diurnal sea breeze effects on inner-shelf cross-shore exchange. Continental Shelf Research, 29, 2195-2206.

Heussner, S., Ratti, C. and Carbonne, J. (1990). The PPS 3 time-series sediment trap and the trap sample processing techniques used during ECOMARGE experiment. Continental Shelf Research, 10, 943-958.

ITGE (1989). Mapa geológico de la plataforma continental española y zonas adyacentes, 1 :200000. Hoja 35/ 42A, Barcelona. Institutto Tecnológico GeoMinero de España, Madrid, mem. Expl, pp. 117.

Jiménez, J.A., Guillén, J., Gracia, V., Palanques, A., García, M.A., Sánchez-Arcilla, A., Puig, P., Puigdefábregas, J. and Rodríguez, G. (1999). Water and sediment fluxes on the Ebro Delta shoreface: on the role of low frequency currents. Marine Geology, 157, 219-239.

Kirincich, R. and Lentz, S.J. (2009). Wave-Driven Inner-Shelf Motions on the Oregon Coast. Journal of Physical Oceanography, 39, 2942-2956.

Krom, M.D., Turekian, K.K. and Cutshall, N.H. (1983). Fate of metals in the sediments of the New York Bight. In Wastes in the Ocean, vol. 1, ed. I.W. Duedall, D.R., Kester, B.H., Ketchum and Kilho, P. John Willey and sons, New York, pp. 209-234.

Law, B.A., Hill, P.S., Milligan, T.G., Curran, K.J., Wiberg, P.L. and Wheatcroft, R.A. (2008). Size sorting of fine-grained sediments during erosion: Results from the western Gulf of Lions. Continental Shelf Research, 28, 1935-1946.

Lentz, S.J., Guza, R.T., Elgar, S., Feddersen, F. and Herbers, T.H.C. (1999). Momentum balances on the North Carolina inner shelf. Journal of Geophysical Research, 104 (18), 205–226.

Lentz, S.J. (2001). The influence of stratification on the wind-driven cross-shelf circulation over the North Carolina shelf. Journal of Physical Oceanography, 31, 2749–2760.

Lentz, S.J., Fewings, M., Howd, P., Fredericks, J. and Hathaway, K. (2008). Observations and a Model of Undertow over the Inner Continental Shelf. Journal of Physical Oceanography, 38, 2341-2357.

Liquete, C., Canals, M., Lastres, G., Amblas, D., Urgelés, R., De Mol, B., De Batis, M., Hughes-Clarke, J.E. (2007). Long-term development and current status of the Barcelona continental shelf: a source-to-sink approach. Continental Shelf Research, 27, 1779-1800.

Liquete, C., Canals, M., Ludwig, W., Arnau, P., (2009). Sediment discharge of the rivers of Catalonia, NE Spain, and the influence of human impacts. Journal of Hydrology, 366, 76-88.

Liquete, C., Lucchi, R.G., Garcia-Orellana, J., Canals., M., Masque, P., Pascual, C. and Lavoie, C. (2010). Modern sedimentation patterns and human impacts on the Barcelona continental shelf (NE Spain). Geologica Acta, 8 (2), 169-187.

Modamio, X. (1986a). Heavy Metal distribution on the Coast of California. Marine Pollution Bulletin, 17, 383-385.

Modamio, X. (1986b). Distribución de metales pesados en las desembocaduras de los ríos Besós y Llobregat (Mediterráneo Occidental). Investigación Pesquera, 50, 203-211.

Nittrouer, C.A., DeMaster, D.J. (editors) (1987). Sedimentary processes on the Amazon continental shelf. Pergamon Press, Oxford, pp. 379.

Ogston, A.S. and Sternberg, R.W., (1999). Sediment transport events on the northern California continental shelf. Marine Geology 154, 69-82.

Ogston, A.S., Cacchione, D.A., Sterberg, R.W., Kineke, G.C. (2000). Observations of storm and river flood-driven sediment transport of the northern Californian continental shelf. Continental Shelf Research, 20, 2141-2162.

Ogston, A.S., Drexler, T.M., Puig, P. (2008). Sediment delivery, resuspension, and transport in two contrasting canyon environments in the southwest Gulf of Lions. Continental Shelf Research 28, 2000–2016.

Palanques, A., Plana, F., and Maldonado, A. (1990). Recent influence of man on Ebro margin sedimentation system (Northwestern Mediterranean sea). Marine Geology, 95, 247-63.

Palanques, A. and Diaz, J.I. (1993). Transport and fate of heavy metal pollution dumped in the Besòs River and the Barcelona littoral area (Northwestern Mediterranean). In: Arnaldos, J. and

Mutjé, P. (Editors), Chemical industry and environment. Palahí, Arts Gràfiques. Girona, pp. 21-30.

Palanques, A. (1994). Distribution and heavy metal pollution of the suspended particulate matter on the continental shelf (North-Western Mediterranean). Environmental Pollution, 85, 205-215.

Palanques, A. and Diaz, J.I. (1994). Anthropogenic heavy metal pollution in the sediment of the Barcelona continental shelf (Northwestern Mediterranean). Marine Environmental research, 38: 17-31.

Palanques, A., Sánchez-Cabeza, J.A., Masqué, P., Leon, L. (1998). Historical record of heavy metals in a highly contaminated Mediterranean deposit: The Besòs Prodelta. Marine Chemistry, 61, 209-217.

Palanques, A., Puig, P., Guillén, J., Jiménez, J., Gràcia, V., Sánchez Arcilla, A., Madsen, O. (2002). Near-bottom suspended sediment fluxes on a river-influenced, tideless fetch-limited shelf (the Ebro continental shelf, NW Mediterranean). Continental Shelf research, 22 (2), 285-303.

Palanques, A., Durrieu de Madron, X., Puig, P., Fabres, J., Guillén, J., Calafat, A., Canals, M., and Bonnin, J. (2006). Suspended sediment fluxes and transport processes in the Gulf of Lions submarine canyons. The role of storms and dense water cascading, Marine Geology, 234, 43–61.

Palanques, A., Guillén, J., Puig, P., and Durrieu de Madron, X. (2008). Storm-driven shelf-to-canyon suspended sediment transport at the southwestern end of the Gulf of Lions, Continental Shelf Research, 28, 1947–1956.

Palanques, A., Puig, P., Latasa, M. and Scharek, R. (2009). Deep sediment transport induced by storms and dense shelf water cascading in the northwestern Mediterranean basin, Deep-Sea Research, Pt. I, 56, 425-434.

Palanques, A., Puig, P., Guillén, J., Durrieu de Madron, X., Latasa, M., Scharek, R. and Martin, J. (2011). Effects of storm events on the shelf-to-basin sediment transport in the southwestern end of the Gulf of Lions (Northwestern Mediterranean). Nat. Hazards Earth Syst. Sci., 11, 843–850.

Palinkas, C.M., Nittrouer, C.A., Wheatcroft, R.A., Langone, L. (2005). The use of Be-7 to identify event and seasonal sedimentation near the Po River delta, Adriatic Sea. Marine Geology, 222, 95-112.

Palinkas, C.M., Ogston, A.S. and Nittrouer, C.A. (2010). Observations of event-scale sedimentary dynamics with an instrumented bottomboundary-layer tripod. Marine Geology, 274, 151-164.

Puertos del Estado. Oceanografía y Meteorología. Banco de datos. Punto WANA 2066051. http://www.puertos.es/es/oceanografia_y_meteorologia/banco_de_datos/oleaje.html

Puig, P. and Palanques, A. (1998). Nepheloid structure and hydrographic control in the Barcelona continental margin. Marine Geology, 149, 39–54.

Puig, P., Palanques, A., Sánchez-Cabeza, J.A., Masqué, P. (1999). Heavy metals in particulate matter and sediments in the southern Barcelona sedimentation system (Northwestern Mediterranean). Marine Chemistry, 63, 311-329.

Puig, P., Palanques, A., Guillén, J. (2001). Near-bottom suspended sediment variability caused by storms and near-inertial internal waves on the Ebro mid continental shelf (NW Mediterranean). Marine Geology, 178, 81-93.

Puig, P., Ogston, A.S., Guillen, J., Fain, A.M.V. and Palanques, A. (2007). Sediment transport processes from the topset to the foreset of a crenulated clinoform (Adriatic Sea). Continental Shelf Research 27, 452–474.

Radakovitch, O., Roussiez, V., Ollivier, P., Ludwig, W., Grenz, C., and Probst, J. L. (2008). Input of particulate heavy metals from rivers and associated sedimentary deposits on the Gulf of Lion continental shelf. Estuar. Coast. Shelf S., 77, 285–295.

Reynolds, C. S., Wiseman, S. W. and Gardner, W. D. (1980). An annotated bibliography of aquatic sediment traps and trapping methods. Freshwater Biol. Assoc. Occ. Publ. No. 11, 54 pp.

Roussiez, V., Aloisi, J.C., Monaco, A. Ludwig, W. (2005). Early Buddy deposits along the Gulf of Lions shoreline: a key for better understanding of land-to-sea transfer of sediments and associated pollutant fluxes. Marine Geology, 222-223, 345-358.

Roussiez, V., Ludwig, W., Probst, J. L., Monaco, A., Bouloubassi, I., Buscail, R., and Saragoni, G. (2006). Sources and sinks of sediment-bound contaminant in the Gulf of Lions (NW Mediterranean Sea): a multi-tracer approach. Cont. Shelf Res., 26, 1843–1857.

Rubio, A., Arnau, P.A., Espino, M., Flexas, M., Jordà, G., Salat, J., Puigdefàbregas, J. and Arcilla, A.S. (2005). A field study of the behaviour of an anticyclonic eddy on the Catalan continental shelf (NW Mediterranean), Prog. Oceanogr., 66 (2–4), 142–156.

Sanchez-Cabeza, J.A., Masqué, P., Schell, W.R., Palanques, A., Valiente, M., Palet, C., Perez-Obiol, R., Pantaleón Cano, J. (1993). A record of anthropogenic environmental impact in the continental shelf north of Barcelona City. In: Isotope Tecniques in the study of Past and Current Environmental changes in the hydrosphere and the atmosphere. Vienna, IAEA-SM-329/18, pp. 175-184.

Sancho-García A., Guillén, J. and Ojeda, E. (2013). Storm-induced readjustment of an embayed beach after modification by protection works. Geo-marine Letters, 33 (2-3), 159-172.

Schlitzer, R. (2003). Ocean Data View , http://odv.awi.de, 2012.

Servei Meteorològic de Catalunya (Generalitat de Catalunya). Dades de Estacions Meteorològiques Automàtiques (EMA): Barcelonès, 2007-2008. http://www.meteocat.com/mediamb_xemec/servmet/marcs/marc_dades.html

Sherwood, C.R., Butman, B., Cacchione, D.A., Drake, D.E., Gross, T.F., Sternberg, R.W., Wiberg, P.L. and Williams III, A.J. (1994). Sediment transport events of the northern California continental shelf during the 1990–1991 STRESS experiments. Continental Shelf Research, 14, 1063–1099.

Sommerfield, C.K. and Nittrouer, C.A. (1999). Modern accumulation rates and a sediment budget for the Eel shelf: a flood-dominated depositional environment. Marine Geology 154, 227–241.

Soulsby, R.L. (1997). Dynamics of marine sands. Publisher Thomas Telford, London, UK.

Soulsby, R.L. (2006). Simplified calculations of wave orbital velocities. TR-155. HR Wallingford Ltd., Wallingford, 12pp.

Sternberg, R. (2005). Sediment transport in the coastal ocean: a retrospective evaluation of the benthic tripod and its impact, past, present and future. Scientia Marina, 69, 43-54.

Stevens, A.W., Wheatcroft, R.A. and Wiberg, P.L. (2007). Seabed properties and sediment erodibility along the western Adriatic margin, Italy. Continental Shelf Research 27, 400–416.

Traykowsky, P., Geyer, W.R., Irish, J.D., Lynch, J.F. (2000). The role of density driven mud flows for cross-shelf transport on the Eel River continental shelf. Continental Shelf Research, 20, 2113-2140.

Traykovski, P., Wiberg, P.L. and Geyer, W.R. (2007). Observations and modeling of wave-supported gravity flows on the Po prodelta and comparison to prior observations from the Eel shelf. Continental Shelf Research 27, 375–399.

Ulses, C., Estournel, C., Durrieu de Madron, X., and Palanques, A. (2008). Suspended sediment transport in the Gulf of Lion (NW Mediterranean): impact of extreme storms and floods, Cont. Shelf Res., 28, 2048–2070.

Urgeles, R., Cattaneo, A., Puig, P., Liquete, C., De Mol, B., Amblàs, D., Sultan, N., and Trincardi, F. (2011). A review of undulated sediment features on Mediterranean prodeltas: distinguishing sediment transport structures from sediment deformation. Mar Geophys Res (2011) 32:49–69.

Wadman, H.M. and McNinch, J.E. (2008). Stratigraphic spatial variation on the inner shelf of a high-yield river, Waiapu River, New Zealand: implications for fine sediment dispersal and preservation. Cont. Shelf Res., 28, 865–886.

Wheatcroft, R.W. and Borgeld, J.C. (2000). Oceanic flood deposits on the northern California shelf: large-scale distribution and small scale physical properties. Continental Shelf Research 20, 2163–2190.

Wiberg, P. and Smith, J.D. (1983). A comparison of field data and theoretical models for wave–current interactions at the bed on the continental shelf. Continental Shelf Research 2 (2–3), 147–162.

Wiberg, P.L., Drake, D.E. and Cacchione, D.A. (1994). Sediment resuspension and bed armoring during high bottom stress events on the northern California continental shelf: measurements and predictions. Continental Shelf Research 14, 1191–1219.

Wiberg, P.L., Drake, D.E., Harris, C.K. and Noble, M. (2002). Sediment transport on the Palos Verdes shelf over seasonal to decadal time scales. Continental Shelf Research 22, 987–1004.

Wiberg, P.L. and Sherwood, C.R. (2008). Calculating wave-generated bottom orbital velocities from surface-wave parameters. Comput. Geosci., 34, 1243–1262.

Wright, L.D. and Coleman, C.H. (1974). Mississippi River mouth processes-effluent dynamics and morphologic development. J. Geol, 82 (6), 751-778.

Wright, L.D. (1995). Morphodynamics of Inner Continental Shelves. CRC Press, Boca Raton, 241pp.

Wright, L.D., Sherwood, C.R. and Sternberg, R.W. (1997). Field measurements of fairweather bottom boundary layer processes and sediment suspension on the Louisiana inner continental shelf. Marine Geology, 140 (3–4), 329–345.

Wright, L.D., Kim, S.C. and Friedrichs, C.T. (1999). Across-shelf variations in bed roughness, bed stress and sediment suspension on the northern California shelf. Marine Geology, 154 (1–4), 99–115.

Wright, L.D., Friedrichs, C.T. and Scully, M.E. (2002). Pulsational gravity driven sediment transport on two energetic shelves. Continental Shelf Research, 22 (17), 2443–2460.

Wright, L.D. and Friedrichs, C.T. (2006). Gravity-driven sediment transport on continental shelves: a status report. Continental Shelf Research, 26 (17–18), 2092–2107.

Xarxa d'Instruments Oceanogràfics i Meteorològics (Generalitat de Catalunya). Boia direccional del Delta del Llobregat. http://www.boiescat.org/descequips2.asp?boia=boia_llobregat.